University of Stavanger

Faculty of Science and Technology

MASTER'S THESIS

Study program/ Specialization: **MSc Petroleum Engineering / Drilling Technology**	Spring semester, 2015 **Open**
Writer: **Therese Vu**	…… (Writer's signature)
Faculty supervisor: **Mesfin Belayneh** External supervisor(s): **Hayes Chow, Jakob Toftkaer**	
Title of thesis: **Finite Element Method Simulation and Modeling of Tubing Wear**	
Credits (ECTS): **30**	
Key words: Wear Burst Collapse FEM Barlow Tubing Von Mises, Tresca	Pages: 129 pages Stavanger, 15.06.2015

Abstract

This thesis presents finite element method (FEM) based on tubing wear simulation studies. Based on wear depth observed from field data, several scenarios were simulated. These are shut-in, production and gas injection. Both burst and collapse failures modes associated with local wear tube were simulated. The results are compared with API burst and collapse models, which assumes uniform wall thickness. Moreover, for each scenario, simulation based local wear depth dependent burst and collapse models are developed.

The results from simulations show that the API models for uniform reduction in wall thickness could not be applied for tubing with local wear. The stress distribution and concentration for tubing with uniform reduction in wall thickness was shown to be very contradictory from tubing with local reduction in wall thickness.

Acknowledgements

This thesis was written for the Department of Petroleum Engineering at the University of Stavanger in cooperation with ConocoPhillips Norway.

I want to use this opportunity to thank all the people that have contributed with knowledge and helped me in the process of writing this thesis. First, I want to express my great appreciation to Professor Ove Mikkelsen, for letting me borrow one, out of only three, licenses the University has to access Abaqus. Also, thanks to Theodor Ivesdal for helping me setting up the software, which saved me a lot of precious time.

My greatest gratitude goes to my Professor and mentor, Mesfin Belayneh. His excellent academic guidance and engagement in the topic has been the most valuable asset in this process. Professor Mesfin has encouraged and supported me through the ups and downs during the whole period of thesis writing.

A great appreciation also goes to the engineers at ConocoPhillips Norway. Thank you to Rick Watts, who have provided the topic for the thesis, Hayes Chow, who have contributed with his expertise within well intervention operations, and to Jacob Toftkaer, who have answered all of my simple questions throughout the project.

Last but not least, a big thanks to my partners-in-crime, Karen Margrete Wisur, Per Kristian Malde and Håvard Stangeland, for encouraging and keeping me company during the whole semester.

Table of contents

List of figures

List of tables

Nomenclature

$\alpha = Drillstring\ curvature$

$\beta = Geometry\ factor$

$\dot{A}_{Tool\ Joint} = Area\ of\ wear\ caused\ by\ tool\ joint$

$A_s = Cross - sectional\ area\ of\ Steel$

$a = Inside\ radius$

$b = Outside\ radius$

$C_{ww} = Wear\ coefficients$

$D, d_o = Outside\ diameter$

$DF = Design\ factor$

$D_t = Total\ depth\ of\ well\ at\ time\ of\ interest$

$D_\delta = Depth\ of\ wear\ point$

$D_w = Depth\ of\ wear$

$E = Young's\ modulus$

$E_{wear} = Wear\ efficiency$

$F = Side\ force$

$F_a = Axial\ pipe\ force$

$F_f = Sliding\ friction\ force$

$H = Brinell\ Hardness$

$ID = Inside\ diameter$

$K = Sliding\ friction\ coefficient$

$L = Distance\ slid$

$L_D = Length\ between\ the\ tool\ joints$

$L_{H,F} = Length\ of\ tool\ joint\ in\ contact\ with\ casing\ (hard\ face\ positions)$

$N_w = Number\ of\ wireline\ runs$

$OD = Outer\ diameter$

$p_a, P_i = Inside\ pressure$

$p_b, P_o = Outside\ pressure$

$r_i, r_a, r_1 = Inside\ radius$

$r_o, r_b, r_2 = Outside\ radius$

$R =$ Any radial distance between $r_1\ and\ r_2$

$R_b = Radius\ of\ the\ bend$

$SF = Safety\ factor$

$t = Nominal\ wall\ thickness$

$T_s = Maximum\ wireline\ tension\ at\ the\ surface$

$U = Energy\ absorbed\ in\ wear$

$U_t = Total\ mechanical\ energy\ input$

$\dot{V}_{Experiment} = Experimental\ wear\ volume\ rate\ caused\ by\ rotation$

$\dot{V}_{Field} = Field\ wear\ volume\ rate\ caused\ by\ rotation$

$V = Volume\ of\ metal\ removed\ by\ wear$

$V_a = Axial\ speed$

$x = Dimensionless\ parameter$

$y = Dimensionless\ parameter$

$z = Dimensionless\ parameter$

$\mu = Sliding\ friction\ constant$

$\omega = Angular\ velocity\ of\ rotation$

$\sigma = Drillstring\ tension$

$\sigma_a = Axial\ stress$

$\sigma_{a\ MIN} = Minimum\ axial\ stress$

$\sigma_{a\ MAX} = Maximum\ axial\ stress$

$\sigma_b = Bending\ stress$

$\sigma_h = Hoop\ stress$

$\sigma_r = Radial\ stress$

$\sigma_z = Total\ axial\ stress$

$\sigma_y = Minimun\ yield\ stress$

$\sigma_{max} = Maximum\ stress\ in\ the\ tubing\ wall$

$\sigma_{min} = Minimum\ stress\ in\ the\ tubing\ wall$

$\sigma_{VME} = von\ Mises\ equivalent\ stress$

Abbreviations

$API = American\ Petroleum\ Institute$

$COPNO = ConocoPhillips\ Norway$

$DLS = Dogleg\ severity, deg/100ft$

$DOF = Degrees\ of\ freedom$

$FEM = Finitie\ element\ method$

$MD = Measured\ depth$

$NCS = Norwegian\ continental\ shelf$

$PSA = Petroleum\ safety\ authority$

$TVD = True\ vertical\ depth$

1 Introduction

According to NORSOK D-10 standard, production tubing is a primary barrier element. It is exposed to high pressure, temperature, corrosive gases, chemicals, mechanical loading during production and intervention operations. Barrier integrity problem associated with the production tubing have been reported to be an issue on the Norwegian Continental Shelf (NCS). This thesis looks into the problem by simulating locally worn tubing under different loading scenarios. For this investigation, finite element method was used.

1.1 Background and Motivation

In 2006, the Petroleum Safety Authority (PSA) performed a pilot survey on well integrity based on input from seven different exploration and production companies (E&P), where ConocoPhillips was one of the contributors. The project preselected 12 offshore facilities and a total of 406 wells. The selected candidates were all active wells and comprised a range of new and old facilities, injectors and producers, subsea and platform wells, which extended from north to south on the Norwegian Continental Shelf (NCS) [Vignes, B. et al., 2006].

Well integrity is defined by NORSOK D-010 as "the application of technical, operational and organizational solutions to reduce risk of uncontrolled release of formation fluid throughout the life cycle of a well". The standard requirements, according to NORSOK D-010, describe that there shall at all times be two barriers between the surface and an over-pressurized hydrocarbon bearing formation. There are various aspects to the term well integrity, where tubing and annulus integrity are two of them [Wikipedia C]. For a production well, the production tubing and casing both act as well barriers.

As a result of the PSA study, 75 out of the 406 wells from the investigation showed well integrity problems. 39% percent of the problems were within the tubing barrier. Figure 1 illustrates the number of wells within the specific category of barrier-element failure.

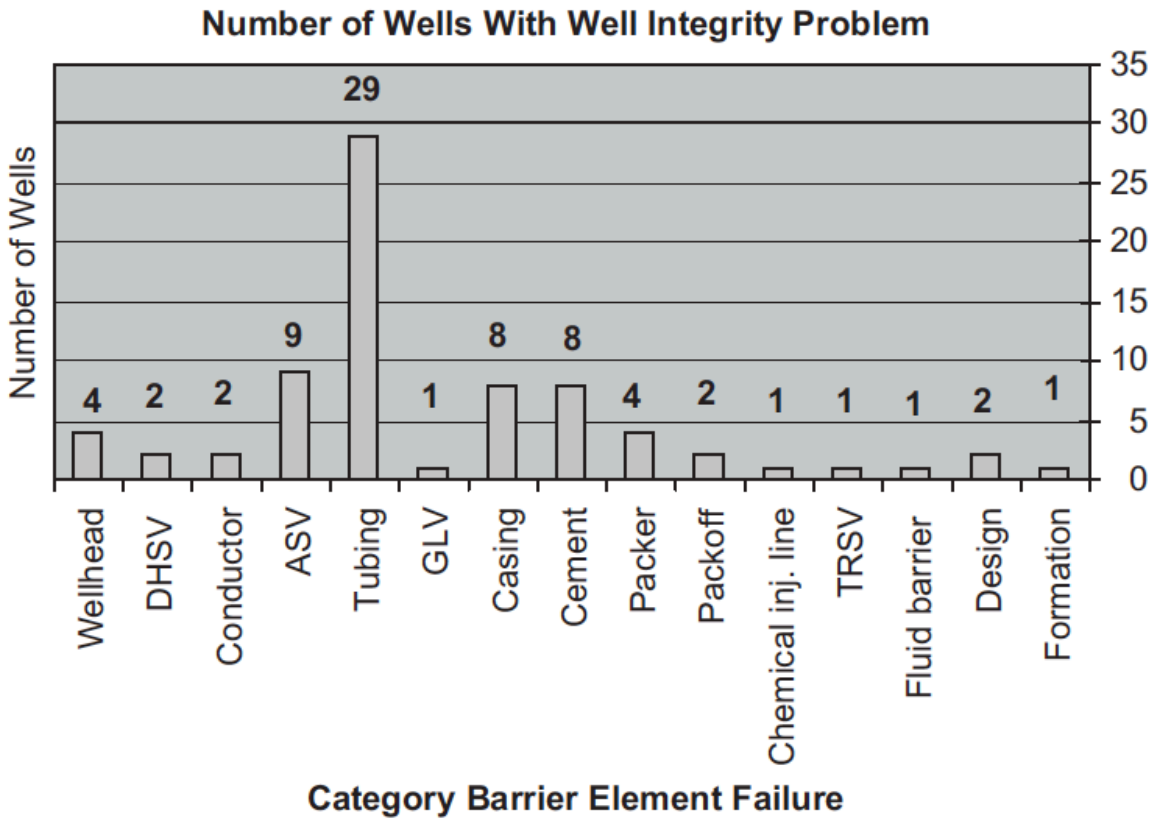

Figure 1: Wells categorized by type of element-barrier failure [Vignes and Aadnoy, 2010]

When a problem has occurred, the time and cost used to repair it can be very extensive. In a worst case it can lead to a permanent abandonment of the well. Therefore, attention should be paid and measures should be taken a step ahead if possible, to avoid the unnecessary expenditure of time and money.

During, and at the end of the productive phase of a well, multiple operations are being done in order to maintain the well integrity. The collective term for these operations is well intervention. Well intervention operations consist of various methods to intervene into a live well, such as coiled tubing, wireline and snubbing. The purpose of well intervention can be to alter the state or geometry of the well, do measurements and tests to provide well diagnostics, or manage the production [Wikipedia A].

ConocoPhillips recently detected wear in the production tubing in some of their wells by analysing multi-fingered caliper data. The wear seems to be local in a cross-sectional point of view, and occurs in different sections of the wells. A comprehensive

study of how the wears have arisen has not yet been performed. The cause could be due to several reasons, among others mechanical damage by tools, erosion and corrosion by the content in the production fluid, which all contributes to deterioration of tubing material [Wikipedia B]. If in addition, an unwanted condition of high differential pressure between the well bore and annulus develops, the consequences can lead to failure of the tubing. The causes of wear will not be extensively discussed in this thesis, but the focus will rather be on the effect that damage has on the safe operational pressure window after it has been worn.

1.2 Problem Description

The wear ConocoPhillips Norway (COPNO) detected in the production tubings showed a range in variation, both in the sense of pattern and where it occurred in the well. Most of the wear appeared to be local wear, which means the reduction in wall thickness around the tubing circumference was not uniform. The focus in this thesis will be to investigate what consequences the wear has for the operating pressure during different scenarios, where very high pressures can occur. The reason that wear is considered as an issue, is that it decreases the burst and collapse pressure resistance of the tubing. In other words, the strength of the tubing is reduced from its original state. Existing models for calculating the de-rated burst pressure for a uniform worn casing are often implemented on locally worn tubing as well, which can be a bit concerning. Per today, ConocoPhillips Norway does not have a consistent model for predicting the deterioration of tubing with local wear.

This thesis uses FEM to simulate tubing with local wear, and from the simulated results, generate a model that predict the wear depth de-rating burst and collapse pressures. It is essential to simulate the conditions that the tubulars may experience during the lifespan of the well, especially when exposed to wear. By simulating the operations during these specific conditions can help to determine the maximum pressure the tubing can withstand after being worn.

This thesis addresses issues such as:

- How uniform vs. local wear affect the burst and collapse strength of the production tubing.

- How does this non-uniform wear affect the safe operational window for the tubing, and which method is the most proper to use in order to get the most precise burst and collapse pressure limit.

1.3 Objectives

The objective of this thesis is to analyse tubing wear caused during well intervention operations. The simulations do not take into account the effect for bending and temperature. The activities include:

1. Study field-data for wear
2. Review literature on the theory of stress, and burst/collapse predictive models.
3. Perform a numerical simulation using Abaqus for different wear depths (in the range of 0-50%), with regards to scenarios where high internal and external pressure occurs. Examples are during well intervention operations, a gas-lift operation or well shut-in.
4. Generate simulation based de-rating burst and collapse model as a function of wear depth

2 Literature Study on Casing Wear

Casing wear is a common phenomenon in drilling wells. In a worst-case scenario, it can cause a blowout leading to full abandonment of the well [Bradley and Fontenot, 1975]. Earlier studies on wear are mostly conducted for casings and rotating drill strings, and less on production tubing wear. Due to lack of an adequate wear measuring technology, a method of wear prediction and a formula that accurately determines the internal pressure capacity of crescent-shaped wear, the aspect of worn casing after installation have been merely overlooked [Song, Bowen and Klementich, 1992]. A production tubing does not have to deal with a rotating drill string, but rather well intervention equipment moving in and out of the well, such as coiled tubing, wireline or slickline. These tools can cause internal wear by scratching and eroding when in contact with the inside of the tubing on the way in or out of the well. This section will review previous studies conducted on casing wear, to get an indication of which method and equations have been used to predict the wear rate and the de-rated pressure limits as a result of the wear.

According to Song et al., 1992, the technology for predicting casing wear already exists. In theory it is possible to build a program, which can both monitor and assess the pressure capacity of a casing after it has been worn, but the lack of a method to accurately calculate the internal pressure capacity makes it difficult. Until now, the equations used to calculate internal pressure for pipes are the standard mechanical equations; API's Barlow or Lame's thick walled cylinder. However, these equations are not sufficient for pipes with non-uniform wear [Song et al., 1992]

Let's first have a look at previous research done on casing wear due to a rotating drill string. A common method used to calculate the burst strength for uniform-wear on casings is the Barlow's equation. The equation is adopted by the API Bulletin and is derived based on uniform wall loss, in which the burst strength reduces linearly with the remaining wall thickness or the wear percentage [Wu, 2005].

By using Barlow's equation for uniform wall-loss to calculate the burst pressure for a crescent-shaped wear pattern, is according to [Song et al., 1992] concerning. The

reason is that the minimum wall thickness is assumed to be the overall wall thickness of the tubing. It does not take into account the fact that only a portion of the circumference has this minimum thickness, while the remaining wall thickness is at it's nominal dimensions. Barlow's equation also oversees the fact that the hoop stress in the worn wall portion increases in order to balance with the internal pressure acting on the inner surface of the tubing. The increase of hoop stress induces a bending moment, which causes the tubing to deform from a circular shape to a slightly oval shape [Wu, 2005]. The calculations based on Barlow for uniform wear does neither account for the ballooning or bending effects caused by the worn section for crescent-shaped wear [Song et al., 1992]. It is of interest to determine the actual ultimate pressure capacity of the production tubing when subjected to crescent-shaped wear, in order to consider the true safety. In this thesis work, the applicability of the Barlow's equation for wear production tubing will be assessed.

2.1 Field Wear Rate From Experimental wear

Bradley and Fontenot (1975) assumed that where the tool joint of a drill string was in contact with the casing, the same amount in volume of material was removed per unit time in the field as in the experiments under the same condition:

$$\dot{V}_{Experiment} = \dot{V}_{Field} \tag{2.1}$$

The area of the wear in a cross-section of a pipe as the tool joints pass by, can be expressed by

$$\left(\dot{A}_{Tool\ Joint}\right)_{Total} = \frac{\dot{V}_{Experiment}}{L_D} = \frac{\dot{V}_{Field}}{L_D} \tag{2.2}$$

Where

$L_D = Length\ between\ the\ tool\ joints$

One can relate the field wear rate, in terms of $\dot{A}_{Tool\ Joint}$, to the experimental wear results by equation (2.3):

$$\dot{A}_{Tool\ Joint} \approx C \begin{pmatrix} Wear \\ Rate \end{pmatrix} \tag{2.3}$$

Equation (2.3) expresses that the for tool joints, the cross sectional wear area can be related to the wear rate. The simplified expression for the wear rate then becomes:

$$\begin{pmatrix} Wear \\ rate \end{pmatrix}_{Field} = \begin{pmatrix} Wear \\ rate \end{pmatrix}_{Experiment} * \left(\frac{L_{H,F}}{L_D}\right) \tag{2.4}$$

Where

$L_{H,F} = Length\ of\ tool\ joint\ in\ contact\ with\ casing\ (hard\ face\ positions)$

2.2 Wear Efficiency and Prediction of Casing Wear

Wear efficiency tells the relationship between the amounts of metal removed to the amount of energy dissipated in the process. Holm's [Holm, 1946] conclusion was that the product of the side force and distance slid is proportional to the volume worn. The volume worn is then inversely proportional to the material hardness *H*.

White and Dawson (1987) later made a modification of this usual wear-coefficient model. They substituted the side-force with friction-force and the way the data were normalized was an important aspect for their study. The wear-efficiency simplified the comparisons between muds, casing grades, side forces, rotation times and rotary speeds. The modification lead to a better understanding of the physical meaning of the force or distance product of the model [White and Dawson, 1987]:

"Friction force multiplied by the distance slid is the mechanical energy dissipated in friction."

Because the wear coefficient measures the efficiency of the wear process, it is called the "wear efficiency"

$$E_{wear} = \frac{U}{U_t} \tag{2.5}$$

Where

$U = Energy\ absorbed\ in\ wear$

$U_t = Total\ mechanical\ energy\ input$

Equation (2.5) can also be expressed in physical properties

$$E_{wear} = \frac{VH}{KFL} \tag{2.6}$$

Equation (2.6) is dimensionless, where

$V = Volume\ of\ metal\ removed\ by\ wear$

$H = Brinell\ Hardness$

$K = Sliding\ friction\ coefficient$

$F = Side\ force$

$L = Distance\ slid$

The distance slid in this equation represents the number of rotations multiplied by the circumference of the tool joint.

By rearranging the equation (2.6) and solving for V, gives the volume of field casing wear prediction. The linear model in combination with the laboratory-measured values of wear efficiency is used to estimate the field volume of wear. The equation becomes

$$V = \frac{EF_fL}{H} \tag{2.7}$$

Where $F_f = Friction\ force$ and $^{E}/_{H} = Proportionality\ constant$

The term $F_f L$ is equal to the energy dissipated in form of friction. One can also see that the volume of worn metal is proportional to this dissipated energy multiplied with a proportionality constant E/H.

2.3 Generalized Contact

To calculate the side force in a casing wear prediction one usually need information about the dogleg, either from measurements or expected values. For a dogleg with the curvature α and the tension σ at the top of the curve, an equation for side force is given as [White and Dawson, 1987]:

$$F = \sigma \sin\alpha \tag{2.8}$$

Equation (2.8) is simplified and excludes gravity. The curvature of the dogleg is associated with a specific length of the drill string, usually 100 feet. This means that the latter equation gives the total side force for the whole length of the drill string, and not only for the sections where the tool joint are in contact with the casing. The reasons for ignoring the fact that the side force is concentrated at the tool joint are two. Firstly, according to the wear-efficiency model the wear is a linear function of the side force. By correlating the side force, one does not have to take into account for contact areas and pressures. Secondly, even though only the tool joints are in contact with the casing in one place at a given time; as the tool joints successes down the curvature one joint after another, it will make a wear scar along whole dogleg. In other words, the tool joint movement will distribute the wear scar uniformly within the dogleg. Even though the distribution turns out to be uniform, the measured wear depth in the scar for the curve may show variations due to presumably differences in curvature locally. Instead of using equation (2.8), there has been developed a table for side-force in API RP-7G [White and Dawson, 1987].

White and Dawson (1987) do make the assumption that the rate of casing metal removed is a linear function of the side force on the tool joint, with the assumption that the friction is constant. In reality when the drill string is rotating, the friction will vary for different rotational speed and the friction coefficient will not be constant.

Figure 2 will show the axial friction coefficient as a function of axial speed for drill strings with different rotational speed. The axial friction coefficient is given as

$$\mu_{axial} = \mu * \sin\alpha \qquad (2.9)$$

Where

$\alpha = \tan\alpha = \frac{V_a}{r\omega}$

$r = Tool\ joint\ radius$

$\omega = Angular\ velocity\ of\ rotation$

$\mu = Sliding\ friction\ constant$

$V_a = Axial\ speed$

Figure 2 shows that for a non-rotating drill string, the friction coefficient is constant for increasing axial speed.

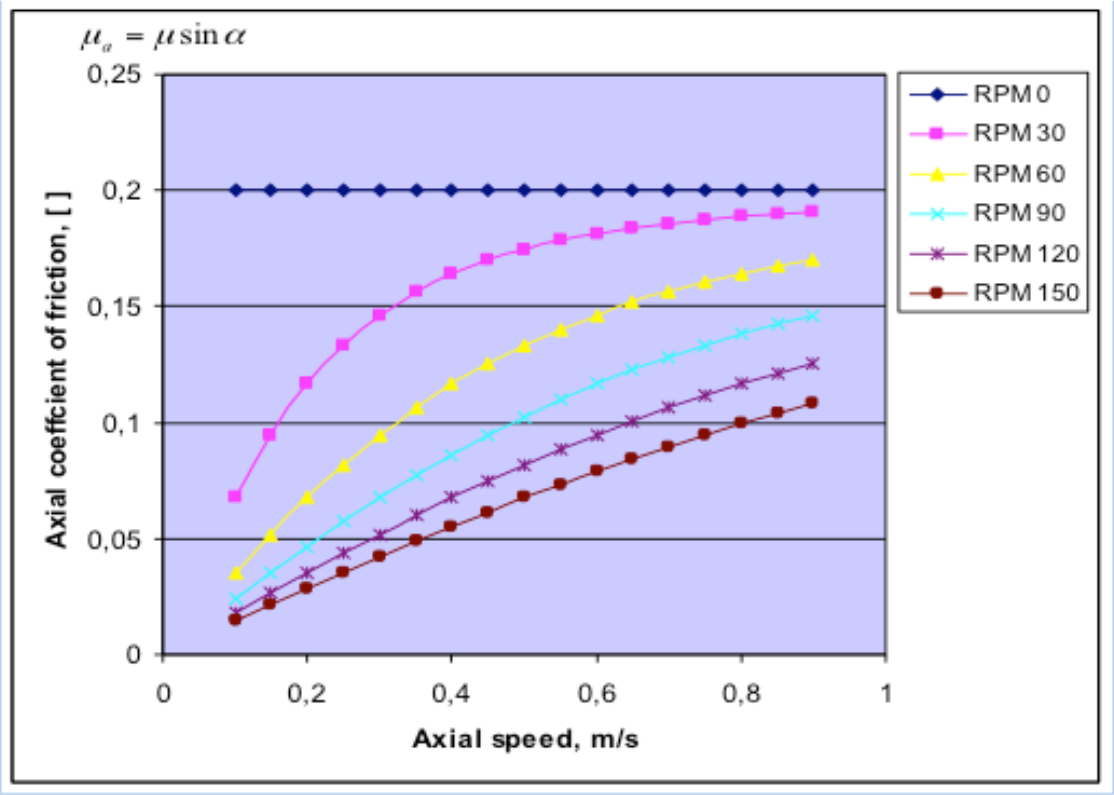

Figure 2: Axial friction coefficient as a function of axial speed

2.4 Wear Depth

According to the results from the wear tests presented by Fontenot and McEver (1974), the wireline wear coefficients are determined in Table 1.The results obtained in this table represent the wireline coefficients as a function of type of mud, contact load and casing grade. These coefficients can be used to determine the volume of wear for a running wireline.

Type of Mud	Contact Load (lb/ft)	Wear Coefficients (C_{ww}) (cu in./lb-ft) K-55	P-110
Water	9.8	1.1×10^{-8}	1.2×10^{-8}
	19.6	2.0×10^{-8}	0.8×10^{-8}
Unweighted water-base mud	4.9	15.0×10^{-8}	11.0×10^{-8}
+ 3 percent sand	9.8	8.6×10^{-8}	8.0×10^{-8}
	19.6	7.1×10^{-8}	7.2×10^{-8}
Weighted water-base mud	9.8	3.9×10^{-8}	3.9×10^{-8}
without drill solids	19.6	1.9×10^{-8}	2.2×10^{-8}
Weighted water-base mud	9.8	5.2×10^{-8}	3.5×10^{-8}
with 2 to 8 percent drill solids	19.6	2.1×10^{-8}	2.2×10^{-8}
Weighted water-base mud	9.8	12.0×10^{-8}	13.0×10^{-8}
with 8 percent drill solids	19.6	5.2×10^{-8}	4.3×10^{-8}
+ 3 percent sand			
Weighted water base mud	19.6	6.1×10^{-8}	5.9×10^{-8}
without drill solids			
+ 3 percent sand			

FEBRUARY, 1975

Table 1: Wear coefficients (C_{ww}) determined from wireline wear tests [Fontenot and McEver, 1974]

The volume of the wear scar from a wireline can according to Bradley and Fontenot (1975) be calculated with the following equation:

$$V_{Wireline} = 2C_{ww}T_sN_w\frac{(D_t-D_\delta)^2}{D_t}sin\left(\frac{\delta}{2}\right) \quad (2.10)$$

Where

$C_{ww} = Wear\ coefficients$

$T_s = Maximum\ wireline\ tension\ at\ the\ surface$

$N_w = Number\ of\ wireline\ runs$

$D_t = Total\ depth\ of\ well\ at\ time\ of\ interest$

$D_\delta = Depth\ of\ wear\ point$

The volume can then be used to calculate the wear depth/indentation depth. Bradley and Fontenot (1975) used the equation from the *Handbook of Chemistry and Physics*, which have been derived from the formula for the area of a circular segment:

$$V_{Wireline}\left[\frac{cu\ in.}{ft}\right] = \frac{\pi D^2}{8} - \left[\left(\frac{D}{2} - D_w\right)\sqrt{D_w(D-D_w)} + \frac{D^4}{4}sin^{-1}\left(1-\frac{D_w}{D}\right)\right] \quad (2.11)$$

Where

$D = Wireline\ or\ tool\ diameter$

$D_w = Depth\ of\ wear$

The latter equation is meant for a circular segment and can therefore be applied for the model for tool joint in a casing wear scenario.

2.5 Corrosion

Corrosion is a naturally occurring process, which deteriorates the material by reacting with its environment. Basically, corrosion downhole is an electrochemical reaction, which requires the presence of metal, water or electrolyte, and a corrodent [Bellarby, 2009]. Corrosion consists of two reactions, an anodic and a cathodic reaction. The anode reaction emits negative electrons, while the cathode reaction receives them, as illustrated in the next figure

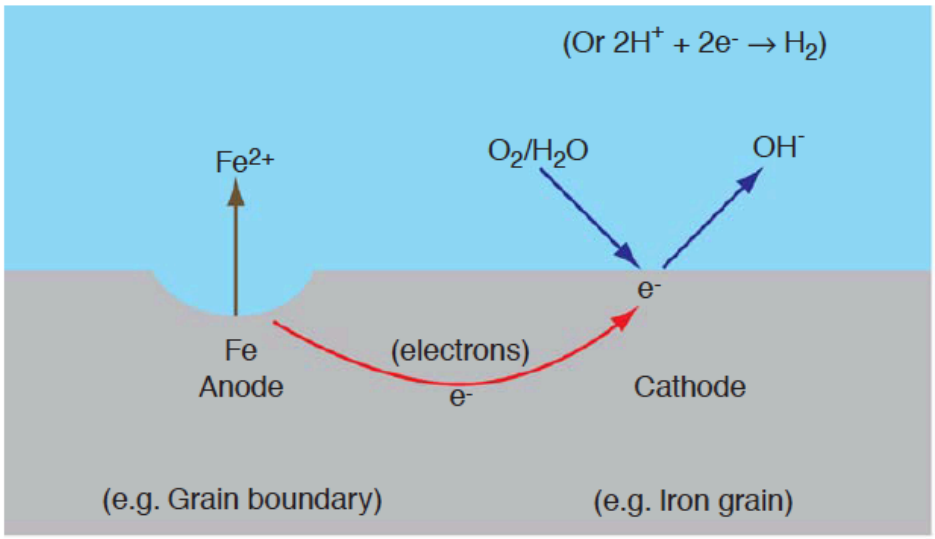

Figure 3: Reactions of corrosion [Bellarby, 2009]

Usually, the production tubing is protected with a coating that prevents corrosion, but when it has been partly removed in portions of the well, corrosion can attack these areas. The solids contained in the flow of production fluids can erode the tubing and remove this protective corrosion film. The mechanical damage from the well interventions can also contribute to the removal of the film. The next picture shows a tubing of grade L80 13Cr that have been corroded locally along a path:

Figure 4: Local corrosion of L80 13Cr tubing [Bellarby, 2009]

3 Theory

This chapter presents the theory of stress in tubing and failure criteria.

3.1 Types of Cylinders

Casings, strings and tubings are all circular cylinders. These metal cylinders are exposed to various loads such as, chemicals, pressures and temperatures. These loadings cause stresses in the body of the cylinder. It is therefore important to perform stress analysis in order to evaluate whether the cylinders can withstand the operational loads. By applying stress analysis, it is possible to evaluate the failure conditions of the cylinders such as burst, collapse, buckling and tensile.

Cylinders in general are classified into two categories as:

1. Thick walled cylinder
2. Thin walled cylinder

3.1.1 Thick-Walled Cylinder

Cylinders are thick-walled if the ratio between the wall thickness t and inner radius r_i satisfies the condition:

$$t > {}^{1}/_{10}\, r_i \qquad (3.1)$$

Figure 6 illustrate a thick walled cylinder along with the state of tri-axial stress. These are along the axial, radial and circumferential directions, $\sigma_z = total\ axial\ stress$, $\sigma_r = radial\ stress$ and $\sigma_h = hoop\ stress$.

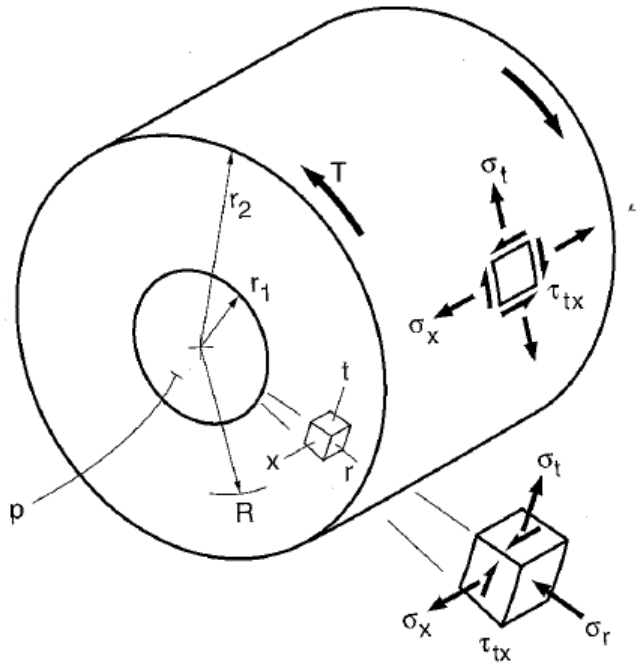

Figure 5: Stress in an internally pressurized thick-walled cylinder [Dowling, 2012]

Where

r_1 = Inner radius, r_2 = Outer radius, R = any radial distance between r_1 and r_2, σ_r = Radial stress, σ_θ = Hoop stress, σ_x = Axial stress, [r, x, t] = cylindrical coordinates

For thick walled cylinders under an applied pressure loading, the stresses are being generated across the whole cylinder wall. In order to design the safe operational limit, one first has to determine the three principal stresses (which will not be derived here): radial (σ_r), hoop (σ_h) and axial (σ_z). By neglecting the effect of temperature and assuming the stress is generated due to pressure only, the stresses are given as follows [Boresi and Schmidt, 2003]:

Radial stress

The radial stress is always compressive and varies from $\sigma_r = -p_a$ at the inner radius to $\sigma_r = -p_b$ on the outer radius:

$$\sigma_r = \frac{p_a a^2 - p_b b^2}{b^2 - a^2} - \frac{a^2 b^2}{(b^2 - a^2) r^2}(p_a - p_b) \qquad (3.2)$$

Tangential stress

The tangential stress, or hoop stress, is always tensile. The highest tensile value is on the inner radius and is decreasing towards the outer radius.

$$\sigma_h = \frac{p_a a^2 - p_b b^2}{b^2 - a^2} + \frac{a^2 b^2}{(b^2 - a^2) r^2}(p_a - p_b) \tag{3.3}$$

Axial stress

The value of the axial stress depends on whether the cylinder has open ends or not. For open-ended tubing the axial stress is equal to zero, while for capped- or closed-end tubing the axial stress is:

$$\sigma_z = \frac{p_a a^2 - p_b b^2}{b^2 - a^2} \tag{3.4}$$

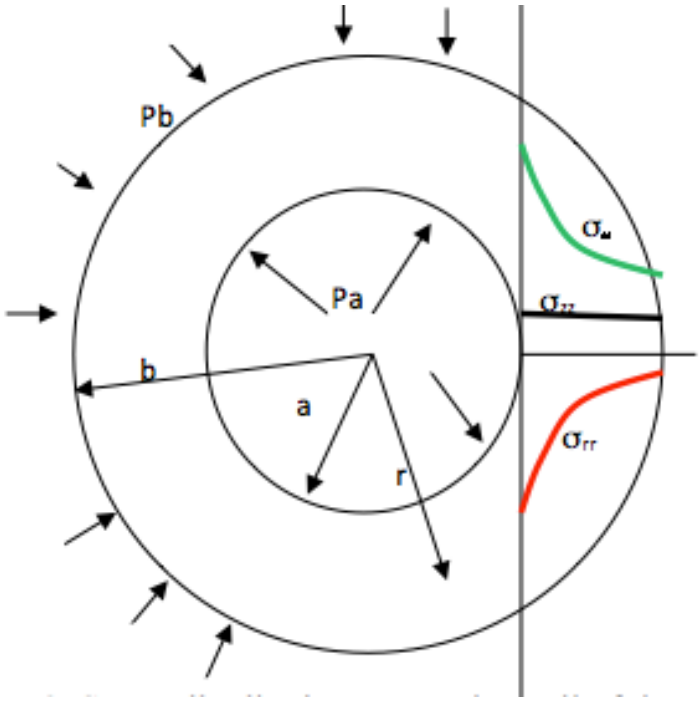

Figure 6: The stress distribution in a thick-walled cylinder [Boresi and Schmidt, 2003]

3.1.2 Thin-Walled Cylinder

A cylinder is considered as a thin walled cylinder when the ratio between the wall thickness t and the inner radius r is less than 0.1 [Dowling, 2012]:

$$t < {}^{1}/_{10}\, r_i \tag{3.5}$$

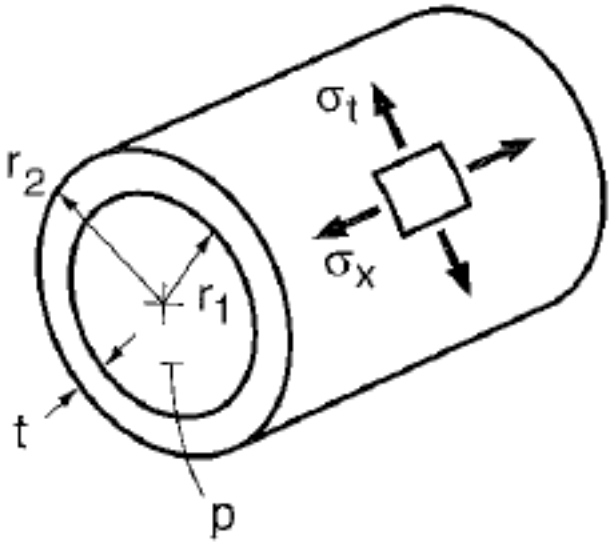

Figure 7: Stresses in an internally pressurized thin-walled cylinder [Dowling, 2012]

The same thick-walled cylinder stress equations apply for the thin walled cylinder, but they can be expressed in a simpler manner. The hoop stress is equally distributed across the wall, the radial stress varies from $\sigma_r = -p$ at the inner radius to $\sigma_r = 0$ at the outer radius, and the axial stress only apply for closed-end cylinders. Given in [Dowling, 2012], the equations for thin-walled cylinder are as follows:

Radial stress

Inner radius

$$\sigma_r = -p \tag{3.6}$$

Outer radius

$$\sigma_r = 0 \tag{3.7}$$

Tangential stress

$$\sigma_h = \frac{pr}{t} \tag{3.8}$$

The hoop stress is equally distributed across the tubing wall

Axial stress

Closed-end tubing:

$$\sigma_z = \frac{pr}{2t} \tag{3.9}$$

Open-end:

$$\sigma_z = 0 \tag{3.10}$$

3.1.3 Tubing sizes

Earlier studies are mostly performed on worn casing, which are thin-walled cylinders. When ConocoPhillips Norway (COPNO) started to conduct studies for wear on the production tubing, which is a similar case, it seems that they have considered the production tubing as a thin-walled cylinder by applying Barlow's equation. The dimensions of the most used production tubing indicates that they are thick-walled cylinders.

Table 2: Common dimensions for production tubings used by COPNO [Toftkaer, 2015]:

	Production Tubing A	Production Tubing B	Production Tubing C	Production Tubing D
Inside Diameter (ID)	4.892 in.	3.958 in.	4.778 in.	4.670 in.
Outside Diameter (OD)	5.5 in.	4.5 in.	5.5 in.	5.5 in.
Inside Radius (r_i)	2.446 in.	1.979 in.	2.389 in.	2.335 in.
Wall Thickness (t)	0.304 in.	0.271 in.	0.361 in.	0.415 in.
Cylinder Type Eq. (3.1)	$0.304 > 0.1 * 2.446$ Thick-walled	$0.271 > 0.1 * 1.979$ Thick-walled	$0.361 > 0.1 * 2.389$ Thick-walled	$0.415 > 0.1 * 2.335$ Thick-walled

As seen on Table 2, all of the common production tubings meet the criteria for thick-walled cylinder. The studies conducted by COPNO to calculate the de-rated burst pressure for a production tubing seems to be based on thin-walled cylinder theory, by applying Barlow's equation.

Other equations are applied for thick-walled cylinders than for thin-walled, as derived earlier in the different burst models. Thin walled theory only takes the hoop stress, σ_h, into account, while Von Mises theory is a combination of all the three principal stresses, σ_h, σ_z and σ_r [Boresi and Schmidt, 2003]

3.2 Tri-axial well design: Failure Criterions and Safety Factors

The uni-axial Barlow equation have for a number of years been the favourite for burst calculations due to the simplicity of it [Craft, Holden and Graves, 1962]. The problem is that this equation is derived assuming the pipe to be a thin-walled cylinder with

zero external pressure. If the hoop stress exceeds a predetermined limit (yield strength or ultimate strength), the pipe will fail in burst. Barlow's formula omits the effects of the axial loads, which is a shortcoming. The equation is accurate for pipes without axial loads and has a large ratio between the diameter and wall thickness (thin-walled cylinders). Barlow is though, very applicable for a thin-walled casing with no axial load, but fails for a drill pipe or tubing [Aasen and Aadnoy, 2006]

During installation and service, the well tubulars may be subjected to a variety of loads. The axial loads and bending in the pipe produces tensile- and compressive axial stresses. The internal and external pressure of the tubulars gives rise to radial and hoop stress in the tubing wall [Aasen and Aadnoy, 2006]. If torque is present, the pipe may experience shear stresses. A positive sign indicates tensile stress, while a negative sign is referred to as compressive.

3.2.1 Tresca failure criterion

The Tresca failure criterion is also known as the maximum shear-stress criterion, and is based on the maximum and minimum principal stresses, σ_{max} and σ_{min}. The intermediate principal stress is not accounted for in this criterion [Boresi and Schmidt, 2003]. For a ductile material subjected to any type of loading, Tresca can be used to predict the failure stress. According to Hibbeler (2011) the Tresca criterion is defined as follows:

*"The yielding of a material begins when the absolute maximum shear stress in the material reaches the shear stress that causes the same material to yield when it is subjected **only** to axial tension."*

$$\sigma_y = \sigma_{max} - \sigma_{min} \tag{3.11}$$

Where

$\sigma_y = Minimum\ yield\ stress$

3.2.2 Von Mises failure criterion

The Von Mises failure criterion is based on the maximum distortion theory, and is used to predict the yielding of steel under combined stress. The initial yield stress is based on a combination of the axial stress, radial stress and hoop stress. These stresses are also called the principal stresses. By neglecting the torque and shear stress effect, the yielding criterion can be calculated from the three principal stresses [Bellarby, 2009]:

$$\sigma_{VME} = \sqrt{{}^{1}/_{2}\{(\sigma_h - \sigma_r)^2 + (\sigma_r - \sigma_z)^2 + (\sigma_z - \sigma_h)^2\}} \quad (3.12)$$

When the σ_{VME} exceeds the yield stress of the material, σ_y, the yielding starts to occur.

3.2.3 Designing Safety Factor

Uni-axial tension tests are performed in order to experimentally determine the yield strength of well tubulars [Aasen and Aadnoy, 2006]. Two out of three principal stresses, σ_r and σ_h, are set to zero in this case. According to Aasen and Aadnoy (2006), the Von Mises equivalent stress, σ_{VME}, for this situation is given as:

$$\sigma_{VME} = \sigma_y \quad (3.13)$$

Aasen and Aadnoy (2006) define the design factor (DF) as "the ratio of the allowable stress to the working stress (σ_y/σ_{VME})". Both dimensional and material (yield strength) properties have manufacturing tolerances. The yield strength of the pipe is the allowable stress, while the Von Mises stress, σ_{VME}, is the applied stress. A high design factor means a higher margin against failure. DF=1 is the predicted failure point according to Aasen and Aadnoy (2006).

$$DF = \frac{\sqrt{2}\sigma_y}{\sqrt{(\sigma_h - \sigma_r)^2 + (\sigma_r - \sigma_z)^2 + (\sigma_z - \sigma_h)^2}} \quad (3.14)$$

Several attempts by different engineers and scientists have been done trying to solve the tri-axial design. Aasen and Aadnoy's approach was to use dimensional analysis to develop a simplified solution of the tri-axial design. The effects of torque and bending are currently neglected in the derivation, and the Lame solution for radial and hoop stresses in a thick-walled tubular is being used. They state that during investigation of the equations they revealed that both the failure of burst and collapse initiates at the inner surface of the pipe.

Aasen and Aadnoy (2006) introduces a geometry factor by Holmquist and Nadai (1939):

$$\beta = \frac{2{r_o}^2}{{r_o}^2 - {r_i}^2} = \frac{\left({d_o}/{t}\right)^2}{2\left({d_o}/{t} - 1\right)} \tag{3.15}$$

The maximum VME stress for most cases arise at the inside surface of the pipe. Therefore, by letting $r = r_i$, the equations for radial and hoop stress for thick-walled cylinder (Eq. (3.2) and (3.3)) can be reduced to [Aasen and Aadnoy, 2006]:

$$\sigma_r = -p_i \tag{3.16}$$

$$\sigma_h = \beta(p_i - p_o) - p_i \tag{3.17}$$

When bending is included, the axial stress can be calculated as follows:

$$\sigma_z = \frac{F_a}{A_s} + \sigma_b = \sigma_a + \sigma_b \tag{3.18}$$

The following dimensionless variables were found as a result of performing a dimensional analysis:

$$x = (p_i + \sigma_z)/\sigma_y \tag{3.19}$$

$$y = \beta(p_i - p_0)/\sigma_y \tag{3.20}$$

When inserting these variables into equation (3.14), one can express the design factor as:

$$z = DF = \frac{1}{\sqrt{x^2 - xy + y^2}} = \frac{\sigma_y}{\sigma_{VME}} \tag{3.21}$$

This is an exact solution to the calculation of burst and collapse. Equation (3.21) describes a surface that fully represents the loads caused by inside- and outside pressure in addition to axial stresses, in relation to the yield limit of the tubing [Aasen and Aadnoy, 2006].

Solving equation (3.21) for y gives:

$$y = \frac{x}{2} \pm \sqrt{\frac{1}{DF} - \frac{3}{4}x^2} \tag{3.22}$$

The positive sign represents the tensile force for burst, while the negative sign indicates compressive forces for collapse. The limit curve calculated from the Von Mises is the equation of an ellipse (3.20). Figure 7 shows an example of ellipses generated for different design factors:

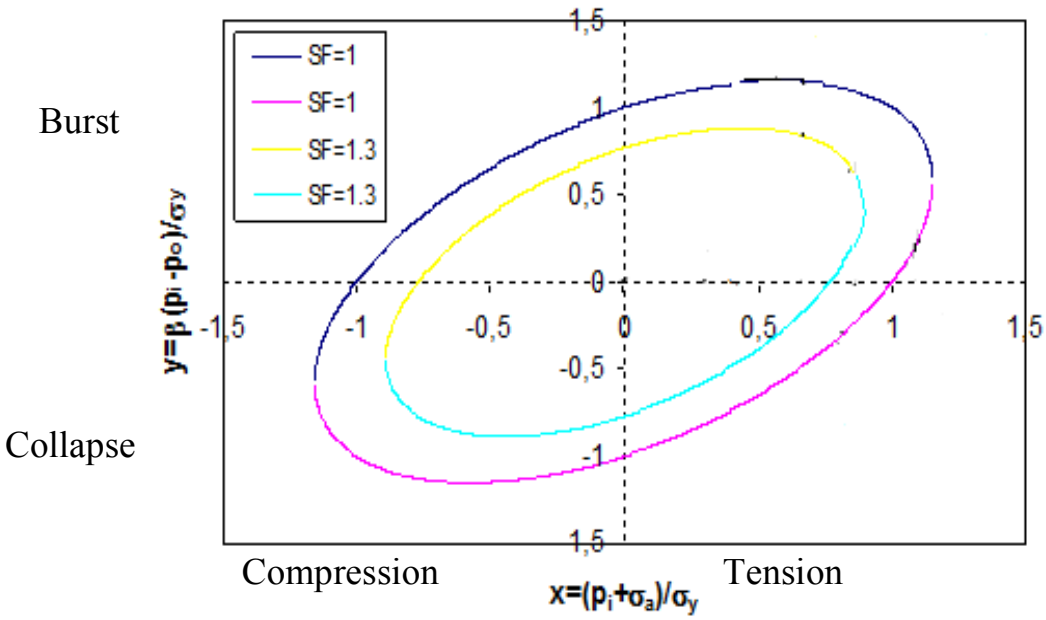

Figure 8: Von Mises failure envelope for various three dimensional Design Factors in 2D plane.

As the design factor increases, the envelopes for burst and collapse in the plot becomes smaller. All the loads acting on the casing or tubing needs to stay within the ellipse through all time, in order to be in the safe operational area. The upper portion of the ellipse corresponds to burst pressures and the lower portion to collapse pressures.

Example 1: Tri-axial limit curves with and without design factors

The two next figures are typical examples of design limit plots by the NORSOK standard, DF=1.25. The figures compares the same load, but with and without the design factor.

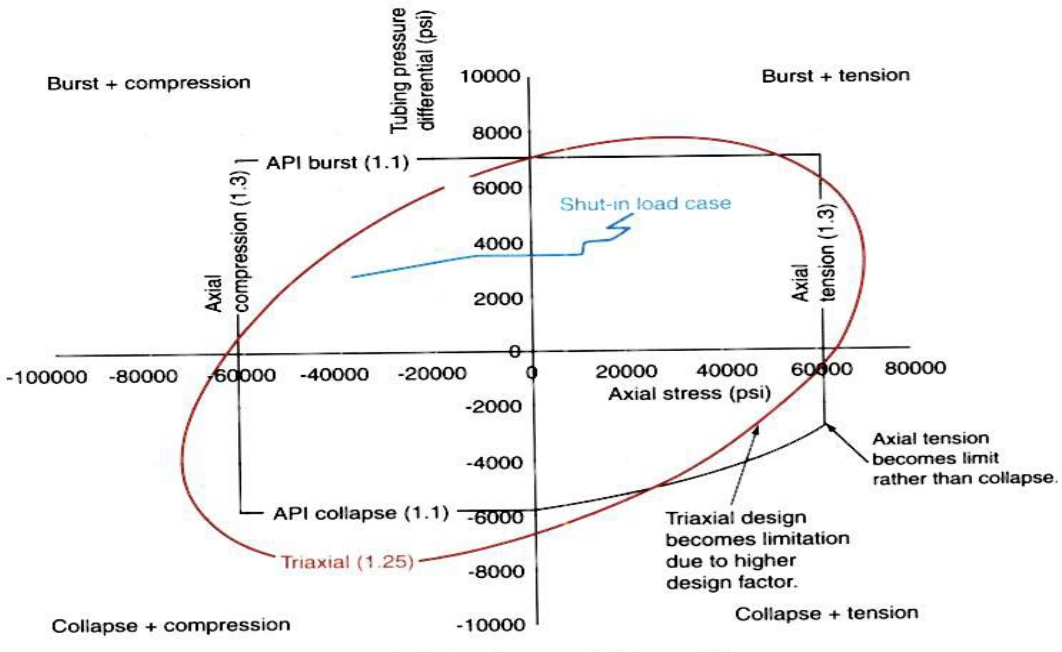

Figure 9: Design limit plot for L80, including the DF of 1.25 [Bellarby, 2009]

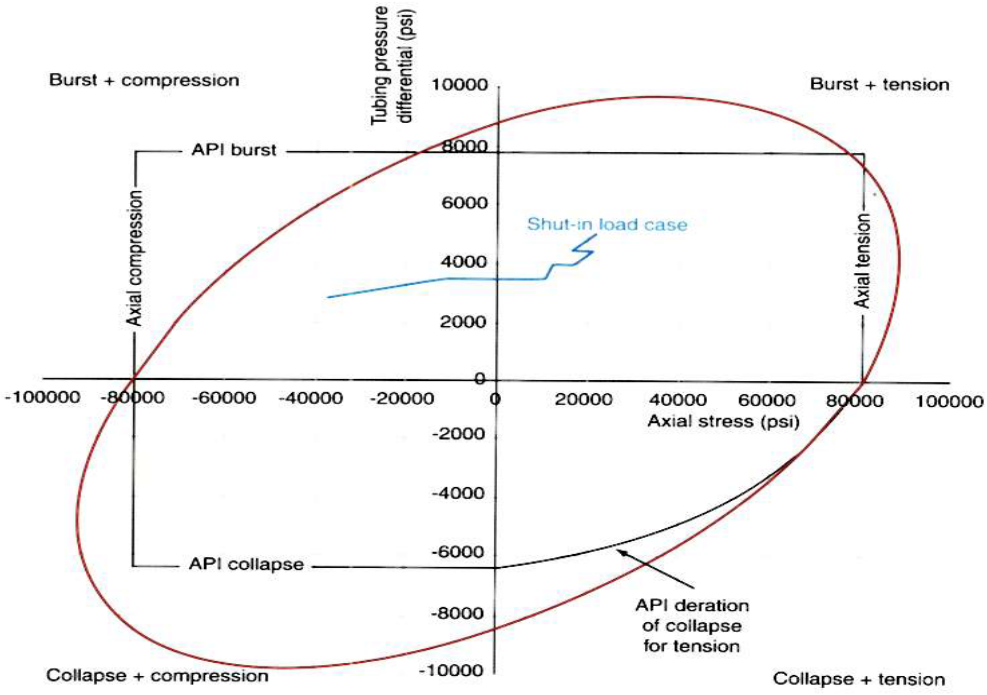

Figure 10: Design limit plot for L80, excluding the design factor (DF=1) [Bellarby, 2009]

3.2.4 Bending stress

In the presence of doglegs in the well path and buckling of the string can cause bending stress, σ_b. One can calculate the bending stress using the beam theory from [Bellarby, 2009]:

$$\sigma_b = \pm \frac{ED}{2R_b} \tag{3.23}$$

$D = Outside\ diameter$
$R_b = Radius\ of\ the\ bend$
$E = Young's\ modulus$

The radius of the bend can be calculated from the dogleg severity, DLS $\left(\frac{degrees}{100\ feet}\right)$ or the angle α. The $\pm$ sign is because the tensile stresses on the outer diameter are positive, while the compressive stresses on the inside diameter are negative. The bending stress appears to be higher on the outer diameter than the inner.

The bending stress can be calculated at any given point in the well. Because the bending stress act locally, unlike the for example the thermal loads, the bending stress in one location does not affect the stress in other locations. Thus, the bending stress is being added to the existing axial stress profile. As stated earlier, the bending stress can be both positive and negative, which means that the axial stresses may be increased or decreased. Simply, by subtracting or adding the bending stress σ_b to the axial stress σ_a, one can calculate the minimum and maximum axial stress, $\sigma_{a\,MIN}$ and $\sigma_{a\,MAX}$[Bellarby, 2009].

Minimum axial stress

$$\sigma_{a\,MIN} = \sigma_a - \sigma_b \tag{3.24}$$

Maximum axial stress

$$\sigma_{a\,MAX} = \sigma_a + \sigma_b \tag{3.25}$$

3.3 Burst theory and models

When an unworn tubular is subjected to internal pressure (P_i) or external pressure (P_o), it induces a hoop stress (σ_h) in the wall, which is always balancing to P_i and P_o as shown in Figure 11:

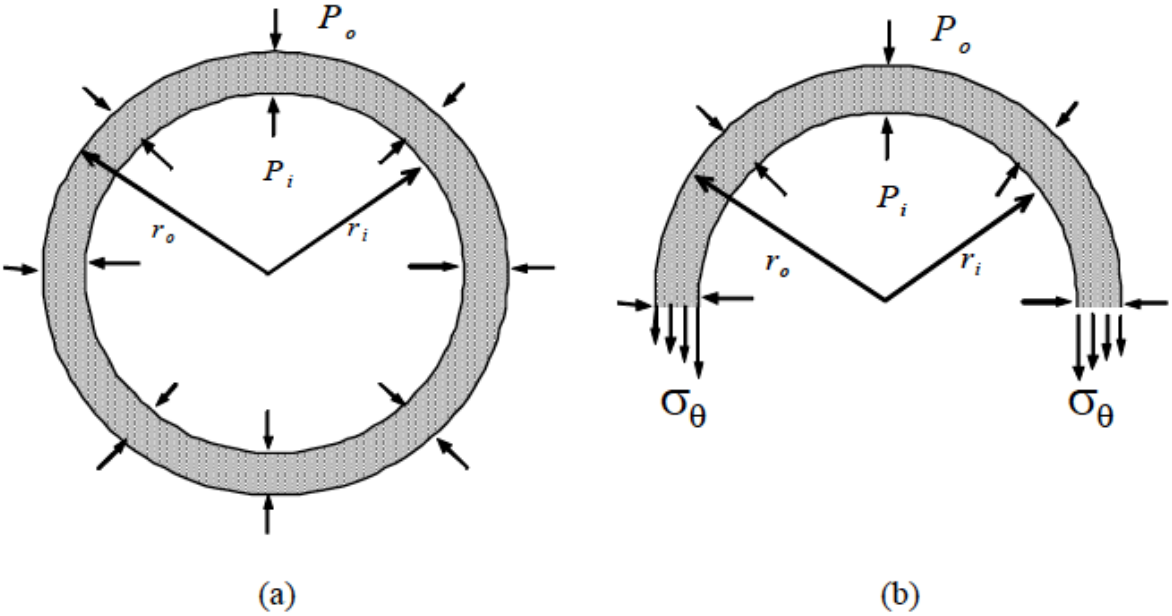

Figure 11: A) Casing hoop stress and internal pressure balance on unworn casing B) Distribution of hoop stress in the wall [Wu, 2005]

If the internal pressure gets very high, the differential pressure increases and the tubular will feel a higher burst pressure loading [Byrom, 2007]. The hoop stress is a tensile stress in the tube wall, and as Figure 11 B) shows, it is higher at the inner diameter and lower at the outer diameter. As the internal pressure (P_i) increases, the tensile hoop stress will increase until the material yields. The failure criterions are used to derive the burst and collapse models, and the derivation can be found in Appendix A.

3.3.1 Burst models based on Thick-Walled cylinder

When assuming inside pressure only, and setting $P_b = 0$ and $\sigma_z = 0$, the principal stresses in equations (3.2), (3.3) and (3.4) can be reduced to:

$$\sigma_r = \frac{p_a a^2}{b^2 - a^2} - \frac{a^2 b^2}{(b^2 - a^2) r^2}(p_a) \tag{3.26}$$

$$\sigma_\theta = \frac{p_a a^2}{b^2 - a^2} + \frac{a^2 b^2}{(b^2 - a^2) r^2}(p_a) \tag{3.27}$$

$$\sigma_z = \frac{p_a a^2}{b^2 - a^2} = 0 \tag{3.28}$$

Using Tresca failure criteria:

By inserting equations (3.26), (3.27) and (3.28) into the equation (3.11), and solving for $P = P_Y$ and at $r = a$ gives an equation for pressure that causes the inner wall of thick-walled cylinders to yield:

$$P_Y = \frac{\sigma_Y}{2}\left(1 - \frac{a^2}{b^2}\right) \tag{3.29}$$

Using Von –Mises failure criteria:

Similarly, inserting the principal stresses [Eq. (3.26), (3.27) and (3.28) into (3.12) and solving for $P = P_Y$ and at $r = a$ gives an equation for pressure that causes the inner wall of thick-walled cylinders to yield:

$$P_Y = \frac{\sigma_{VME}\left(1 - \frac{a^2}{b^2}\right)}{\sqrt{\frac{a^4}{b^4} + 3}} \tag{3.30}$$

3.3.2 Burst models based on Thin-Walled cylinder

Consider the stress equations (3.6) through (3.9) given for thin-walled cylinders, in section 3.1.2.

Inserting the maximum and minimum principal stresses in the Tresca failure criteria (Eq. 3.11), and solving for the pressure that cause the inner wall yielding $P = P_y$ gives:

$$P_y = \frac{\sigma_Y t}{r} \tag{3.31}$$

Equation (3.31) is the Barlow equation. The API (American Petroleum Institute) Burst rating (API Bulletin 5C3, 1999) is based on this formula. The API adds a factor of 0.875, which is the tolerance for the deviation in wall thickness of 12.5% from the manufacturer [Bellarby, 2009]:

$$P_y = 0.875 * \frac{2\sigma_Y t}{D} \tag{3.32}$$

Similarly, insert the principal stresses $(\sigma_h, \sigma_z, \sigma_r)$ of thin-walled cylinder into Von Mises failure criteria (3.12), and solving for the pressure that cause the inner wall yielding $P = P_Y$ gives:

$$P_Y = \frac{2}{\sqrt{3}} \frac{\sigma_Y t}{r} \tag{3.33}$$

3.4 Collapse theory and models

The collapse condition of cylinders is recognized by four different modes of failures. These are defined by the API Bulletin 5C3 (1999) as elastic, transitional, plastic and yield strength. Therefore, establishing a collapse rating for tubulars is a more complex process than for burst. Properties such as tubing diameter, wall thickness and pipe ovality is significant to the collapse rating. The ratio between the outside tubing diameter and thickness, the slenderness ratio, is used to select the appropriate collapse mode. Each mode has an empirical formula associated to it [Bellarby, 2009]:

Elastic collapse

$$P_{elastic} = \frac{46{,}95 * 10^6}{(D/t)[(D/t)-1]^2} \tag{3.34}$$

Because the deformation is purely elastic, the yield stress of the tubing is irrelevant.

Transitional collapse

$$P_{transitional} = Y_p \left(\frac{F}{D/t} - G\right) \tag{3.35}$$

Plastic collapse

$$P_{plastic} = Y_p \left[\frac{A}{D/t} - B\right] - C \tag{3.36}$$

A, B, C, F and G are empirical constants determined through earlier experiments for each pipe material. The constant values are found in API 5C3, and are given in Table 4 and Table 5.

Yield collapse

$$P_{yield} = 2Y_p \left[\frac{(D/t)-1}{(D/t)^2}\right] \tag{3.37}$$

Figure 12 shows the mode of collapse for different values of the slenderness ratio. These curves are specific for the L80 pipe material. Each different grade will have its own distinctive curves.

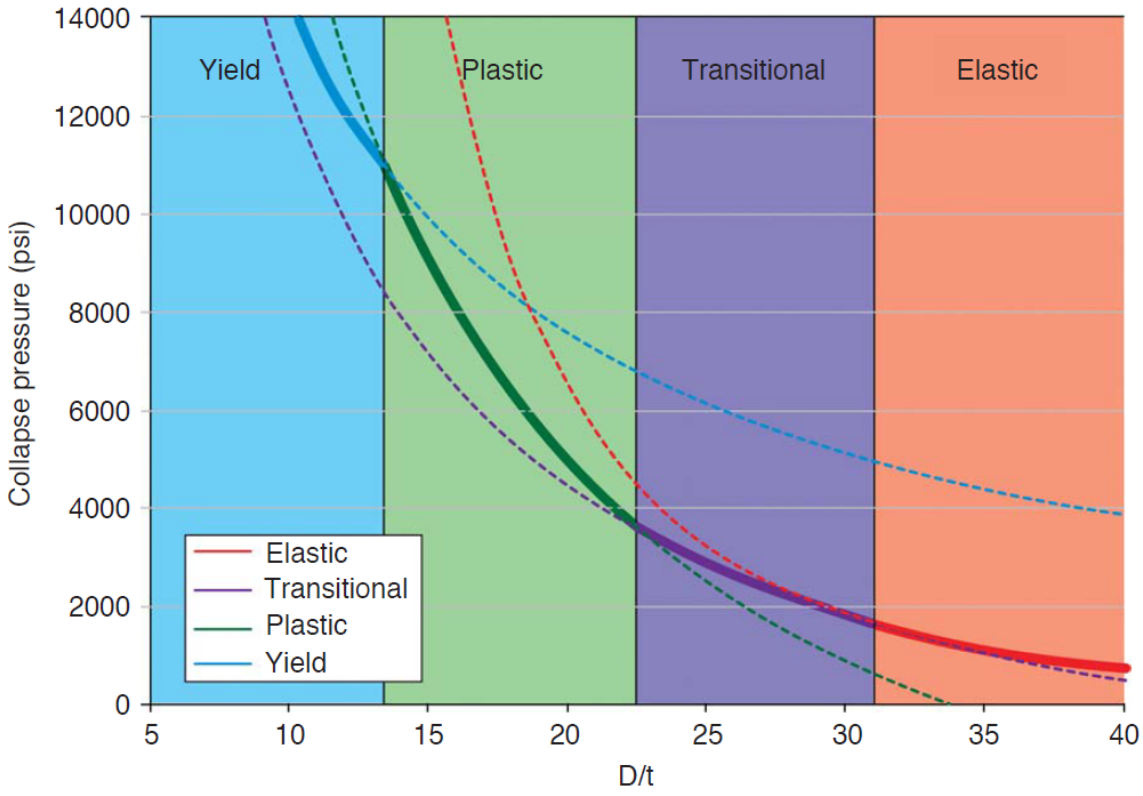

Figure 12: Collapse pressure as a function of slenderness ratio (D/t) for L80 tubing [Bellarby, 2009]

According to Adams and Payne (2001), the equations for the four collapse modes are too conservative for slenderness ratios of 21-24, but for ratios between 11-15 the risk is higher. To unify and modernize these formulas, a revision has been done (Payne, 2001). The effects of ovality, eccentricity and residual stress are directly included in the revised formulas.

Table 3: Collapse modes [API 5C3, 1999]

Grade (ksi)	Elastic Collapse (D/t)	Transitional Collapse (D/t)	Plastic Collapse (D/t)	Yield Collapse (D/t)
40	>42.64	27.01–42.64	16.40–27.01	<16.40
55	>37.21	25.01–37.21	14.81–25.01	<14.81
80	>31.02	22.47–31.02	13.38–22.47	<13.38
90	>29.18	21.69–29.18	13.01–21.69	<13.01
95	>28.36	21.33–28.36	12.85–21.33	<12.85
110	>26.22	20.41–26.22	12.44–20.41	<12.44
125	>24.46	19.63–24.46	12.11–19.63	<12.11
140	>22.98	18.97–22.98	11.84–18.97	<11.84
155	>21.70	18.37–21.70	11.59–18.37	<11.59

Table 4: Transitional collapse factors [API 5C3, 1999]

Grade (ksi)	F	G
40	2.063	0.0325
55	1.989	0.036
80	1.998	0.0434
90	2.017	0.0466
95	2.029	0.0482
110	2.053	0.0515
125	2.106	0.0582
140	2.146	0.0632
155	2.188	0.0683

Table 5: Plastic collapse factors [API 5C3, 1999]

Grade (ksi)	A	B	C
40	2.95	0.0465	754
55	2.991	0.0541	1206
80	3.071	0.0667	1955
90	3.106	0.0718	2254
95	3.124	0.0743	2404
110	3.181	0.0819	2852
125	3.239	0.0895	3301
140	3.297	0.0971	3751
155	3.356	0.1047	4204

4 Ekofisk Field and Data Gathering

The Greater Ekofisk Area is located in the southern region of the Norwegian Sea, about 300 kilometres southwest for Stavanger. It consists of the fields Ekofisk, Eldfisk, Embla and Tor, which are all operated by ConocoPhillips and included in the same production license PL 018. The license is situated in block 2/4 on the Norwegian Continental Shelf (NCS) [ConocoPhillips B].

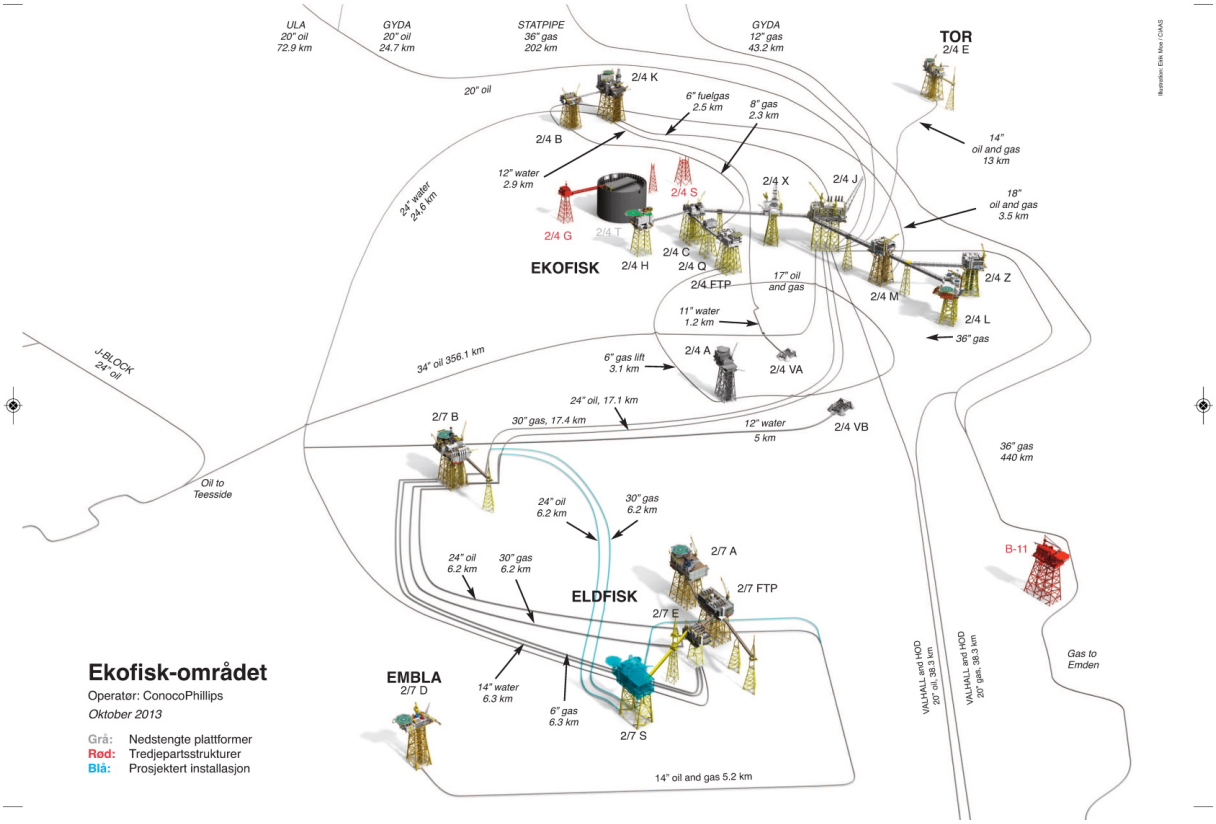

Figure 13: The Greater Ekofisk Area [ConocoPhillips A]

Phillips Petroleum Company first discovered the Ekofisk field in 1969, and the first drop of hydrocarbon was produced by June 19th 1971 [ConocoPhillips B]. The reservoir is located 3000 meters beneath the seabed and consists of chalk with an oil column of 300 meters. The Ekofisk field produces both oil and gas, and is the largest producing field on the NCS. Its area extends over a region of 50 square kilometres (10km x 5km) [Oljefakta].

Figure 14shows the Ekofisk Complex, which comprises all the installations that are linked together by pedestrian bridges. Per 2014, this includes 9 platforms in an area with a water depth of approximately 70 to 80 meters. Since the development started in the early 1970's, the complex has served as a junction-centre for the production of the Ekofisk Area [ConocoPhillips C].

Figure 14: The Ekofisk Complex. [ConocoPhillips A]

Due to pressure depletion in the reservoir as a consequence following production, subsidence of the seabed started to occur. Already in 1985, one had to take measures in order to secure the platforms from sinking further. In 1987, all of the platforms had to be jacked up by 6 meters and a wall was built to protect the oil tank.

Water injection was introduced in 1987, in the desire to increase the recovery rate. The platform EKO Kilo had the mission to inject water into the reservoir to maintain the pressure. Eventually the rate of subsidence declined [ConocoPhillips B].

4.1 WellView

WellView is a database that is a part of an integrated well lifecycle analysis and visualization solution. It is a complete corporate well file. From well planning to abandonment, WellView tracks all changes and operations throughout the well's lifecycle [Peloton, 2015]. From this database one can track all the jobs and operations a well have been exposed to in its life, like well intervention, sidetracking and plug and abandonment activities. If wear is detected, WellView can help to track down which operations have been performed through time.

4.2 Tenaris

Among others, Tenaris deals with tubings that are pulled from holes offshore and transported to onshore. Tenaris has one office located in Tananger next to the main COPNO base. Specific portions of the tubing can be ordered into land for a more accurate investigation. It is important to know in which location the tubing have been at downhole, in order to know how much bending it has been subjected to. Tubings exposed to severe bending may have been subjected to very high side forces exerted from well intervention equipment, such as coiled tubing for example.

The luxury of having Tenaris right next to the office is the possibility to examine the pulled tubings physically and visually. After the tubings are pulled and examined on the base, some of it is forwarded to another location to be cleaned and internally scanned [Rohde, 2015]. The scanning reveals any damage that exists on the inside of the tubing. The essential part of this information is to figure out whether the wear is evenly distributed, where the thickness is reduced uniformly across the whole circumference, or if the wear is concentrated in one place to form a crescent-shaped pattern. Figure 15 is illustrating a tubing with a crescent-shaped wear scar.

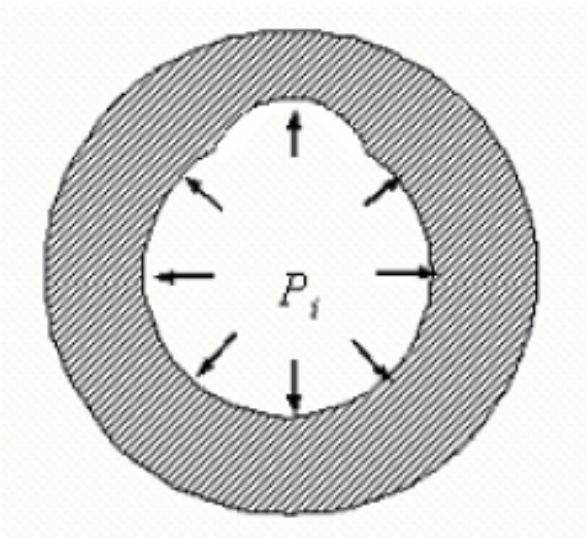

Figure 15: Crescent-shaped wear on tubing [Wu, 2005]

4.3 "Well X"

Tenaris pulled a tubing from a well, hereafter referred to as "Well X", which was available for viewing and examination on the ConocoPhillips base in Tananger. Well X have had a coiled tubing operation of 15 runs [Toftkaer, 2015], Figure 16clearly shows the wear inside the tubing was concentrated in a groove. In this well, as the pictures shows, the coiled tubing has most likely worn through a layer of scale that have deposited on the tubing wall. The depth of the indentation, if requested, can later be determined after washing and lacer scanning the tube [Rohde, 2015]

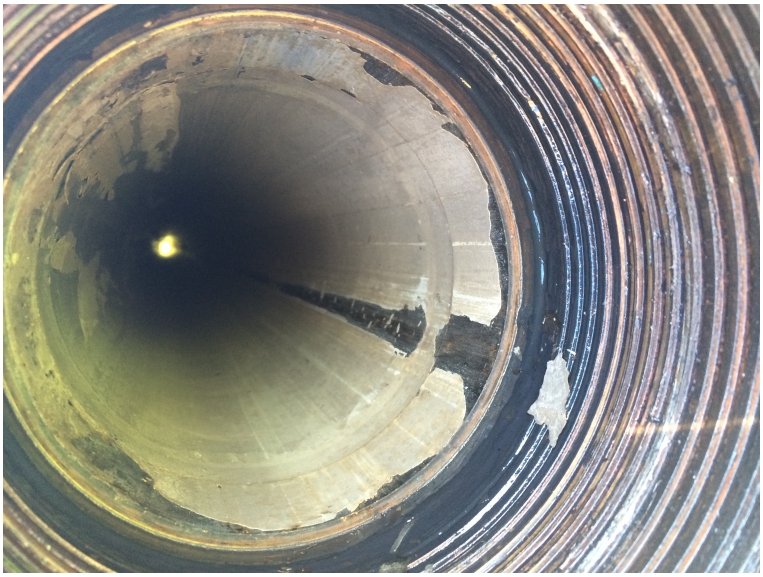

Figure 16: Pulled tubing from "Well X" [Private picture taken at Tenaris]

4.4 "Well Y"

The well referred to as "Well Y" is located on the southeastern part of the field as an upper horizontal Ekofisk Formation producer. The well is in an area with a few water injection wells, which supports the reservoir pressure. "Well Y" is the main wellbore and was drilled and completed in 2007-2008 as a part of 30 wells [Chow, 2015].

The wellbore is deviated with a maximum dogleg severity of 4 degrees per 100ft at a depth of 2588 ft. MD. There were performed two coiled tubing operations in the time period from 2009 to 2010 with a total of 16 runs. 13 of those runs were to perform straddle stimulations with acid. A multi-fingered caliper tool, which is a tool that measures the internal diameter of the tubing, was run across the full length of the well. The purpose of the tool was to assess the condition of the production tubing with respect to mechanical and corrosive damages following the acid stimulation. The tool identified a grooved wall penetration, were the maximum indentation depth was 47% of the wall thickness at 1626 ft. There have been speculations within ConocoPhillips that these two coiled tubing operations may have contributed to cause the wear [COPNO, 2011]. For simplicity, the simulations in this thesis use the dimensions of the coiled tubing to build the crescent-wear geometry in the tubing.

Table 6: Production Tubing Specifications [Rohde, 2015]

PIPE BODY DATA					
GEOMETRY					
Nominal OD	**5.500** in.	Nominal Weight	**17.00** lbs/ft	Standard Drift Diameter	**4.767** in.
Nominal ID	**4.892** in.	Wall Thickness	**0.304** in.	Special Drift Diameter	**N/A**
Plain End Weight	**16.89** lbs/ft				
PERFORMANCE					
Body Yield Strength	**397** x 1000 lbs	Internal Yield	**7740** psi	SMYS	**80000** psi
Collapse	**6290** psi				

According to the report from COPNO (2010), the inspection indicated that the 5,5" tubing appeared to be in good condition with respect corrosion damage. Some exceptions are three pup joints were the caliper tool detected general corrosion on a range from 23-27% of the wall thickness.

4.4.1 Maximum recorded wall penetrations

The data from the caliper tool indicates that some areas have more wear than others, especially in the first dogleg were the maximum dogleg severity is located. Figure 17 correlates the damage in percent wall loss to the borehole profile. Clearly, the damage is most severe in the deviated hole section .

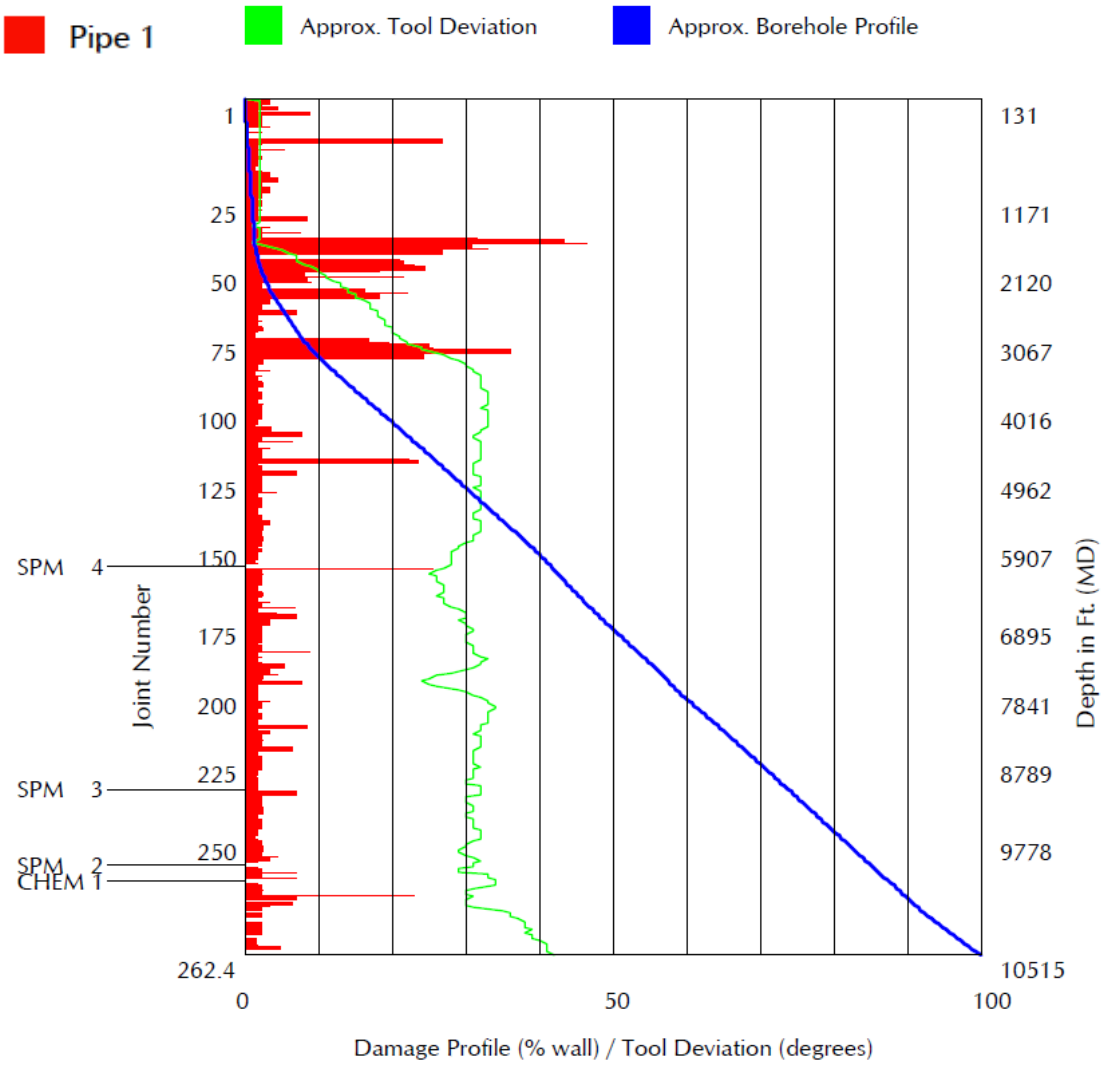

Figure 17: Correlation of recorded damage to borehole profile [COPNO, 2010]

Table 7 shows where in the wellbore there has been detected most severe wear in the tubing. The maximum wear depth appears to be 47% of tubing wall thickness at joint number 26 at 1626 ft.

Table 7: Maximum recorded wall penetrations with multi-finger caliper log

Apparent Wear		
Joint no.	**Wear %**	**Measured depth**
34	32%	1550 ft.
35	43%	1587 ft.
36	47%	1626 ft.
38	33%	1701 ft.
75	36%	3068 ft.

The multi-fingered caliper data for "Well Y" are visualized in Figure 18. The green colour illustrates the wear scar, and the wear seems to rotate as it successes down the well. The penetration depth is according to COPNO (2012), defined as a measure of the value read by one finger, expressed as a penetration fraction from the inner to the outer surface of the pipe. There is, thus, one penetration value for each finger. "Maximum penetration" is a single number for each depth.

Metal loss is defined as the fraction of metal at a cross section of the pipe that has been "lost", as determined from the log. That is, for a mechanical caliper, only considering the inner surface. "Maximum metal loss" within a joint is the metal loss at that depth, within that joint of pipe, where the most metal has been lost [COPNO, 2012].

SEAWELL

Multifinger Caliper 3D Log Plot

Company : **ConocoPhillips**
Field : **Ekofisk**
Well : [redacted]
Date : **September 4, 2010**

Description : ***Detail of Caliper Recordings Across Apparent Wear Recorded in 5.5" Tubing.***

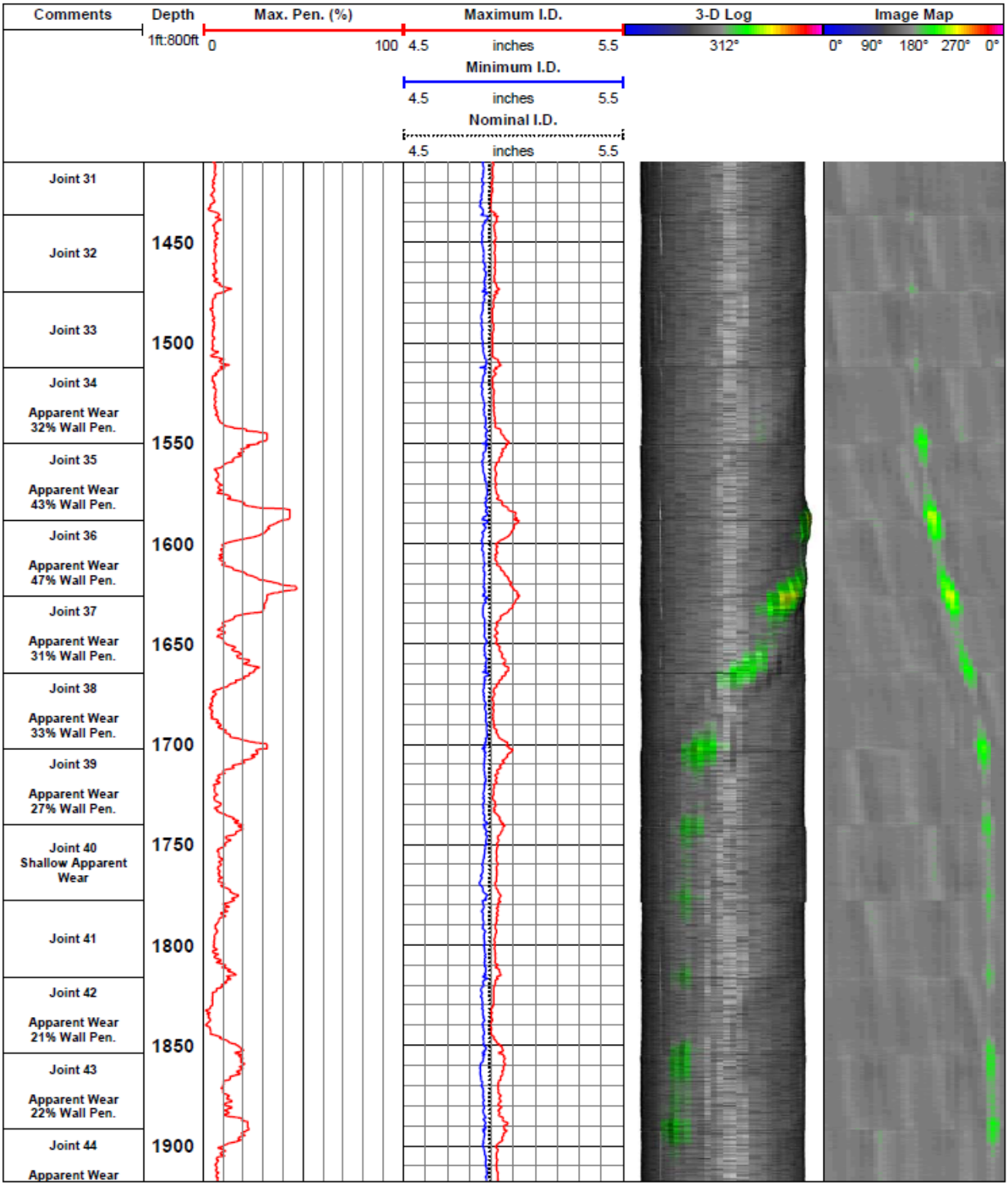

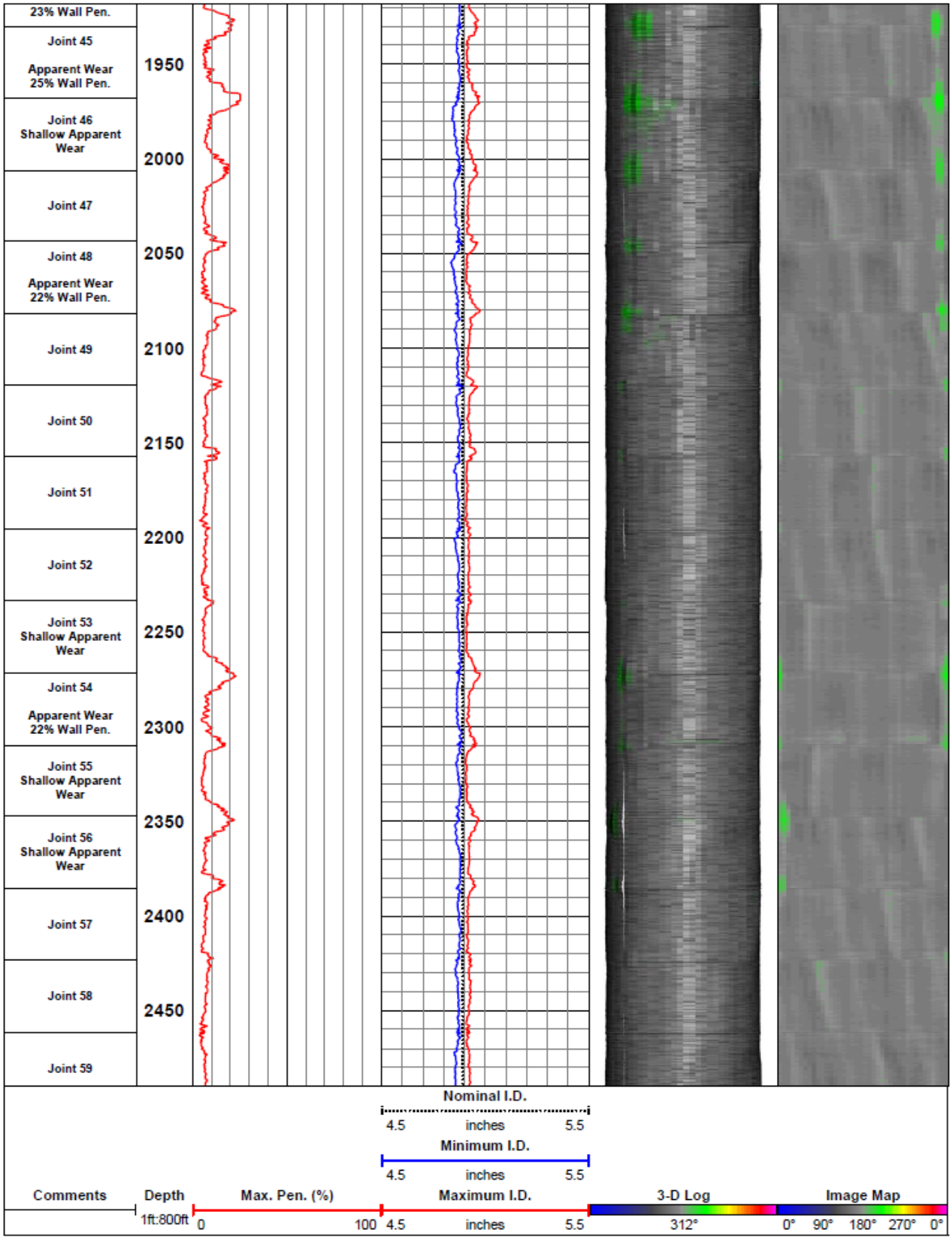

Figure 18: Interpreted multi-fingered caliper data [COPNO, 2010]

5 Finite Element Method modelling

The simulation in this thesis is specifically based on the input data obtained from Well Y. The purpose of the simulation is to find a model that predicts the safe/failure zone for the operating internal pressure for the well, which has been subjected for extensive well intervention. The model simulates the portion of the tubing in Well Y, where the multi-fingered caliper-logging tool detected the maximum penetration. The content of this chapter is based on part of the curriculum from the subject "Introduction to Finite Element Methods (FEM) (ASEN 5007)" at the University of Colorado at boulder [Felippa, 2014A and 2014B].

5.1 Introduction to FEM

According to Felippa (2014 A), the term "Mathematical Modeling" is used when converting from an actual physical system to a mathematical model of the system. He also defines a model as follows:

"A model is a symbolic device built to simulate and predict aspects of behaviour of a system."

Because a mathematical model only predicts aspects of a system, and not the whole system, the process is called idealization. The results obtained from the numerical or analytical solution is basically a re-interpretation of the chosen aspects. Engineering systems can be very complex, and in order to simulate a system it needs to be simplified to bring the complexity down to a manageable level. This is obtained by filtering out physical details that are not relevant to the design and analytical process; it is called "Complexity Control".

5.2 Discretization

Even though mathematical modeling is a simplification of a reality, it does not necessarily mean that the models of the physical systems are easy to solve. The models with an infinite number of "degrees of freedom" (DOF) often include coupled

partial differential equations in two dimensions, space and time, that are subjected to both boundary and interface conditions.

In order to do a numerical simulation, one has to reduce the infinite number of DOF to a finite number. The reduction process is called *discretization* and the result is a discrete model.

5.3 Approximation and Sources of Error

Figure 19 illustrates a simplified model of the physical simulation process. Error in solutions occurs frequently during simulations. Every step in the simulation process introduces a new source of error. The modelling errors are not the most severe ones, but to validate a model it requires comparison with actual experimental results. This is expensive and one actually also need access to experimental results.

There can also be errors in the discretization, because solutions computed from the discrete model is basically only an approximation of the exact solution of the mathematical model.

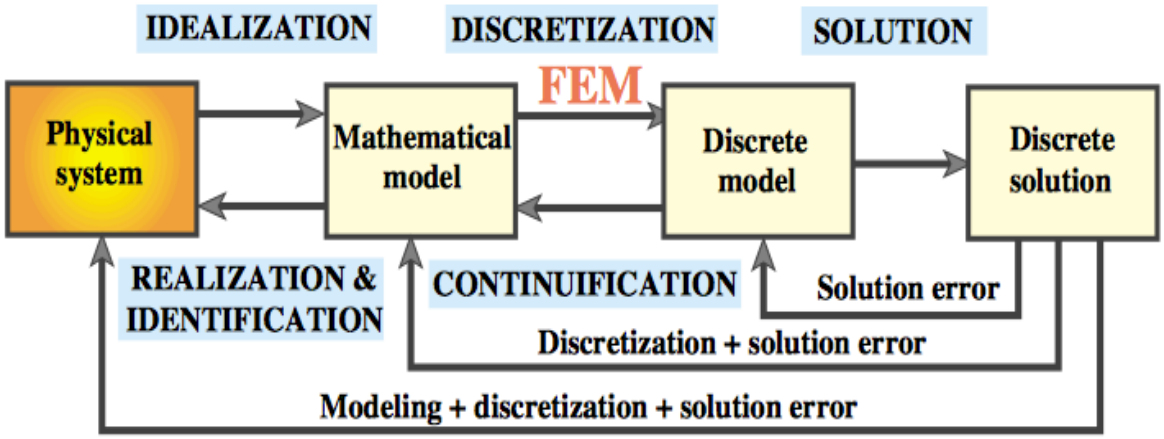

Figure 19: Simplified model of the physical simulation process [Felippa, 2014A]

5.4 Finite Element Method

In structure mechanics, the most used and dominating discretization technique is the finite element method, also referred to as FEM. One can interpret the FEM from either a mathematical or physical point of view. In the physical FEM, the basic concept is to subdivide the mathematical model into "finite elements". These elements are non-overlapping and of simple geometry. In a mathematical interpretation of the FEM, it is called disjoint support.

The finite number of degrees of freedom expresses the response of each element. At a set of nodal points, the response is characterized as the value of an unknown function. Assembling or connecting all the finite elements creates a discrete model. It is from the discrete model that the mathematical model is approximated from.

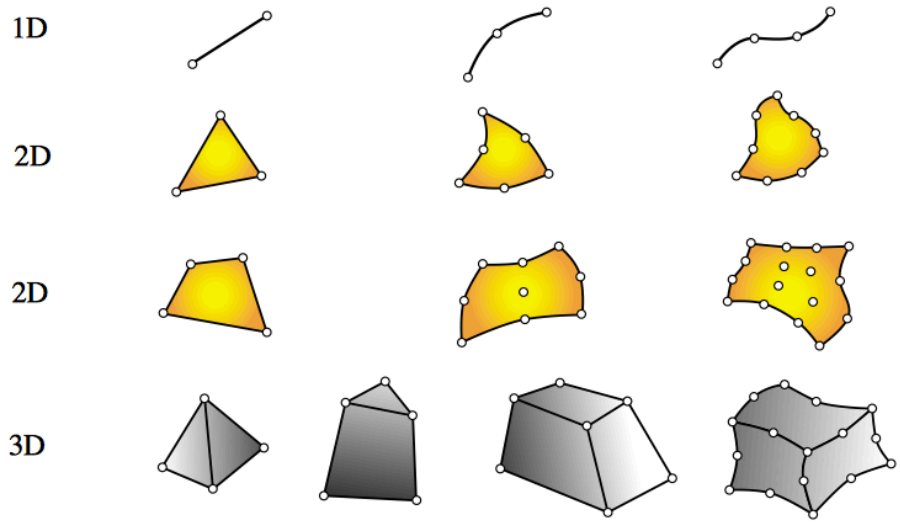

Figure 20: Simple geometries in 1D, 2D and 3D [Felippa, 2014A]

5.4.1 Element Nodes

As seen on the Figure 20, the geometrical elements have so-called nodal points. These nodes both define the geometry of the element (geometric nodes) and serve as a home for degrees of freedom (connection nodes). The nodes are normally located at the corners or end points of the elements. For elements of higher dimensions or with more

complicated structures, the nodes can also be placed in the interior or on the faces. It is the position of the geometric nodes that defines the geometry of the element.

5.4.2 Degrees of Freedom

The state of the element is specified by number of element degrees of freedom. The DOFs acts as a connection between elements adjacent to each other. According to Felippa (2014A) the DOFs are defined as "*the values, and possibly derivatives, of a primary field variable at connector node points"*. How the primary variable appears in the mathematical model is the key factor. The degrees of freedom are for many mechanical elements the displacement components at the nodes, while the primary variable is the displacement field.

5.4.3 FEM Model Generation: Geometry, Material Properties and Loading

The procedure of creating a model starts with the processing step, where one builds the geometry and meshes, adding parameters as loads, material properties, problem type and possibly boundary conditions if they are present. When modeling, it is wise to keep it simple. Choose the simplest possible finite element that will do the job, and never choose complicated elements unless you know what you are dealing with. The steps of generating the models go in the order of:

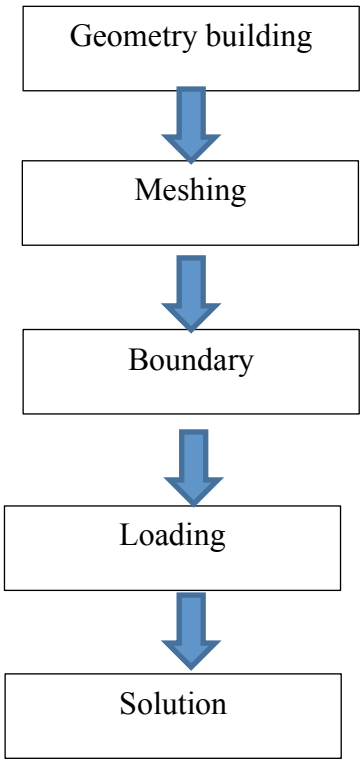

Figure 21: Structure of experimental arrangement in Abaqus

The input data used to build the models in the simulations are provided in Table 8 through Table 10.

Table 8: Input data [COPNO, 2011]

Well Data	
Well name	Well Y
Completion fluid density	8,6 ppg
DLS @ max penetration	2,9 deg.
TVD @ max penetration	1626 ft.

Table 9: Tubing Specifications [COPNO, 2011]

Production tubing L80 13Cr	
Inside radius, r_i	2,446 in.
Outside radius, r_o	2,750 in.
Wall thickness, t	0,304 in.
Material yield strength	80.000 psi
Original Burst pressure (Barlow's Equation)	7740 psi
Original Collapse pressure	6280 psi

Table 10: Coiled Tubing Specifications [COPNO, 2011]

Coiled Tubing	
OD	2,875 in.
r_O	1,4375 in.

Geometry Building

The geometrical model was built based on the tubing dimensions used in actual wells in the Ekofisk field. For the simplicity, the geometry of the grooved wear scar is assumed to have the dimensions of coiled tubing, even though it is not certain it is main cause of the wear.

For each indentation depth, the tubing with grooved wear was built manually. The geometry building takes place in a X-Y-Z coordinate system, were all the coordinates entered is relative to the origin at (0,0). In the beginning of the building process one only uses the X-Y coordinates to build the geometry; the length of the object is added in the second step. For simplicity, the tubing centre is chosen to be at the origin and the inside and outside radius positions are inserted with respect to this point. The position of the coiled tubing centre and outer radius varies for each wear depth and depends on how deep the wear scar is.

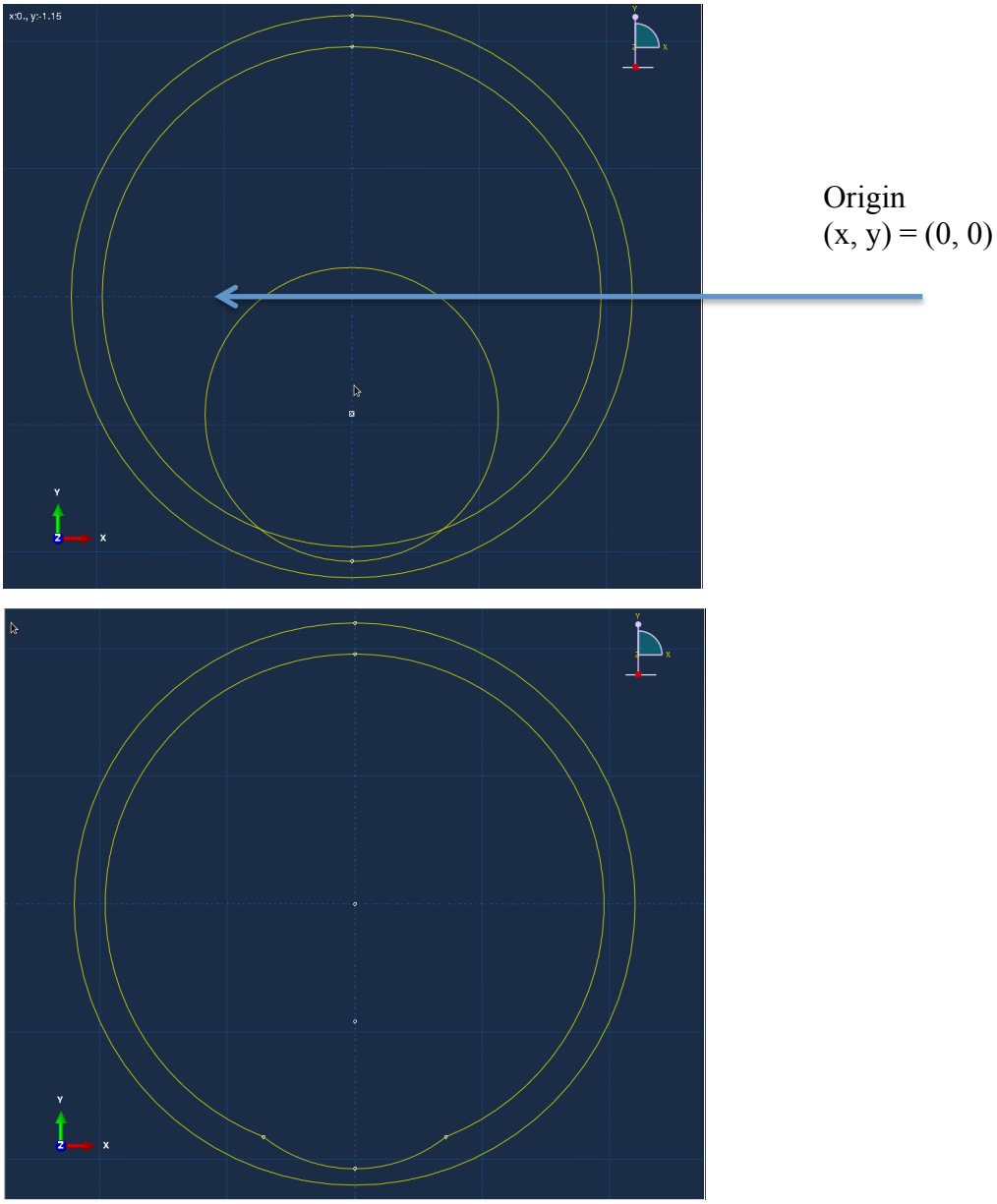

Figure 22: Geometry Building Step 1

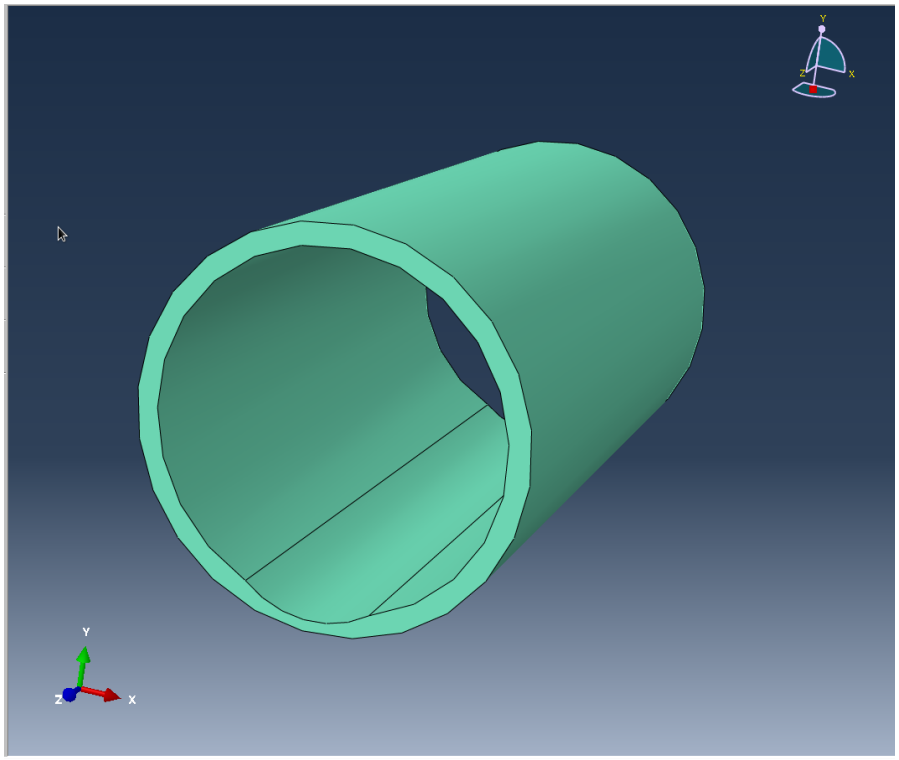

Figure 23: The geometry of tubing after being extruded.

An example of how the coordinates for the coiled tubing is calculated are shown in Appendix B.

Meshing

The principle of meshing is to use the coarsest mesh possible that will cover the dominating physical behaviour of the system, especially in the design applications. By creating a mesh of varying density minimizes the DOF's. In areas one expects the stress to be concentrated, like for example in corners or cracks, are areas of interest and importance. Only in these areas does the mesh need to be fine [Liu and Quek, 2003].

For meshing of models in this thesis, the bilinear Q8 element has been used. It has a degree of freedom of 8 and gives a good solution. Figure 24 shows the meshed model.

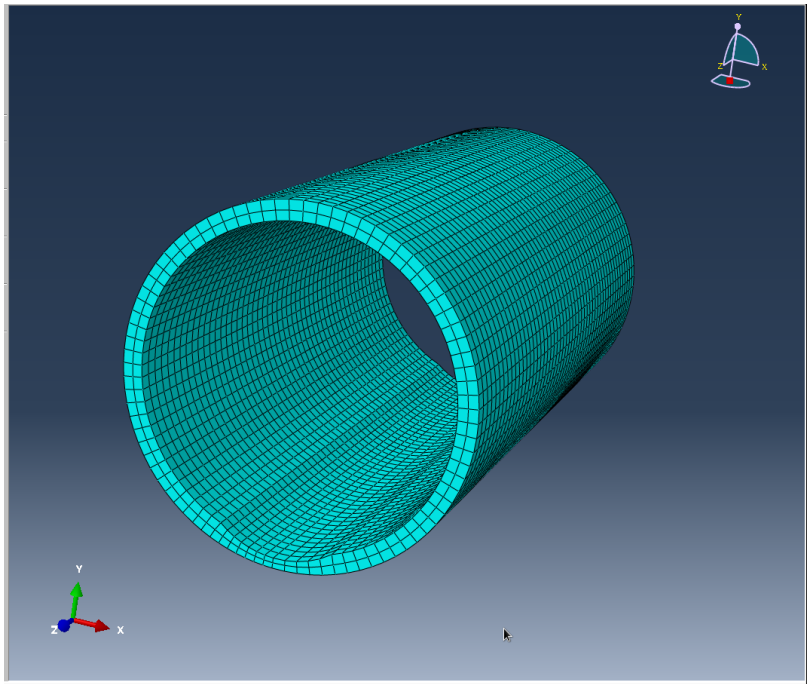

Figure 24: Meshing

Boundary Conditions

As shown on Figure 25, the boundary conditions are both free ends since only a cross-section of the tubing is being simulated and analysed.

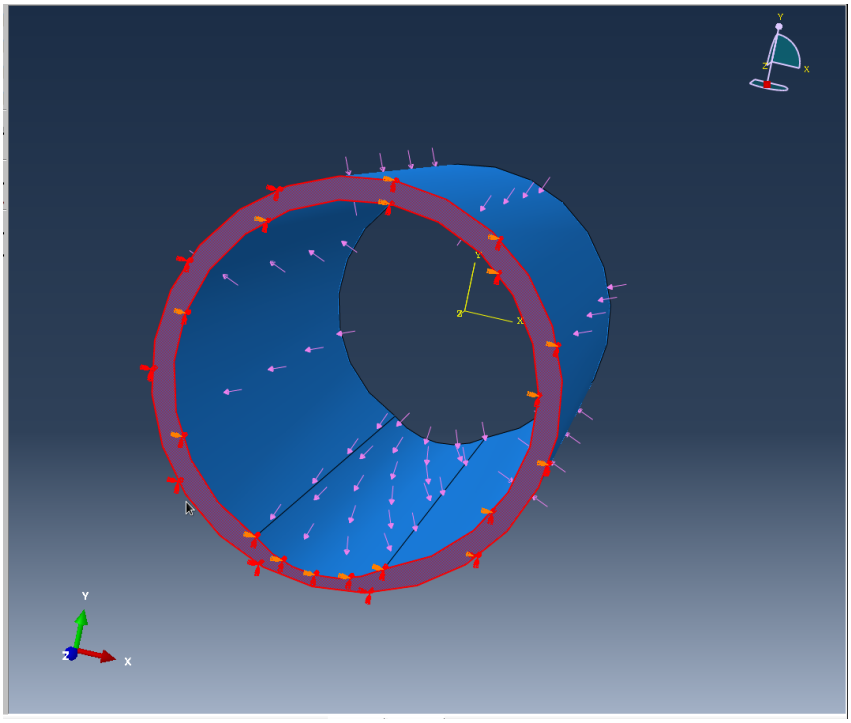

Figure 25: Boundary conditions

Loading

For each wear depth several simulations have been done. The loads applied within one single simulation are constant, but is increased or decreased between the simulations in order find a trend line. As shown on Figure 26, the internal pressure is in reality exerted from the fluids inside the well, and the external pressure is exerted from the fluids in the annulus.

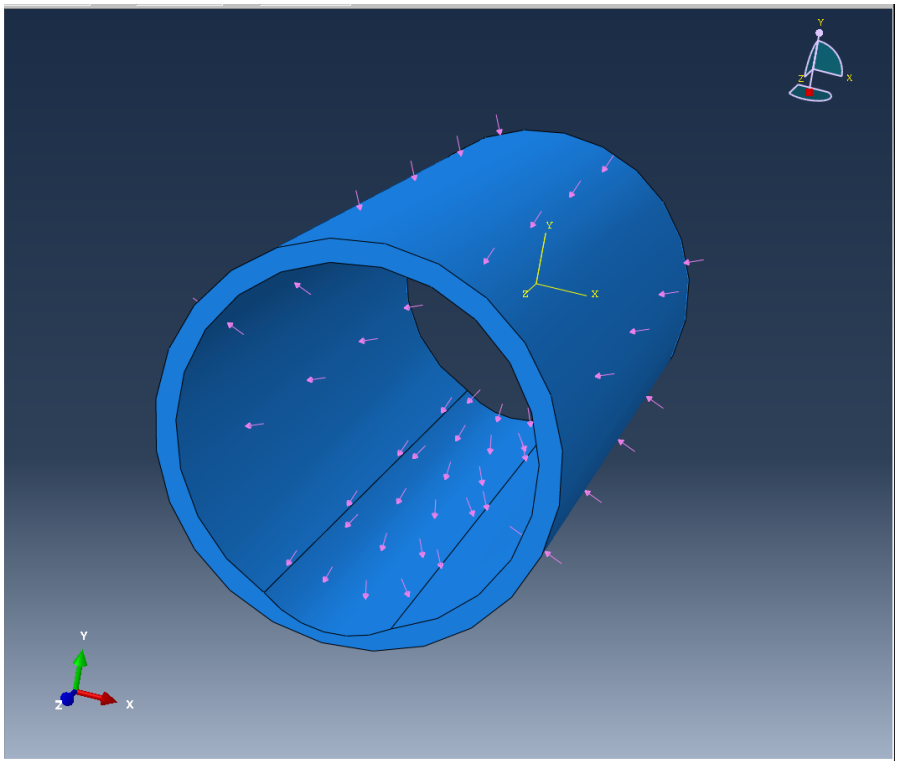

Figure 26: Internal and external loads

Material Properties

Young's modulus (E), Poisson's ratio (v) and the tubing wall thickness are the material properties. The chosen properties for the model used in this thesis are linear, elastic and isotropic are shown on Figure 27.

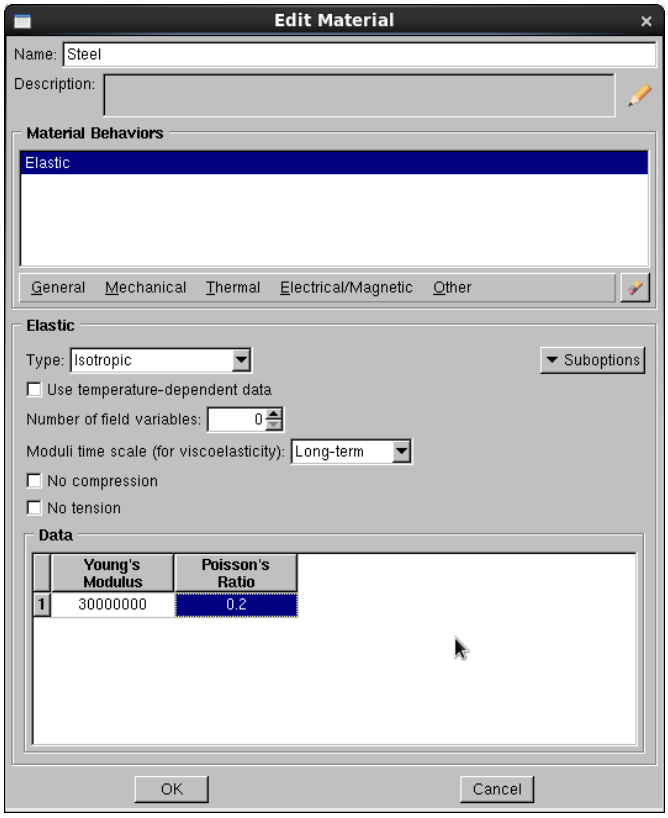

Figure 27: Material properties

6 FEM Simulation solution results and analysis

The FEM simulation is based on input data from Well Y. The field and survey data are both provided by ConocoPhillips. Based on the results from the caliper data the maximum wear depth appears to be 47% of wall thickness at a depth of 1626 ft. TVD. The tubing material is L80, the completion fluid has a density of 0,86 ppg and the fluid gradient inside the well is approximately 0,3 psi/ft. The simulations in this thesis are based on these specific well settings.

The purposes of these simulations are to study the effect of increasing wear depth on the tubing burst and collapse strength for different scenarios. It is desirable to determine the true burst and collapse pressure for the increasing local wear depths, and compare it to the standard methods of uniform wear.

6.1 Simulation Scenarios

During a lifetime of a well, it is being subjected to several different types of loading events. It is important to determine how much load the tubing can withstand before it starts to yield, considering the wear caused by equipment and tools during service and production. Three different loading scenarios are being simulated to study these problems.

For each scenario, the first model was built for a reference purpose. The base model simulates the tubing without any form of wear, with maximum internal pressure applied to see if it could withstand the calculated maximum pressure. The original burst pressure is according to ConocoPhillips [COPNO, 2011], calculated to be 7740 psi for unworn tubing by using Barlow's equation, and the original collapse pressure calculated to be 6280 psi. The internal load can in real life either be exerted by the fluids produced from the reservoir, or by injected fluids during a well intervention operation, like for example bull-heading or acid stimulation. The hydrostatic column of completion fluid in the A-annulus exerts the external load. The pressure may be increased during a gaslift operation because of the additional pressure from the pump, or also if a leak occurs in the tubing barrier.

Abaqus uses these input data to calculate the Von Mises stress, σ_{VME}, in the tubing wall. The material yield strength for L80, is $\sigma_{\mathrm{y}} = 80000\, psi$. According to the simulation results, an unworn pipe has no problem to withstand the maximum applied internal pressure without starting to yield. The Von Mises stress, σ_{VME}, in the tubing wall does not therefore exceed the material yield strength limit for burst in an unworn state, when 7740 psi is applied internally. Neither does the pipe yield when 6280 psi is applied externally in the collapse scenario.

The models were simulated with different wear depths; starting from the reference model with no wear and increasing with five percent wear for each model. An example of how the different indentation depths were calculated is illustrated in Appendix B. For each indentation depth or wear percent, several simulations were conducted with different applied constant pressure, with the intent of finding the point where the σ_{VME} exceeds the yield stress. Six simulations with different pressures where conducted on every single wear depth for all the three scenarios in order to find slope. As mentioned in chapter 5 (Geometry Building), the dimension of the wear groove is based on the dimensions of the coiled tubing.

With wear %, means the wear depth of the tool relative to the wall thickness of the tubing. The recorded maximum wear depth for Well Y was 47% of wall thickness. Therefore, an increment of 5 % in the interval of 0-50%, with an additional model for 47%, where simulated for the different scenarios.

Table 11: Calculated wear positions. The tool center relative to the tubing center is referred to as eccentricity.

Wear %	*Wear depth [in.]*	*Eccentricity [in.]*	*Indentation Depth [in.]*
0%	0	1,0085	2,4460
5%	0,0152	1,0237	2,4612
10%	0,0304	1,0389	2,4764
15%	0,0456	1,0541	2,4916
20%	0,0608	1,0693	2,5068
25%	0,0760	1,0845	2,5220
30%	0,0912	1,0997	2,5372
35%	0,1064	1,1149	2,5524
40%	0,1216	1,1301	2,5676
45%	0,1368	1,1453	2,5828
47%	0,1428	1,1514	2,5889
50%	0,1520	1,1605	2,5980

6.2 Scenario 1 – Burst

When simulating for burst scenario, the external pressure exerted from the completion fluid was calculated to be 727 psi at the point of maximum wear, and is kept unchanged throughout this scenario.

6.2.1 Investigating the application of Barlow's Equation

A test model was built to check if Barlow's method was applicable for local wear, when only a portion of the internal circumference was worn away. Local wear means that the wall thickness is only reduced in certain portions of the tubing. As mentioned in the beginning of chapter 3, Barlow does not account for the fact that only these portions have a reduced wall thickness, while the remaining part is intact. To look at this closer, one has to study and compare the tri-axial stresses in the tubing wall for

uniform- and locally worn tubing. The next figure illustrates local wear compared to uniform wear.

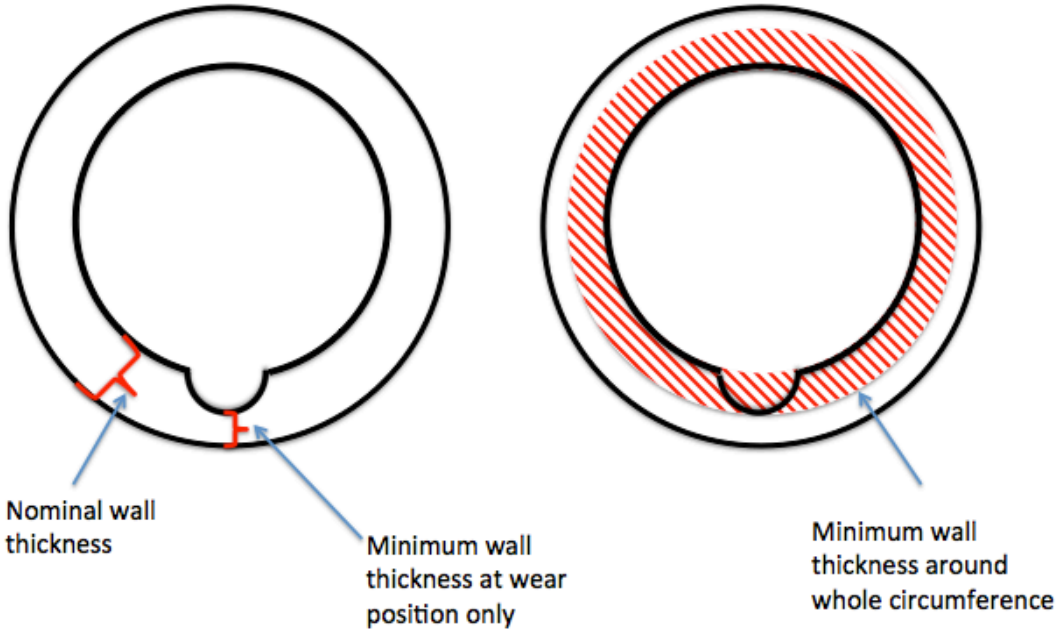

Figure 28: A) Local vs. B) Uniform wear

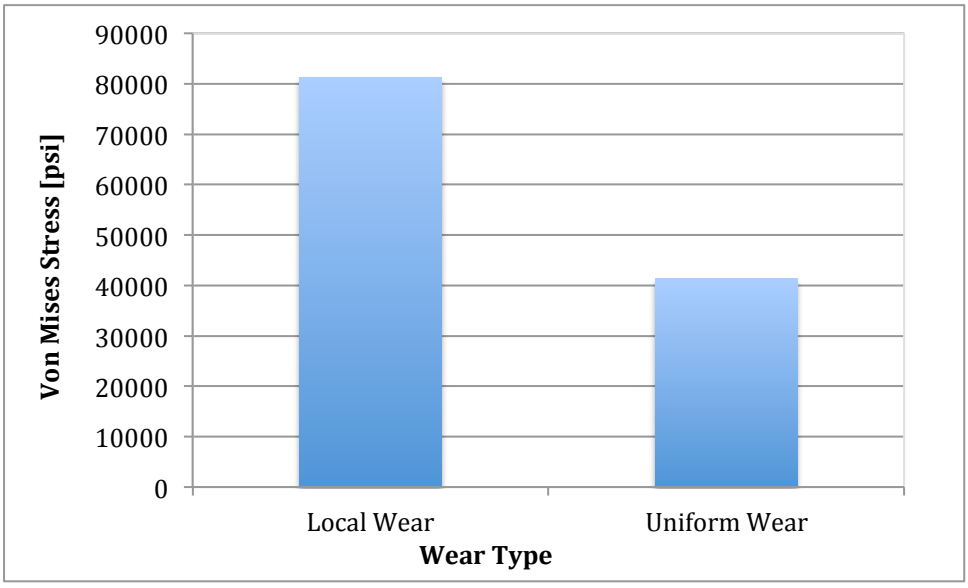

Figure 29: Maximum Von Mises Stress in the tubing wall for the same applied pressure (3200psi).

Figure 29 shows the level of maximum σ_{VME} stress in the tubing wall for the different wear types under the same pressure at 47% wear depth. When simulating the locally worn model, the maximum σ_{VME} was equal to 81350 psi, and the stress in the tubing wall was concentrated at the wear groove. By applying Barlow's method and using minimum wall thickness for the whole circumference, the simulation result shows a maximum σ_{VME} value being 41370 psi. In the uniform wall thickness the stress is also equally distributed along the circumference of tubing. Whereas, the stress concentration in the local wear part shows a higher value and more is prone for failure. Figure 30 a & b illustrate the stress distribution on local wear and uniform thickness tubing respectively.

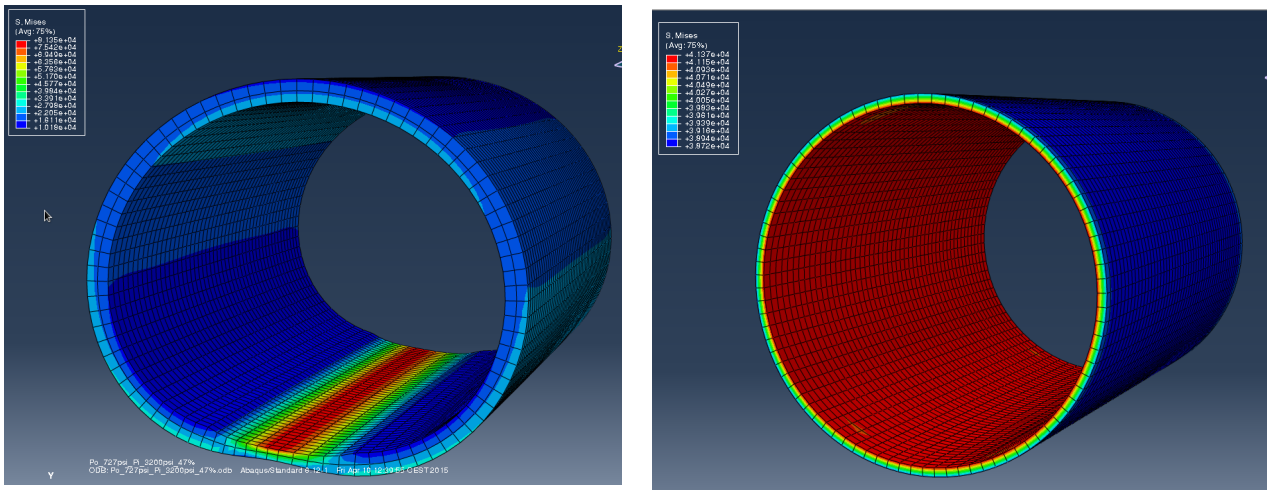

Figure 30: A) Local wear B) Uniform Wear

Clearly, the stress distribution in Figure 30 A) and B) is very dissimilar. Therefore, the assumption of uniform wear for locally damaged tube using Barlow's equation leads to incorrect prediction of burst pressure. This thesis simulation result claims that Barlow's equation cannot be used to calculate the de-rated burst pressure for locally worn thick/thin walled tubing.

On the other hand, for an actual uniform wear, and for a thickness-to-inside radius-ratio of $t < {}^{1}/_{10}\, r_i$ (thin-walled cylinder), Barlow accurately predicts the de-rated burst pressure and matches the simulation results. However, for thick walled, the model derived in section § 3,31 (Eq. 3.29 & 3.30) is believed to be better than Barlow's equation.

6.2.2 Results From Abaqus Simulation – Burst

The next three figures show the stress distribution in the tubing wall, where the red colour indicates the maximum stress the wall is subjected to for the given applied pressure, and the blue colour indicates minimum stress.

When simulating the problems, internal pressure is applied to the inside of the tubing. The results of the simulations tell if the value of the Von Mises stress, σ_{VME}, in the tubing wall has exceeded the material yield strength. If σ_{VME} is above $\sigma_y = 80\,000\,psi$, one has to proceed the next simulation with applying a lower internal pressure, until the value of σ_{VME} is less than the value of σ_Y. The opposite procedure is implemented if σ_{VME} turns out to be below σ_y at first. The reason is to determine where the σ_{VME} intersects with σ_y.

Reference model – 0% wear depth

Figure 31 shows the reference model with the applied internal pressure of 9700 psi, which is excluded any safety factor. From the simulated results, the Von Mises Stress in the wall is equal to $\sigma_{VME} = 80200psi$, and have just exceed the material yield strength. For 0% wear, the σ_{VME} exceeds the material yield strength, $\sigma_y = 80\,000\,psi$, somewhere between 9600 and 9700 psi internal pressure. The red cells in Table 12 indicate at which pressure the material yield-strength is exceeded.

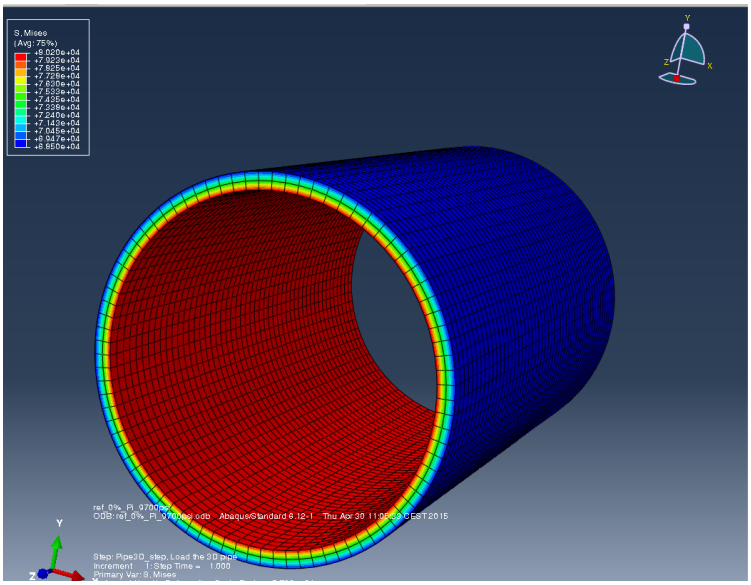

Figure 31: Simulated reference model for burst, without any form of wear

Table 12: Simulated burst pressure results for model with 0% wear

Internal Pressure [psi]	Reference 0% wear Von Mises stress [psi]
9900	82000,00
9800	81100,00
9700	80200,00
9600	79310,00
9500	78410,00
9400	77510,00

Yield point 8000 psi

Tubing model with 25% wear depth

For this model, the tubing started to yield to an internal pressure of only 4927 psi. Figure 32 shows the tubing under an internal loading of 5000psi. Compared to the reference model, this was a significant decrease of approximately 4700 psi in pressure limit, which means almost 50% reduction in burst resistance. Table 13 shows the data for simulation of this model.

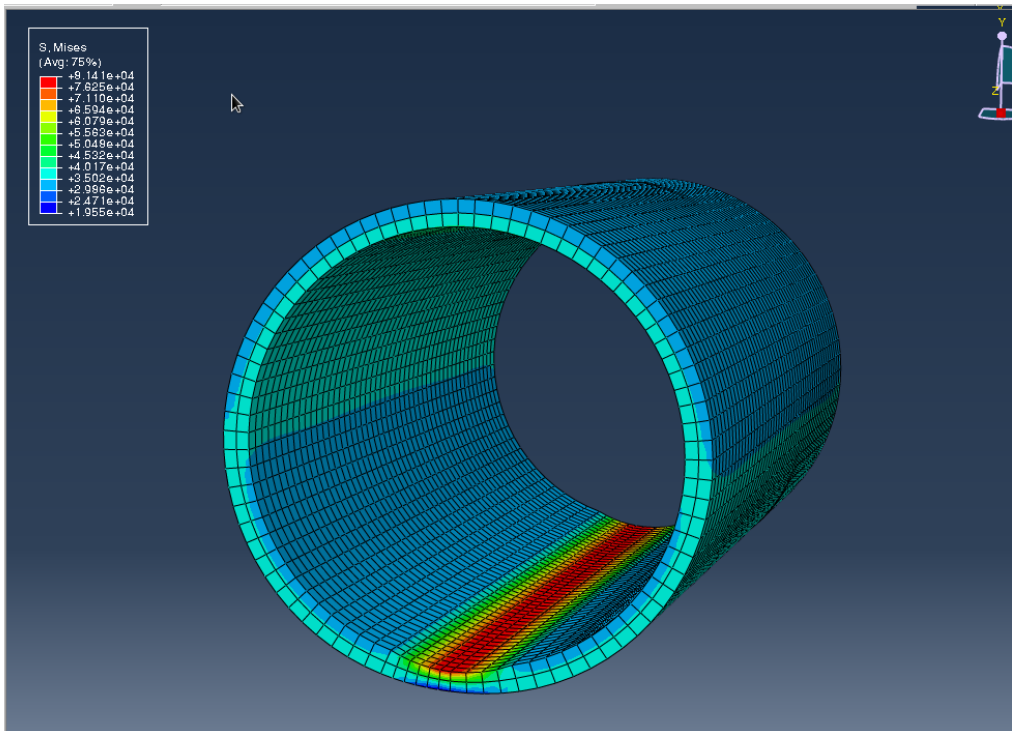

Figure 32: Simulated burst model with 25% wear

Table 13: Simulated burst pressure results for model with 25% wear

Internal Pressure [psi]	25% wear Von Mises stress [psi]
5200	85230,00
5100	83320,00
5000	81410,00
4900	79490,00
4800	77580,00
4700	75670,00

Tubing model with 47% wear depth

The recorded maximum penetration from the multi-fingered caliper log that was conducted showed a grooved wear scar of 47% of the wall thickness. This was simulated in order to determine the true burst strength of the tubing after it has been highly worn, which is based on the actual case of Well Y.

The result from the simulation shows the internal load to be equal to 3159 psi to onset the yielding of the tubing material (see data in Table 14). This means a reduction of approximately 67% of the burst strength from the reference model with no wear. The tubing was considerably deformed to an oval shape.

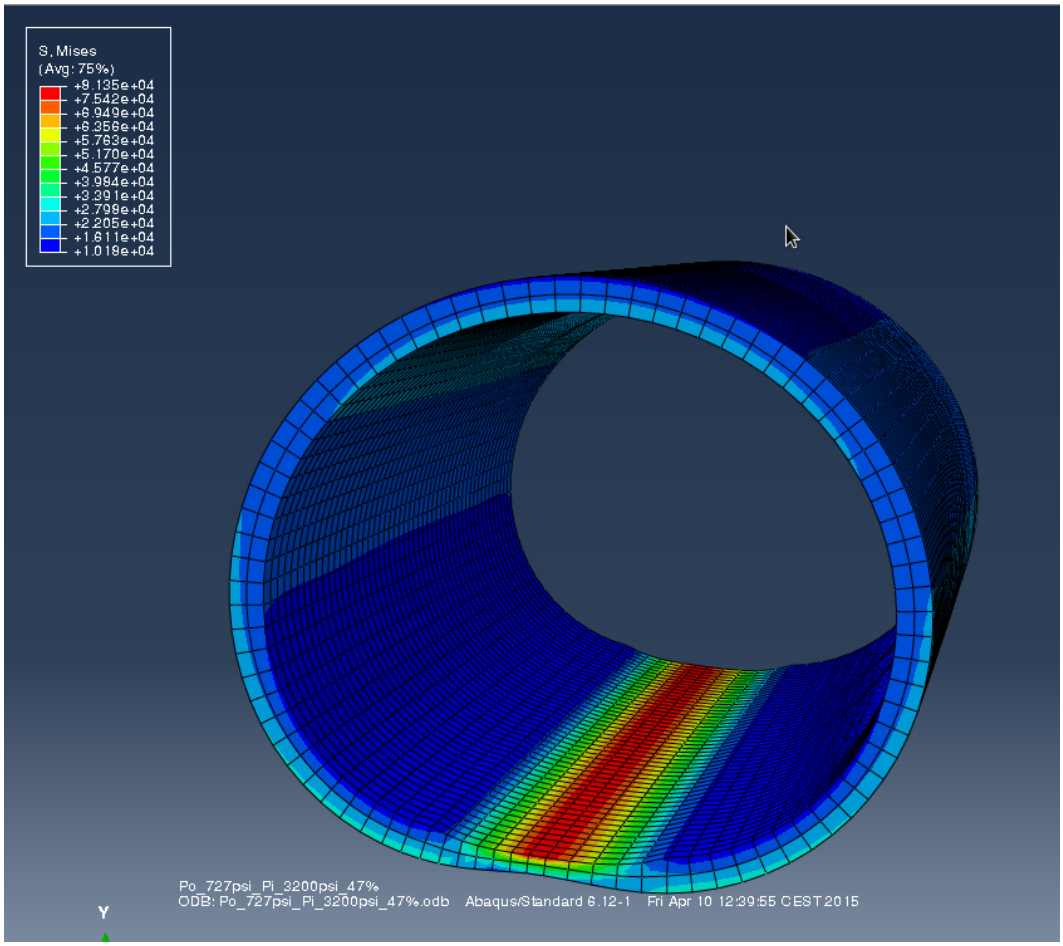

Figure 33: Simulated burst model with 47% wear

Table 14: Simulated burst pressure results for model with 47% wear

Internal Pressure [psi]	47% wear Von Mises stress [psi]
3400	87950,00
3300	84650,00
3200	81350,00
3100	78050,00
3000	74750,00
2900	71450,00

Final result – Burst

The pressure or load, of which the Von Mises stress exceeds the material yield strength, decreases with increasing wear depth, as illustrated in Figure 34. All of the slopes seems to be linear, but not necessary parallel to each other.

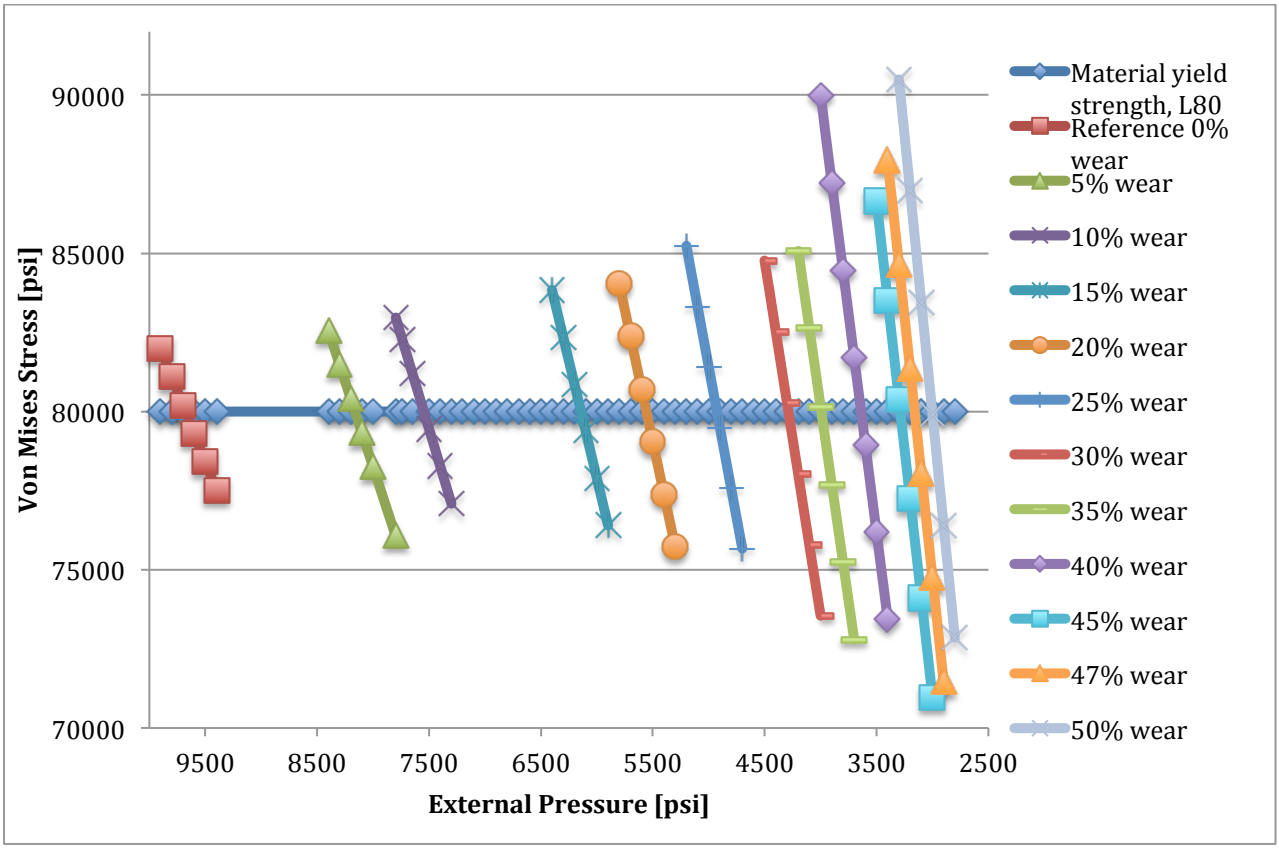

Figure 34: Burst pressure limit as a function of increasing tubing wear

By the implementation of linear interpolation it is desired to determine the pressure of which where σ_{VME} and σ_Y intersects each other. The resulting pressures from linear interpolation are those with which the material starts to yield, for the given wear percent. From the results in Table 15, one can generate a graph for the true burst pressure, following increasing wear. The equation for linear interpolation is given as [Wikipedia D]:

$$y = y_0 + (y_1 - y_0) * \frac{x - x_0}{x_1 - x_0} \qquad (6.1)$$

Table 15: Results from linear interpolation for burst – The pressure at intersection between $\boldsymbol{\sigma_{VME}}$ and $\boldsymbol{\sigma_y}$

Linear Interpolation	
Wear %	**Pressure [psi]**
0,00 %	9677,53
5,00 %	8162,04
10,00 %	7546,61
15,00 %	6141,89
20,00 %	5557,23
25,00 %	4926,56
30,00 %	4288,00
35,00 %	3993,50
40,00 %	3638,04
45,00 %	3287,58
47,00 %	3159,09
50,00 %	3002,27

The plot in Figure 35 shows the safe and failure zones for operating internal pressure, regardless of operation type. The area under the curve represents the safe operational zone for internal pressure. According to the simulations, exceeding this limit for a given wear grade (area above the curve) will lead the tubing to start yielding.

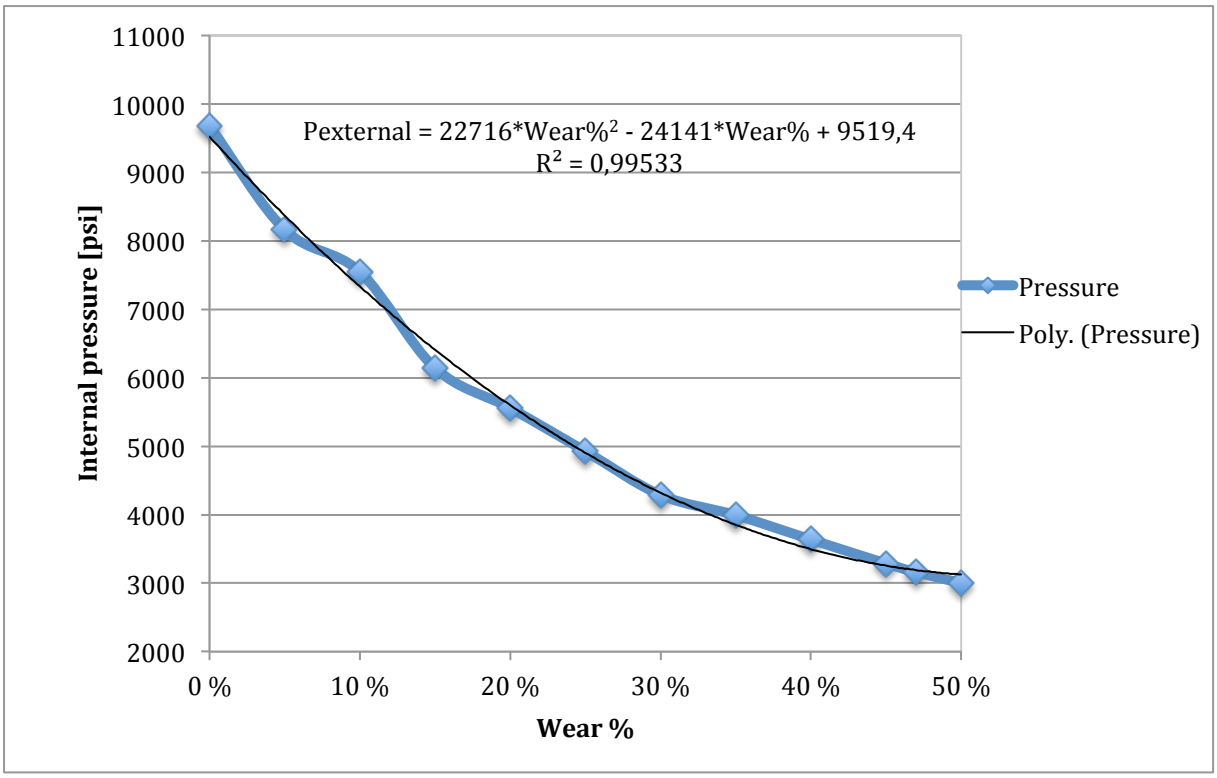

Figure 35: Safe/failure zone for operating internal pressure. "True burst" without any safety factor.

A simulation-based model for de-ration of burst pressure was generated from the curve in Figure 35:

$$P_{external} = 22716 * Wear\%^2 - 24141 * Wear\% + 9519{,}4 \qquad (6.2)$$

The value of the coefficient of determination, $R^2 = 0{,}99533$, tells how well the simulated data fits a statistical model. By implementing this model, the following blue curve is generated in Figure 36. A design factor of 0,8 was applied to the simulation-based model (red curve), in order to match Barlow's model for burst pressure for an unworn tubing. Barlow's slope (green curve) was calculated by using Eq. (3.32).

When comparing Barlow's method for uniform wear to the simulation-based model for local wear, there is a significant difference. Barlow's de-rating curve is linear, while the model is non-linear. The generated model seems to have a much narrower safe operational window when the design factor is considered. At the start of the project, Barlow's equation was thought of as too conservative to use for local wear. According to the results from the simulation, the opposite seems to be applicable. As it turns out, Barlow allows the safe operating window to be greater than the simulations, rather than too conservative.

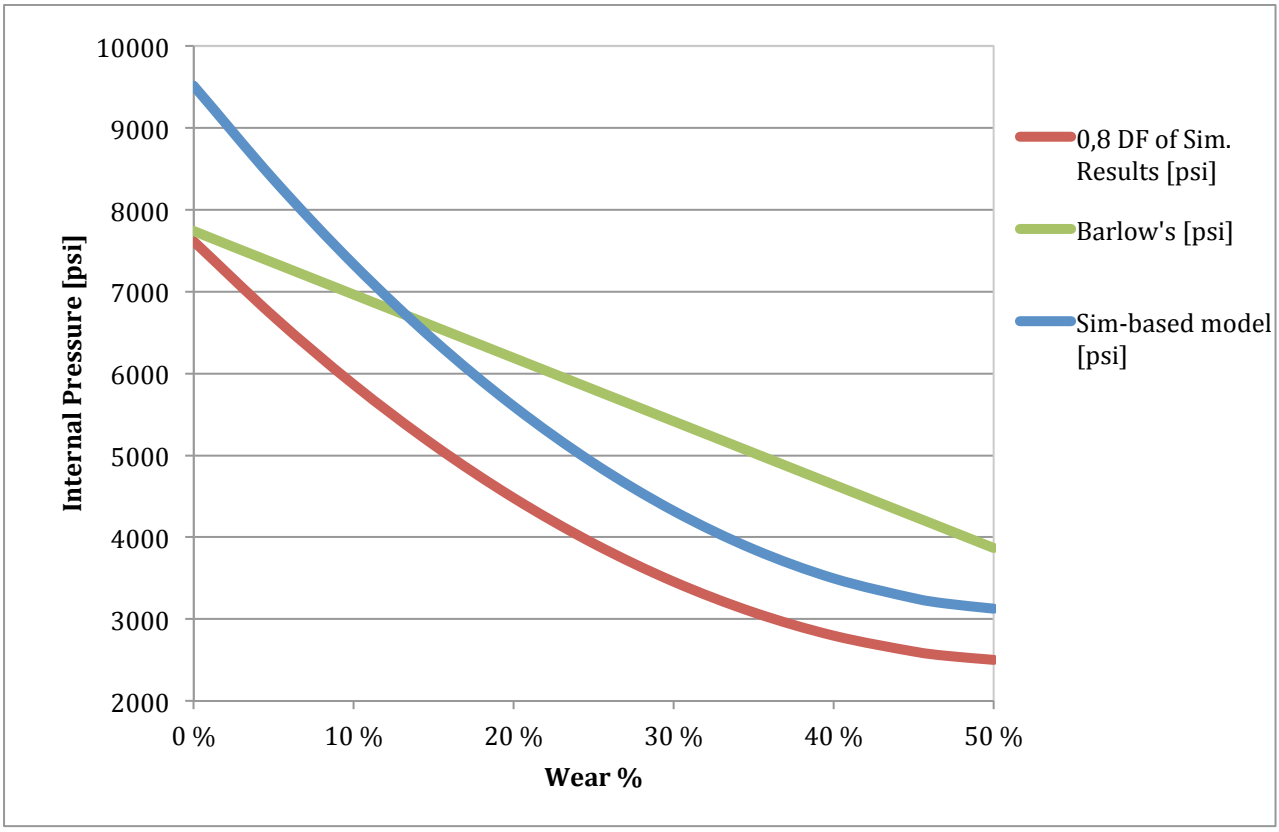

Figure 36: Simulation-based model, one curve with and one curve without design factor, compared to Barlow's model.

Table 16: Summary table for the data in Figure 36

Wear %	Simulated Results [psi]	Simulation-based model [psi]	0,8 DF of Simulation-based model [psi]	Barlow's [psi]
0 %	9677,5	9519,4	7615,5	7738,2
5 %	8162,0	8369,1	6695,3	7351,3
10 %	7546,6	7332,5	5866,0	6964,4
15 %	6141,9	6409,4	5127,5	6577,5
20 %	5557,2	5599,8	4479,9	6190,5
25 %	4926,6	4903,9	3923,1	5803,6
30 %	4288,0	4321,5	3457,2	5416,7
35 %	3993,5	3852,8	3082,2	5029,8
40 %	3638,0	3497,6	2798,0	4642,9
45 %	3287,6	3255,9	2604,8	4256,0
47 %	3159,1	3191,1	2552,9	4101,2
50 %	3002,3	3127,9	2502,3	3869,1

6.3 Scenario 2 – Collapse

This scenario is inspired by a case study from a North Sea well [Torbergsen et al., 2012]. The well had a tieback solution. Pressure tests were performed repeatedly after installation because the pressure in the well could not be maintained. This was an indication of a leak somewhere in the system. After a thorough check the problem was eliminated, pressure tests were again performed and accepted, and the well was set on production.

After a while, it was discovered that the production tubing and casing had collapsed at a depth of approximately 700 m, and it had to be pulled out of hole. A picture of the collapsed pulled tubing is shown in Figure 37. A possible cause of the failure could be a leak in the production casing, leading to pressure build-up behind the casing during pressure testing. Another cause could be expansion of the fluids behind the casing due to thermal effects, leading to an increase in pressure, which possibly could have exceed the collapse resistance of the casing.

During inspection of the retrieved casing and tubing, they discovered that the collapsed section of the tubing consisted of a weaker material grade than the rest of it. The production casing should be of a 9-5/8" N80 53 lbs/ft grade, while the collapsed section was 47 lbs/ft. This yields a 28% reduction in collapse resistance between the grades. Fortunately, only one section of this quality was found, but still, the well was shut-in for a long period causing loss in income.

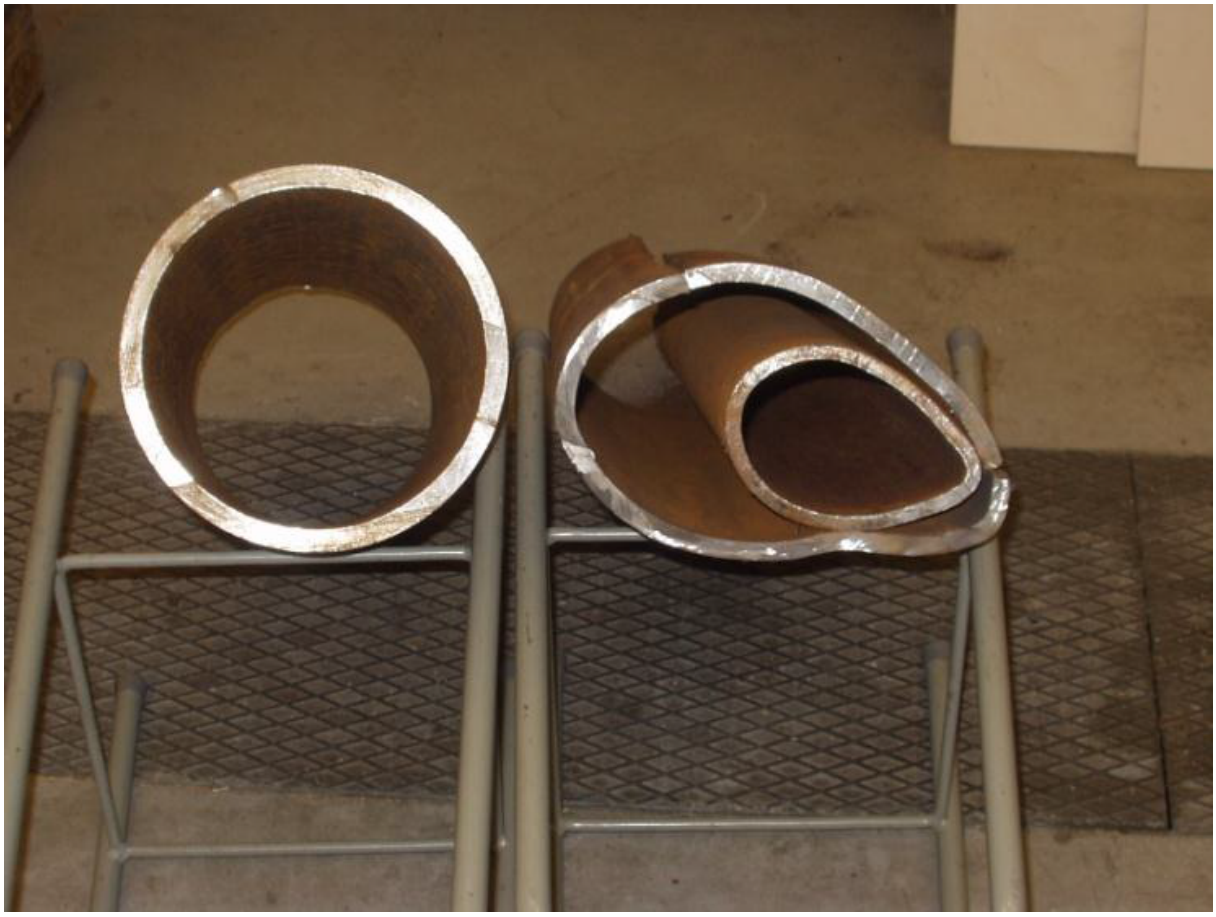

Figure 37: Collapsed casing and tubing from a North Sea well [Torbergsen et al., 2012]

The Ekofisk field commonly uses gas lift technique on wells to help the production. Gas is injected down the A-annulus and enters the tubing above the production packer through gas-lift valves. The applied pump pressure on the surface varies depending on available equipment and material on the platform, ranging from approximately 1800 to 2200 psi [Toftkaer, 2015]. This causes a significant amount of pressure to arise in the A-annulus, similar to the North Sea Well case.

The gas has the purpose of reducing the density of the producing fluids to help lift the fluids to surface [PetroWiki]. The external pressure at a given point in the annulus is then equal to the pump pressure plus the hydrostatic column of completion fluid on top of the desired point.

$$P_o = P_{pump} + \rho_{Comp.Fluid} g h \quad (6.3)$$

The internal pressure used in the simulation is assumed to be static because the reservoir pressure is not sufficient to flow the well. With an oil-gradient of 0.3 psi/ft. in Well Y, leaves the internal pressure of the non-flowing well equal to the hydrostatic column of the oil, which is 488 psi at 1626 ft. (MD = TVD at 1626ft):

$$P_i = \rho_{oil} g h \tag{6.4}$$

$$P_i = 0.3\ {}^{psi}/_{ft.} * 1626\ ft. = 488\ psi$$

According to ConocoPhillips [COPNO, 2011], the original collapse pressure was calculated to be equal to 6280 psi. The purpose of simulating this scenario is to find out the actual safe operational collapse pressure for locally worn tubing. Similar to the burst simulation, a reference model was first simulated to find the actual pressure limit for an unworn pipe in a collapse scenario.

6.3.1 Simulation Results – Collapse

Reference model – 0% wear depth

According to the simulation results, unworn tubing has no problem to withstand the maximum external pressure of 6280 psi. Figure 38 show tubing exposed to 8925 psi before the stresses in the wall exceeds the yield limit.

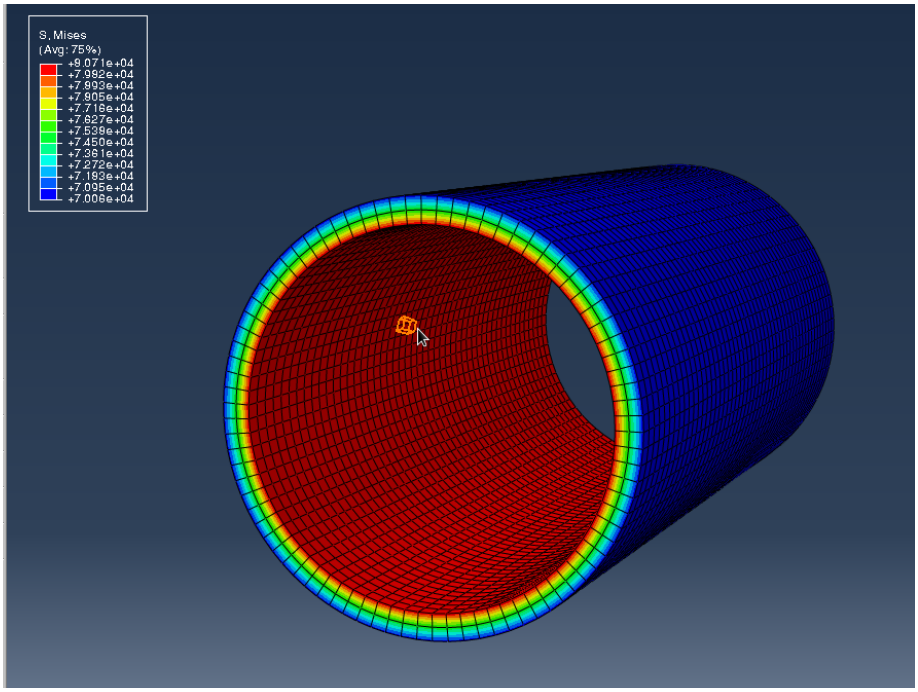

Figure 38: Simulated reference model for collapse scenario without wear

Table 17: Simulated collapse pressure results for model with 0% wear

External Pressure [psi]	Reference 0% wear Von Mises stress [psi]
9200	82600,00
9100	81650,00
9000	80710,00
8900	79760,00
8800	78820,00
8700	77870,00

Tubing model with 25% wear depth

Figure 39 shows tubing with a 25% wear depth of the wall thickness. This model starts to yield under an applied pressure of 4562 psi, which is a 49% reduction in collapse resistance compared to the reference model. Clearly, one can see that the deformation of the tubing resembles the case for the North Sea collapsed casing (Figure 37).

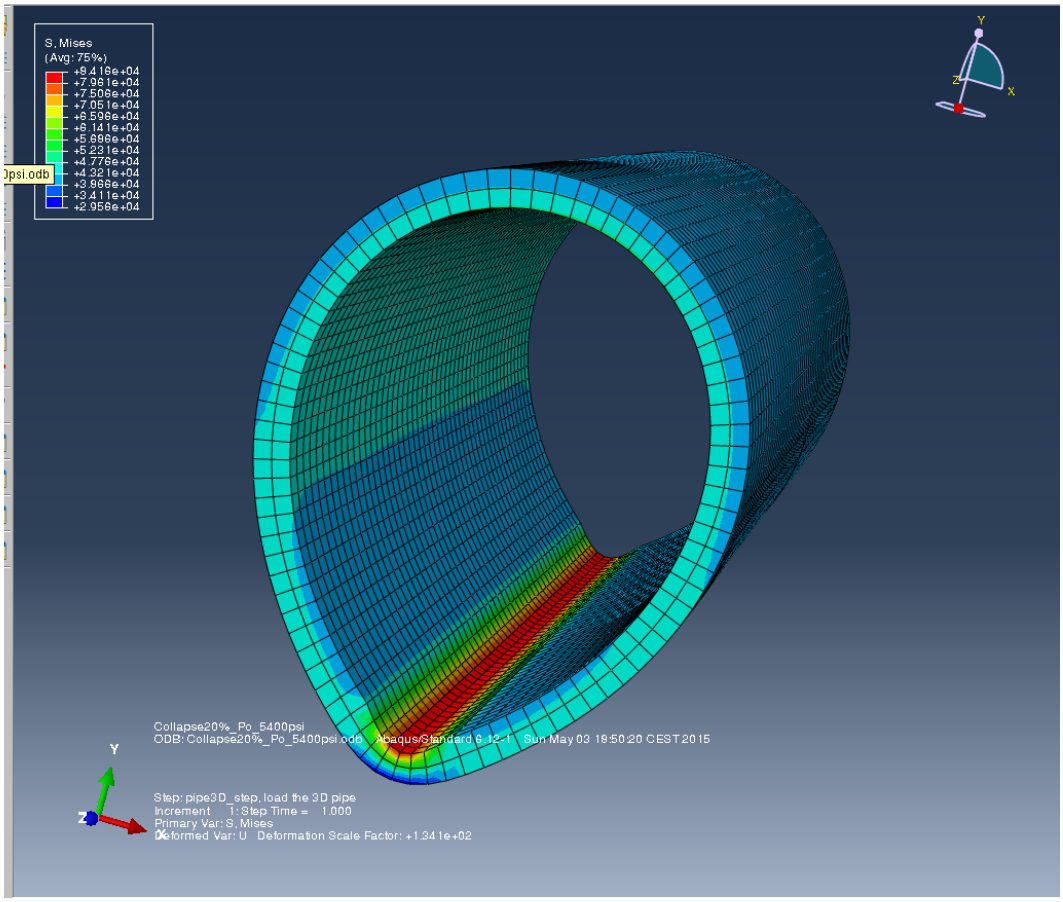

Figure 39: Simulated collapse model for collapse scenario with 25% wear

Table 18: Simulated collapse pressure results for model with 25% wear

External Pressure [psi]	25% wear Von Mises stress [psi]
4800	84650,00
4700	82690,00
4600	80740,00
4500	78780,00
4400	76820,00
4300	74860,00

Tubing model with 47% wear depth

This scenario is inspired by the actual case of Well Y, where the tubing has been extensively worn. The simulation is conducted in order to study the consequences if the tubing were to be subjected to high external pressure, either due to gas lift, a leak situation or other possible causes. Figure 40 shows the tubing under an external load of 2900 psi, with a static internal load of 488 psi. The Von Mises stress in the wall has just exceeded the material yield strength by these applied parameters. A reduction of 68% in collapse pressure has occurred due to severe wear. The simulation procedure for collapse is the same as for burst, and the results are presented in the next section.

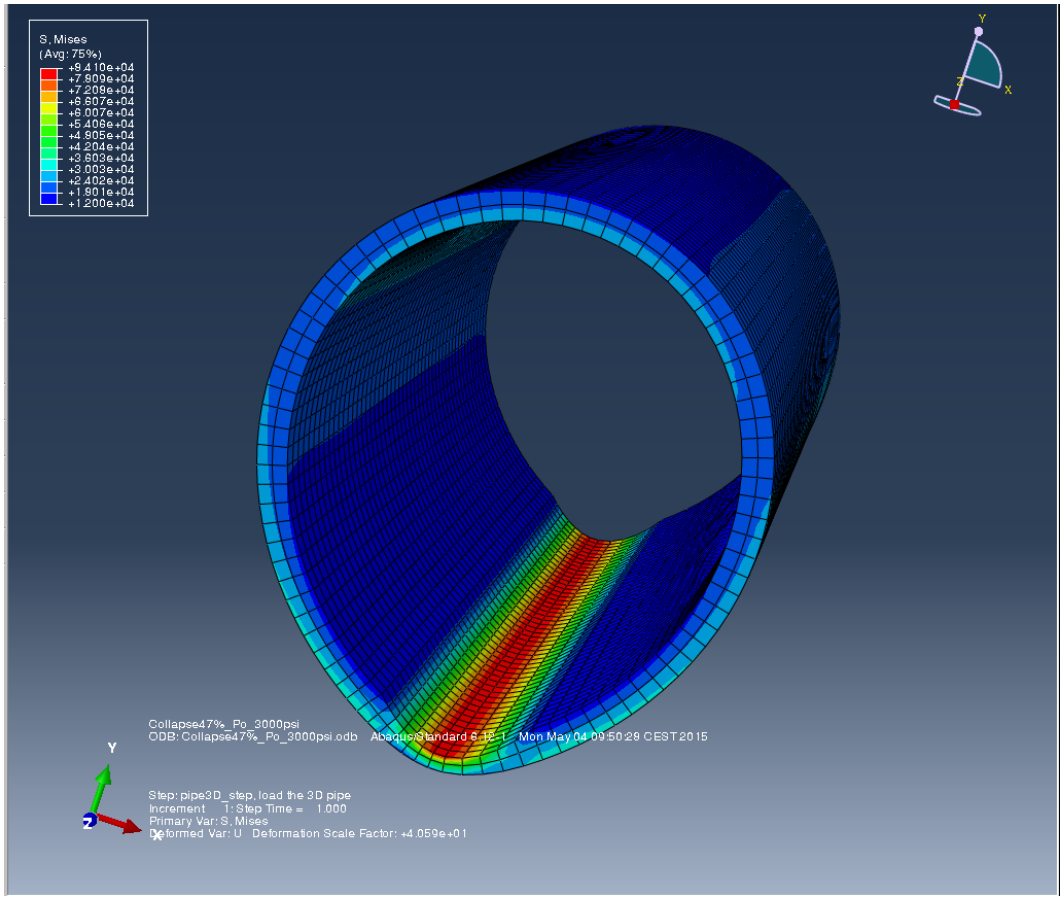

Figure 40: Simulated collapse model for collapse scenario with 47% wear

Table 19: Simulated collapse pressure results for model with 47% wear

External Pressure [psi]	47% wear Von Mises stress [psi]
3100	87440,00
3000	84100,00
2900	80760,00
2800	77420,00
2700	74080,00
2600	70740,00

Final Results – Collapse

The collapse resistance of the tubing obviously decreases with increasing wear, as Figure 41 illustrates. The decrease in yield strength seems to be greater within the first increments of wear percent.

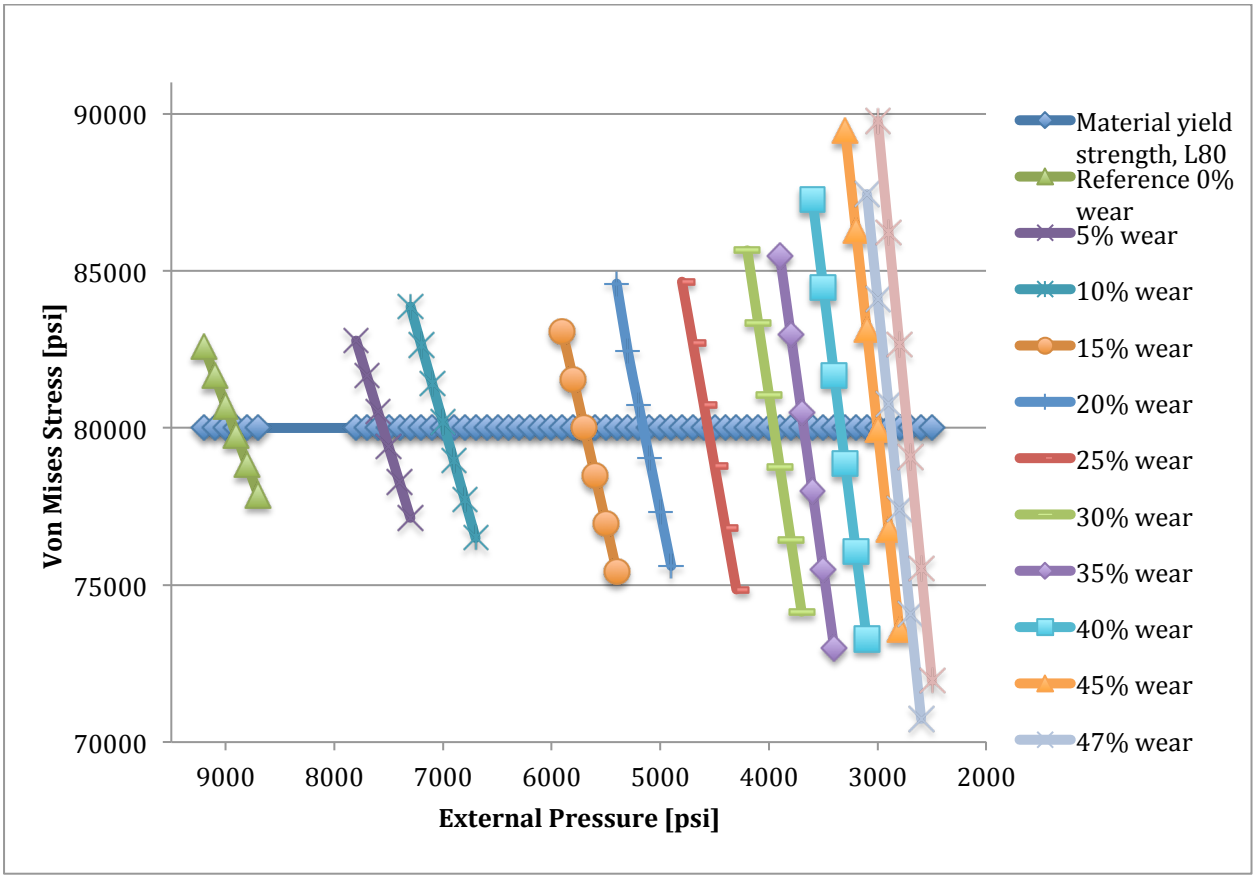

Figure 41: Collapse pressure limit as a function of increasing tubing wear

After using linear interpolation to find the intersection between σ_{VME} and σ_y, the pressure limits for a collapse scenario are represented in

Table 20.

Table 20: Results from linear interpolation for collapse – The pressure at intersection between $\boldsymbol{\sigma_{VME}}$ and $\boldsymbol{\sigma_y}$

Linear Interpolation	
Wear %	**Pressure [psi]**
0,00 %	8925,26
5,00 %	7553,57
10,00 %	6984,55
15,00 %	5699,35
20,00 %	5156,73
25,00 %	4562,24
30,00 %	3954,35
35,00 %	3680,40
40,00 %	3340,36
45,00 %	3001,89
47,00 %	2877,25
50,00 %	2725,77

The curve in Figure 42 represents the simulated results for a collapse scenario, where the high pressure in the annulus causes the tubing to yield. The model generated from these results is as follows:

$$P_{external} = 20328 * Wear\%^2 - 22074 * Wear\% + 8790{,}3 \qquad (6.5)$$

The value of $R^2 = 0{,}99569$ means the correlation between the data and the generated model is good.

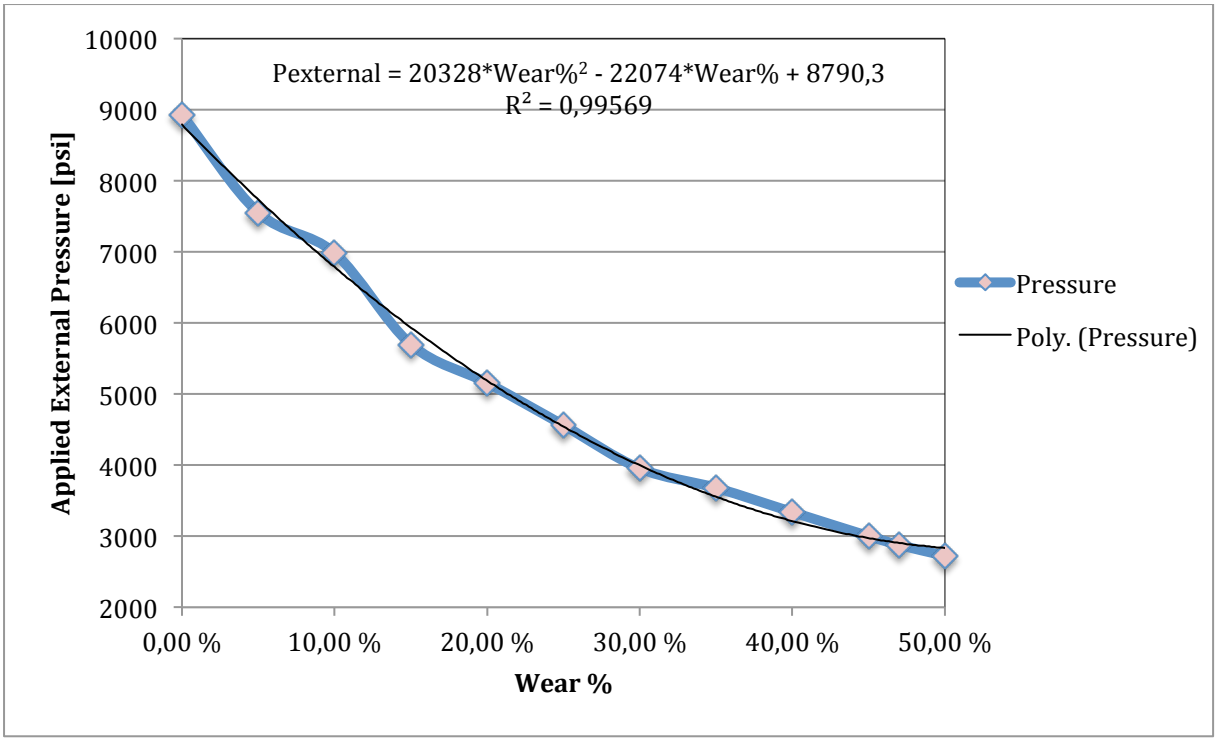

Figure 42: Safe/failure zone for operating external pressure. "True collapse"

A safety design factor of 0,7 is added to the simulation-based model to match the theoretical maximum collapse pressure of 6280 psi for an unworn tubing. For tubing with uniform wall thickness the collapse mode changes with different values of slenderness ratio (D/t). A curve for theoretical collapse was created, where the minimum wall thickness was assumed to be the overall thickness of the tubing. In order to calculate the theoretical collapse curve for the decreasing wall thickness, one had to use three out of four collapse modes. Applying the equations for plastic, transitional and elastic collapse modes generates the theoretical curve. The collapse modes were explained in chapter 3.

Surprisingly, as Figure 43 illustrates, safety factor included simulation-based model for local wear overlaps pretty accurately with the theoretical collapse curve for uniform wall loss. When the wear depth approximately exceeds 30% of the wall thickness, the simulation-based model for local wear seems to have a higher collapse resistance than for uniform wear. Table 21 shows the collapse model calculated using data obtained in Figure 43

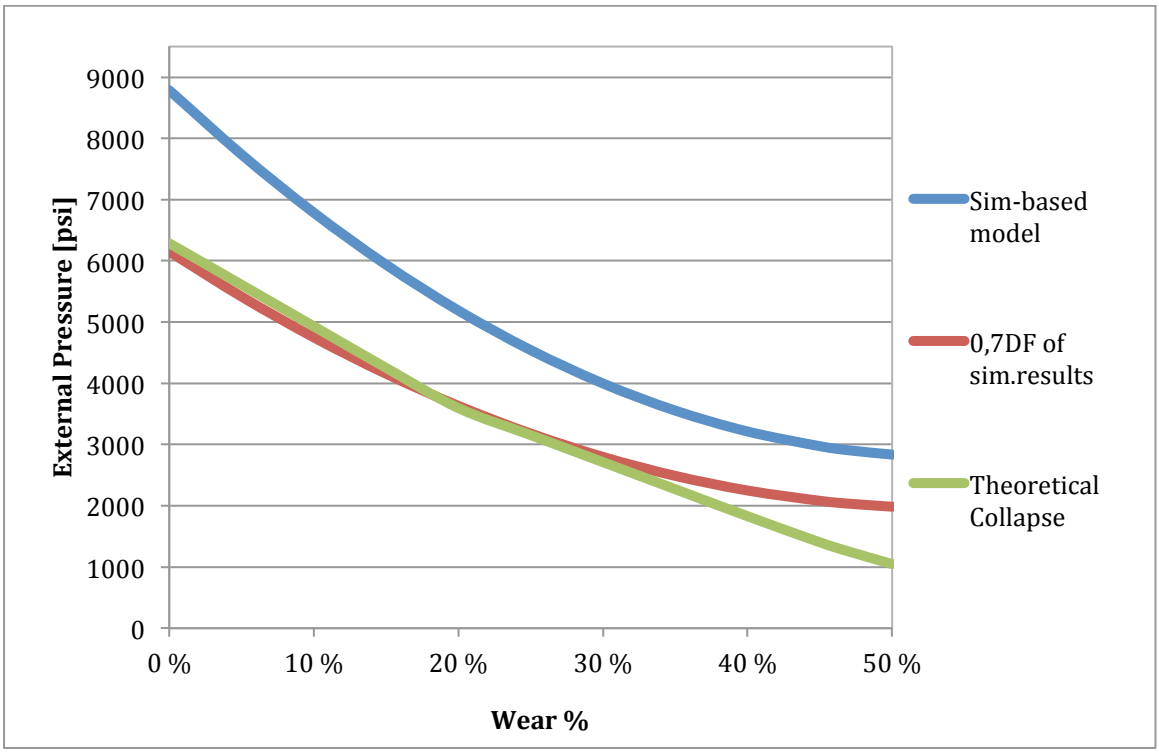

Figure 43: Simulation-based model, with and without design factor, compared to theoretical collapse models for uniform wall thickness.

Table 21: Summary table for the data in Figure 43

Wear %	Simulation-based model [psi]	DF=0,7 of model [psi]	D/t ratio	Collapse mode	Theoretical Collapse [psi]
0 %	8790,30	6153,21	18,09	Plastic	6288,40
5 %	7737,42	5416,19	19,04	Plastic	5609,43
10 %	6786,18	4750,33	20,10	Plastic	4930,46
15 %	5936,58	4155,61	21,28	Plastic	4251,49
20 %	5188,62	3632,03	22,62	Transitional Collapse	3595,83
25 %	4542,30	3179,61	24,12	Transitional Collapse	3154,09
30 %	3997,62	2798,33	25,85	Transitional Collapse	2712,35
35 %	3554,58	2488,21	27,83	Transitional Collapse	2270,62
40 %	3213,18	2249,23	30,15	Transitional Collapse	1828,88
45 %	2973,42	2081,39	32,89	Elastic	1403,34
47 %	2905,98	2034,18	34,14	Elastic	1252,89
50 %	2835,30	1984,71	36,18	Elastic	1048,37

6.4 Scenario 3 – Two wear scars

Well intervention includes several trips in and out of the well with either the same, or different types of equipment and tools. The likelihood of the tools wearing on the exact same spot during all the runs is small [Chow, 2015]. Tripping into the well will exert compressive forces on the tools, while tripping out will exert tensile forces. This causes for example the coiled tubing to be in contact with the tubing in different places on the way down and up. This scenario simulates the tubing with two wear scars. The results are then compared to the tubing models with one scar.

6.4.1 Burst pressure limit for tubing with two wear scars

Tubing model with two wear scars and 10% wear depth

Similar to scenario 1 for burst, the maximum stresses in the tubing wall are concentrated in the two wear scars. At 10% wear depth on both of the scars, the pipe yields at 7245 psi, resulting in approximately 25% reduction in burst resistance from reference model. The magnitude of the stress in the scars seems to be equal.

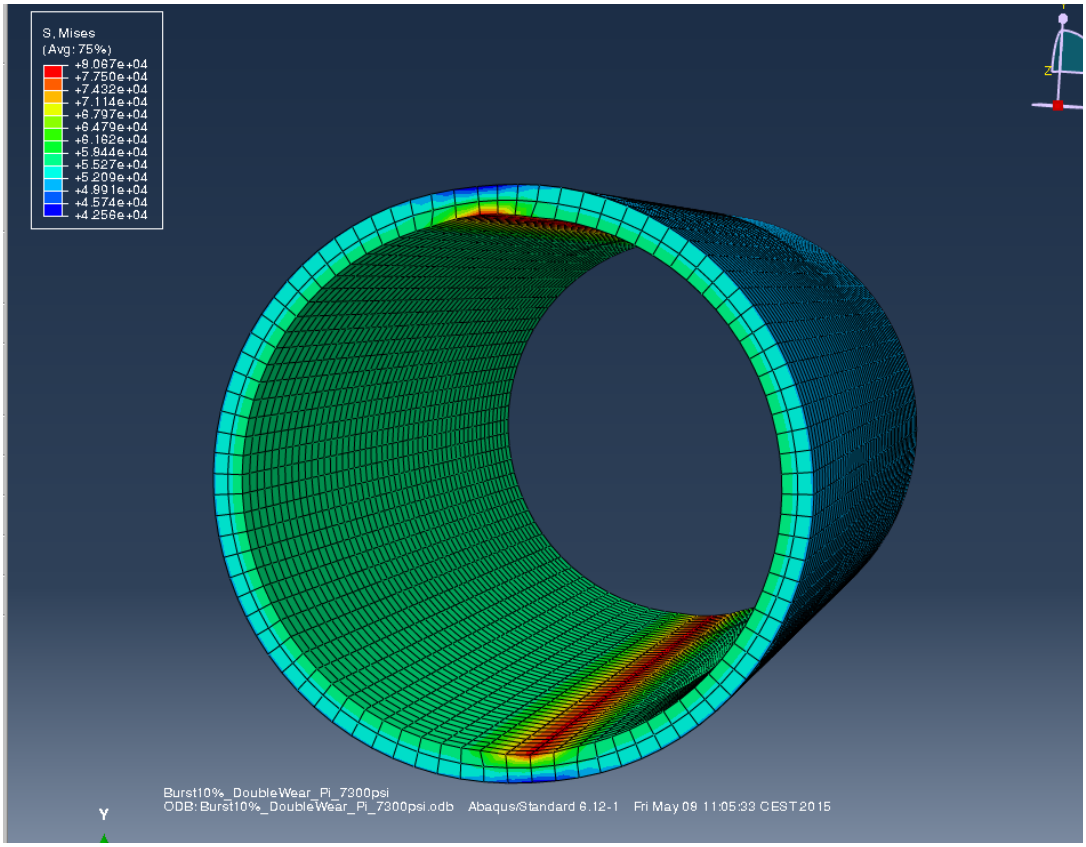

Figure 44: Simulated burst model with 10% wear depth and two wear scars.

Tubing model with two wear scars and 25% wear depth

A pipe with scars of 25% wear depth of the wall thickness, yields to 4639 psi of internal pressure, which corresponds to 48% reduction in burst resistance.

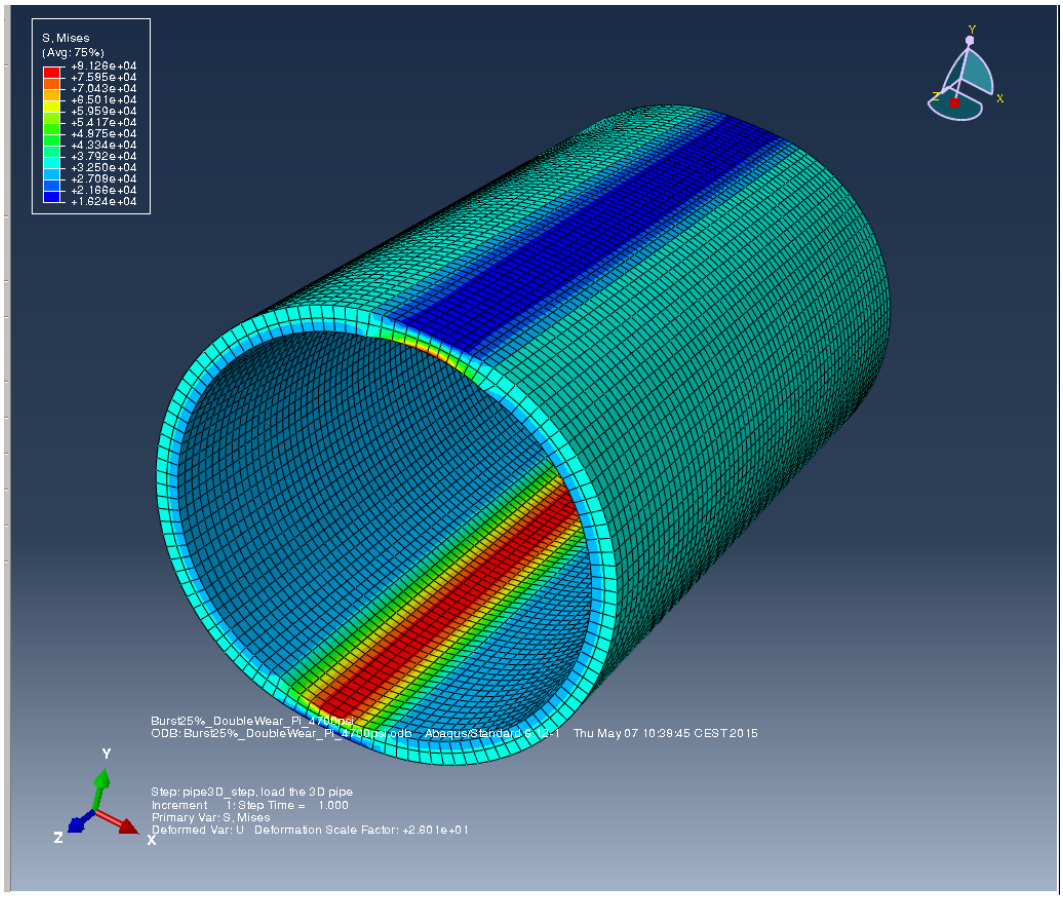

Figure 45: Simulated burst model with 25% wear depth and two wear scars.

Tubing model with two wear scars and 47% wear depth

The model for 47% wear depth shows a severe deformation of the tubing to an oval shape. The reduction in burst resistance from the reference model is at 71%. The pipe yields at a pressure of only 2790 psi at 47% wear.

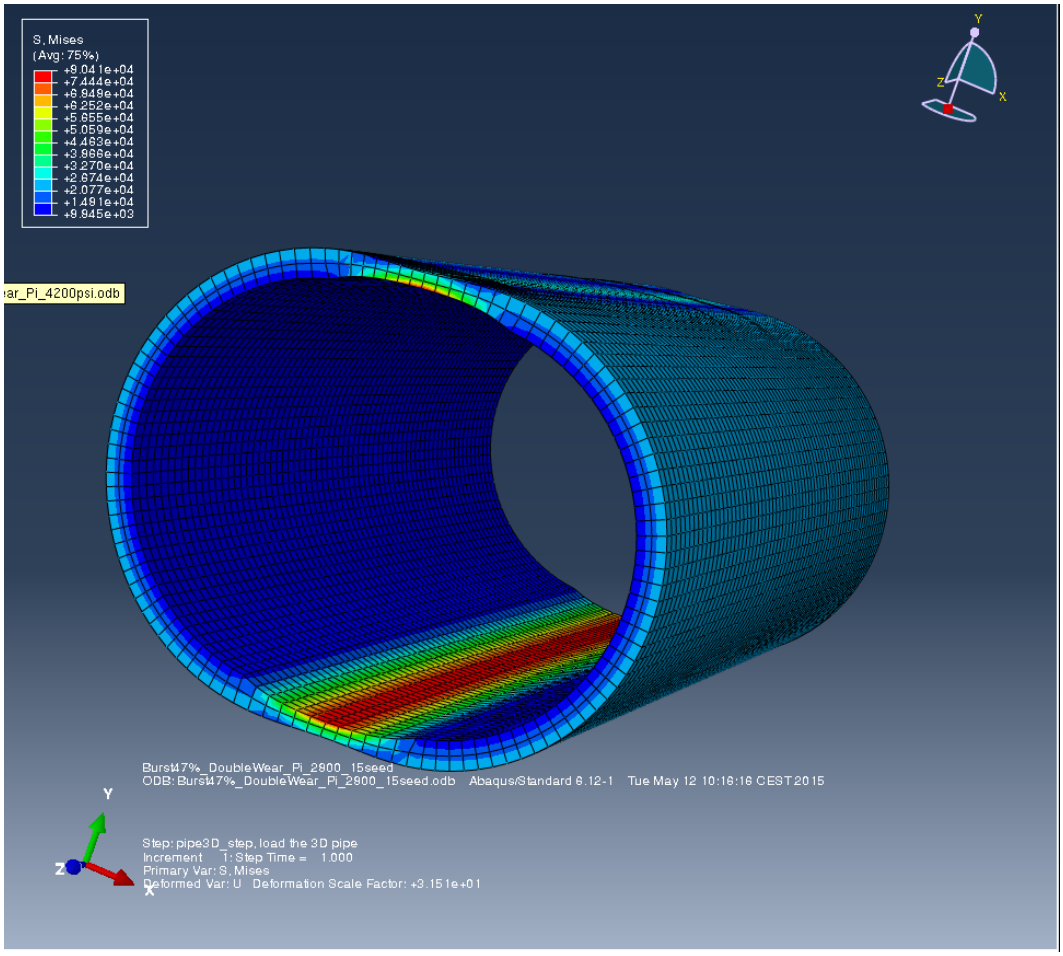

Figure 46: Simulated burst model with 47% wear depth and two wear scars.

Final Results – Two wear scars – Burst

The burst resistance for the tubing with two wear scars seems to decrease in the same pattern as for the tubing with one scar. The reduction in burst pressure with increasing wear depth is more rapid in the range of 0-25% wear, and seems to stabilize for wear depth above 25%.

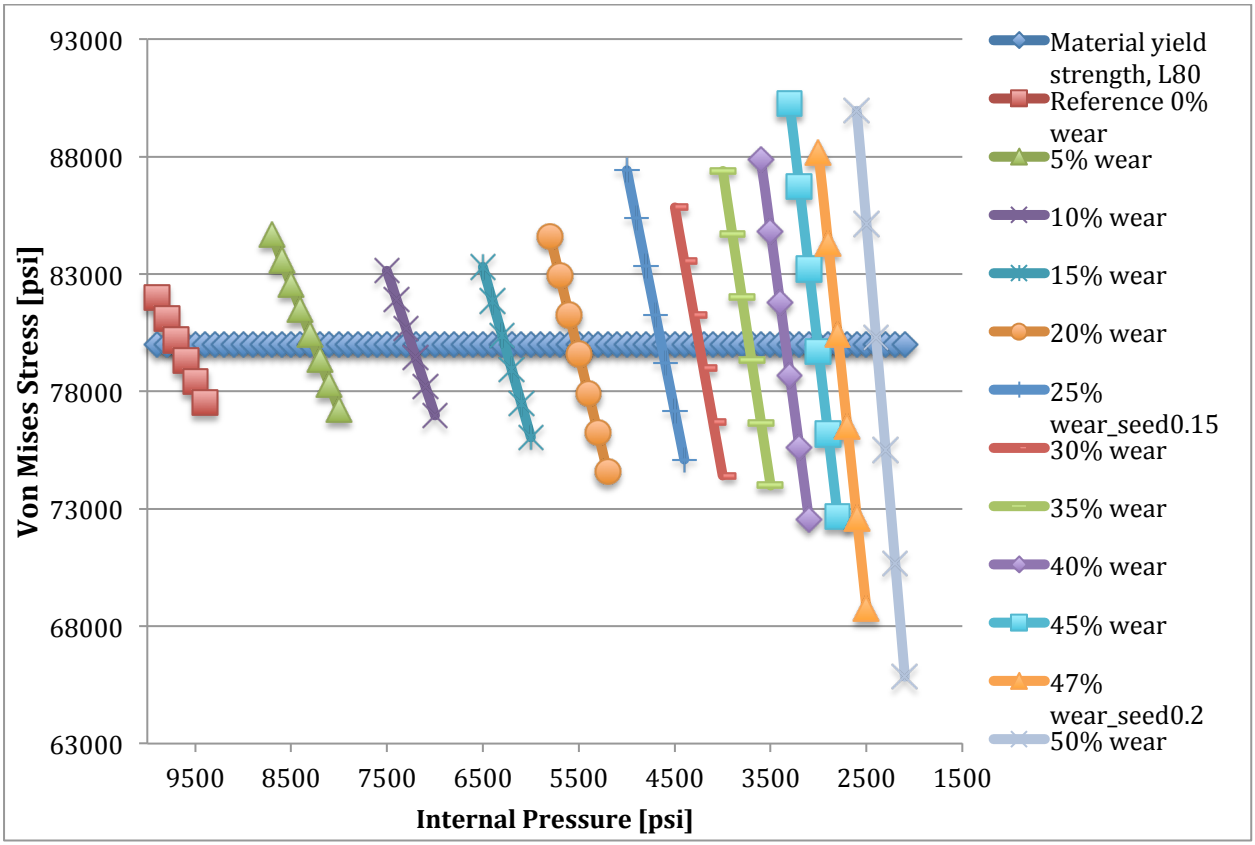

Figure 47: Burst pressure limit for tubing with two wear scars as a function of increasing wear depth

As done for the previous scenarios, the intersection between the σ_{VME} and σ_y are calculated by linear interpolation (Table 22) to generate the graph in Figure 48.

Table 22: Interpolated burst pressure results for a tubing with to wear scars

Linear Interpolation	
Wear %	**Pressure [psi]**
0,00 %	9677,53
5,00 %	8260,75
10,00 %	7245,53
15,00 %	6273,10
20,00 %	5525,00
25,00 %	4638,54
30,00 %	4244,74
35,00 %	3724,25
40,00 %	3342,67
45,00 %	3008,81
47,00 %	2789,49
50,00 %	2393,76

The model generated has a coefficient of determination of $R^2 = 0{,}9967$, which indicates a good prediction curve of the simulated data. The equation for the model is as follows:

$$P_{external} = 20513 * Wear\%^2 + 23969 * Wear\% + 9502{,}5 \qquad (6.6)$$

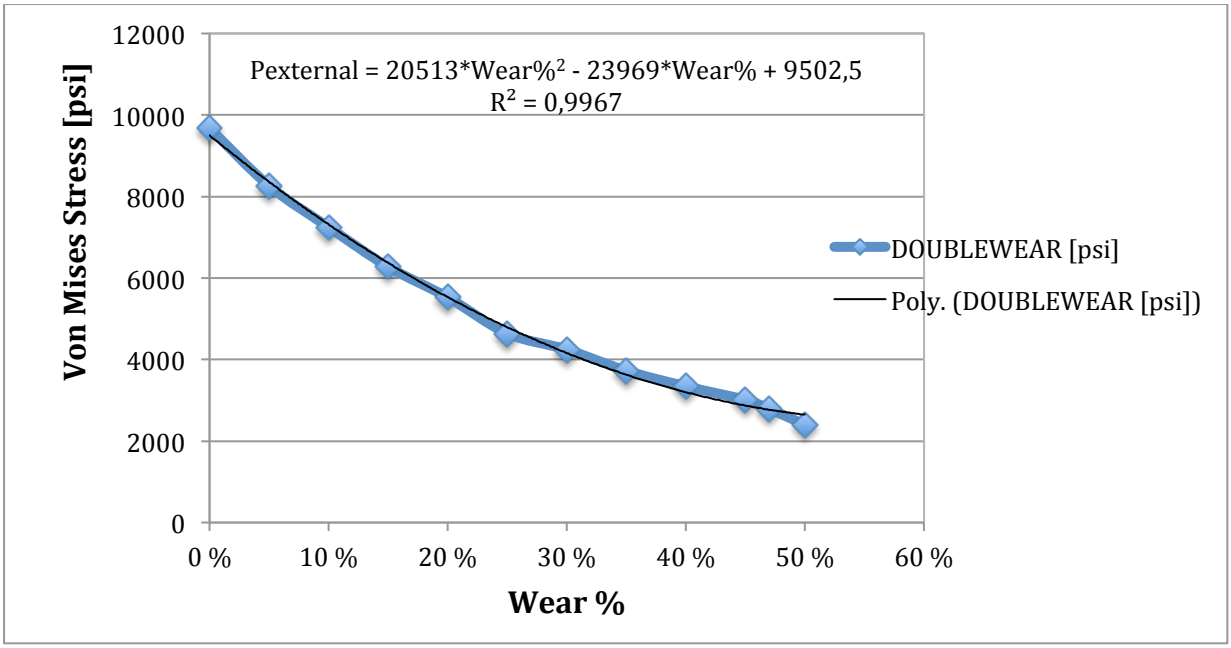

Figure 48: Safe/failure zone for operating internal pressure for tubing with two wear scars.

The trend and values for the curve in Figure 48 resembles a lot the curve modelled for tubing with one wear scar from Figure 35. Figure 49 compares the stress level in the wall for the tubings simulated with one and two wear scars as a function of wear percent. There does not seem to be any significant difference between the safe operational pressure windows, even though one model has one wear scar, and the other has two. The paths overlaps almost entirely in the range of 0-30% wear depth. The curves start to diverge somewhat when the wear groove gets deeper than 30% of the wall thickness.

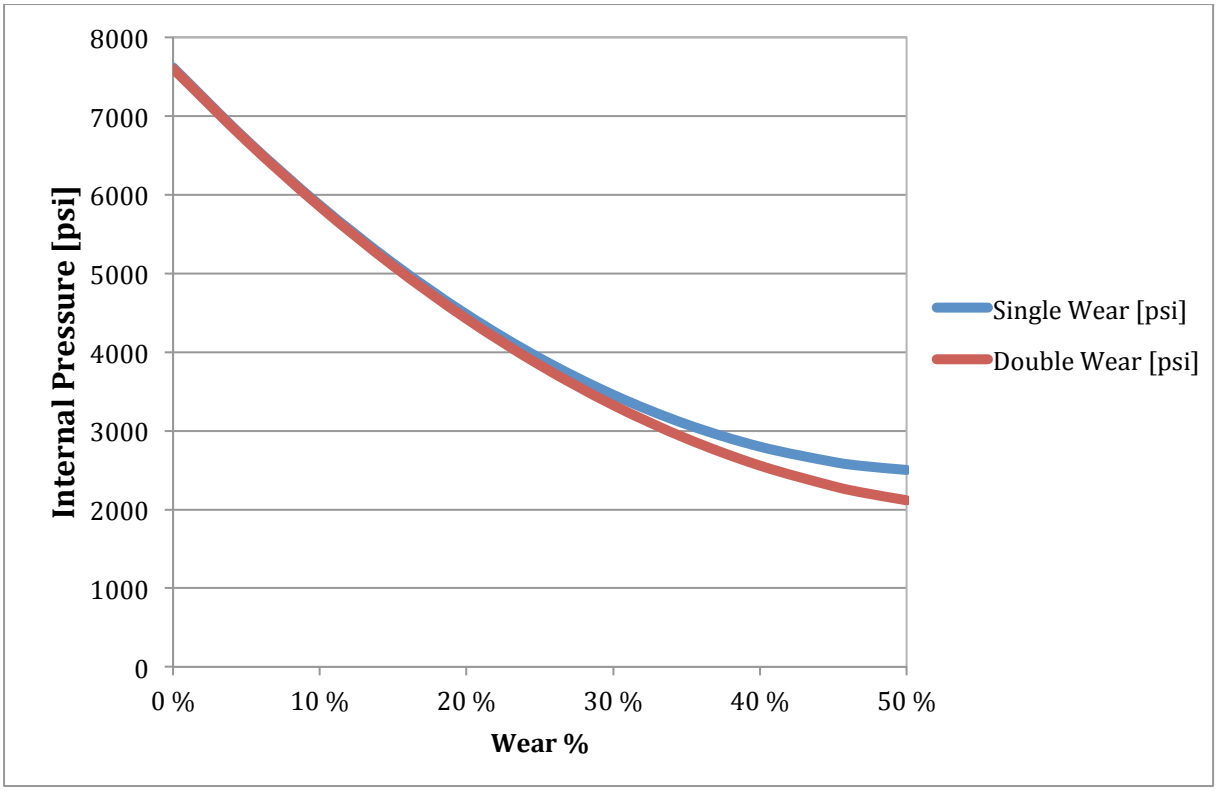

Figure 49: Comparison of burst pressure limit for tubings with one and two wear scars as a function of increasing wear depth

6.4.2 Collapse pressure limit for tubing with two wear scars

The same approach was done for the last scenario as for the previous. Examples of the simulation process, for three different wear depths, are shown with the resulting reduction in collapse resistance in the next sections.

Tubing model with two wear scars and 10% wear depth

The pipe simulated with 10% wear depth on both scars yields at 6720 psi, which is a 25% reduction in collapse resistance compared to the reference model.

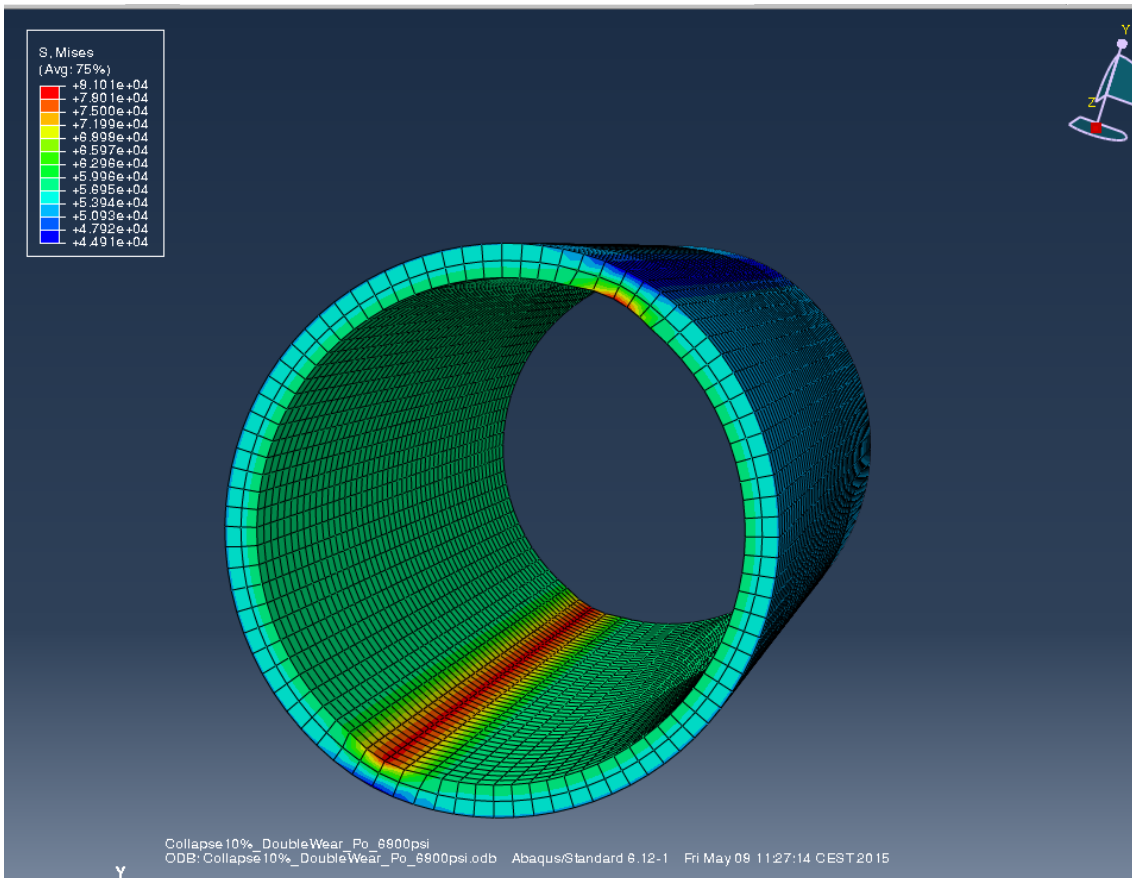

Figure 50: Simulated collapse model with two wear scars at 10% wear depth

Tubing model with two wear scars and 25% wear depth

At 25% wear depth, the pipe yields at 4287 psi, resulting in 52% reduction in collapse resistance. The shape of the tubing starts to deform to an oval shape.

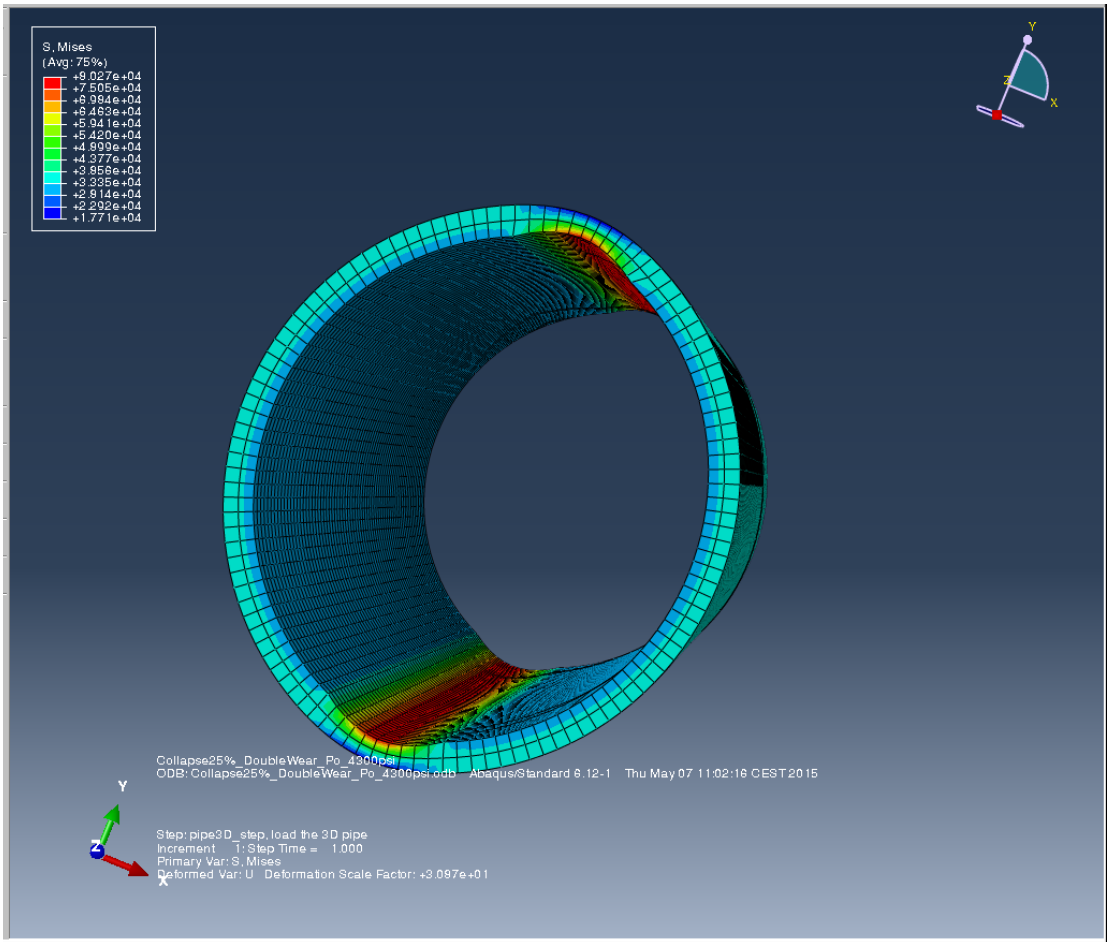

Figure 51: Simulated collapse model with two wear scars at 25% wear depth

Tubing model with two wear scars and 47% wear depth

When the wear depth is as severe as 47% in both wear scars, and subjected to a pressure of 2517 psi, it starts to deform into a pointy oval shape. The reduction in collapse resistance is now at 72% compared to the reference model with no wear.

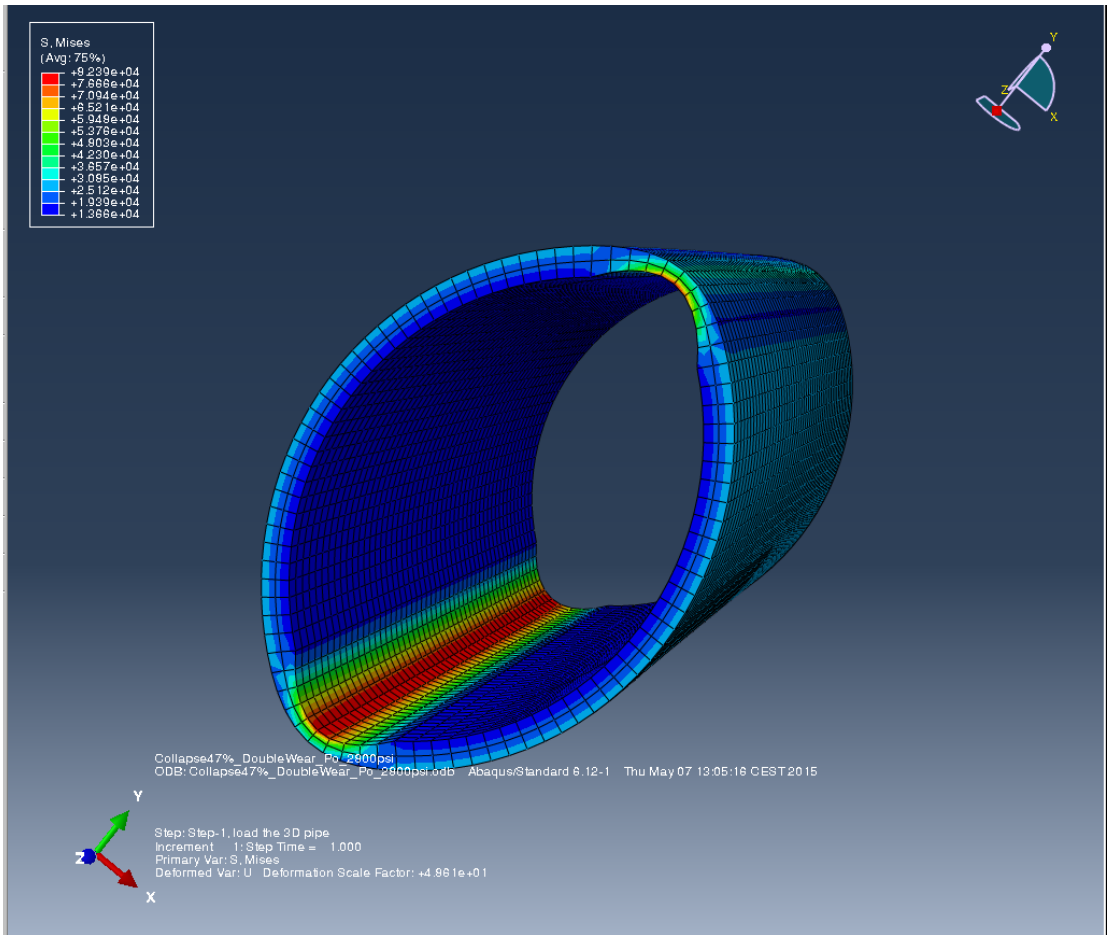

Figure 52: Simulated collapse model with two wear scars at 47% wear depth

Final Results – Two wear scars – Collapse

The graph in Figure 53 shows how the collapse pressure limit for a tubing with two wear scars decreases as a function of increasing wear depth.

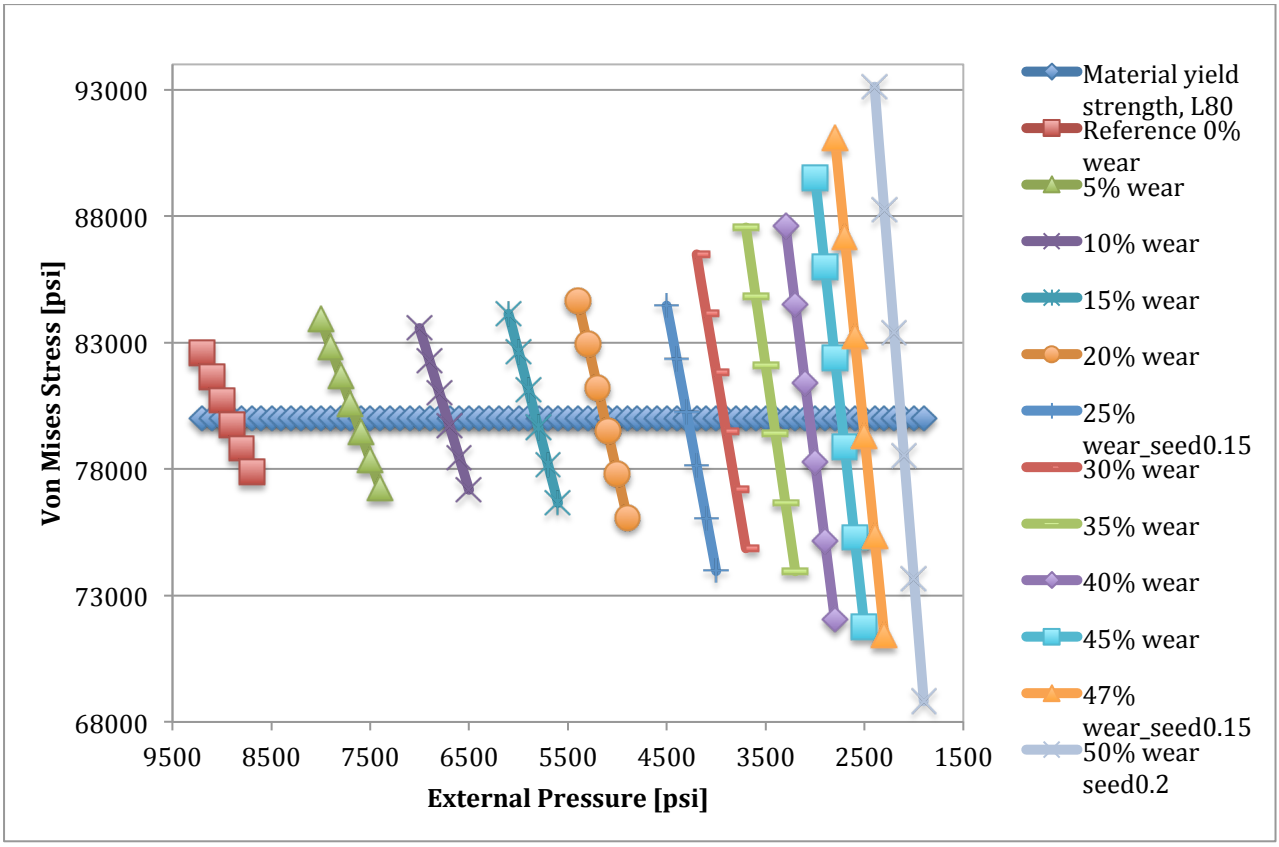

Figure 53: Collapse pressure limit for tubing with two wear scars as a function of increasing wear depth.

By the use of linear interpolation (

Table 23), the safe/failure curve for operating collapse pressure is generated in Figure 54.

Table 23: Interpolated collapse pressure results for a tubing with to wear scars

Linear Interpolation	
Wear %	**Pressure [psi]**
0,00 %	8925,26
5,00 %	7646,85
10,00 %	6720,47
15,00 %	5823,33
20,00 %	5128,07
25,00 %	4287,14
30,00 %	3921,03
35,00 %	3422,43
40,00 %	3055,31
45,00 %	2732,11
47,00 %	2517,56
50,00 %	2130,04

From the simulation results, this model was developed:

$$P_{external} = 18071 * Wear\%^2 - 21860 * Wear\% + 8776{,}1 \qquad (6.7)$$

This model also seems to fit with the simulated data with correlation coefficient, $R^2 = 0{,}99686$.

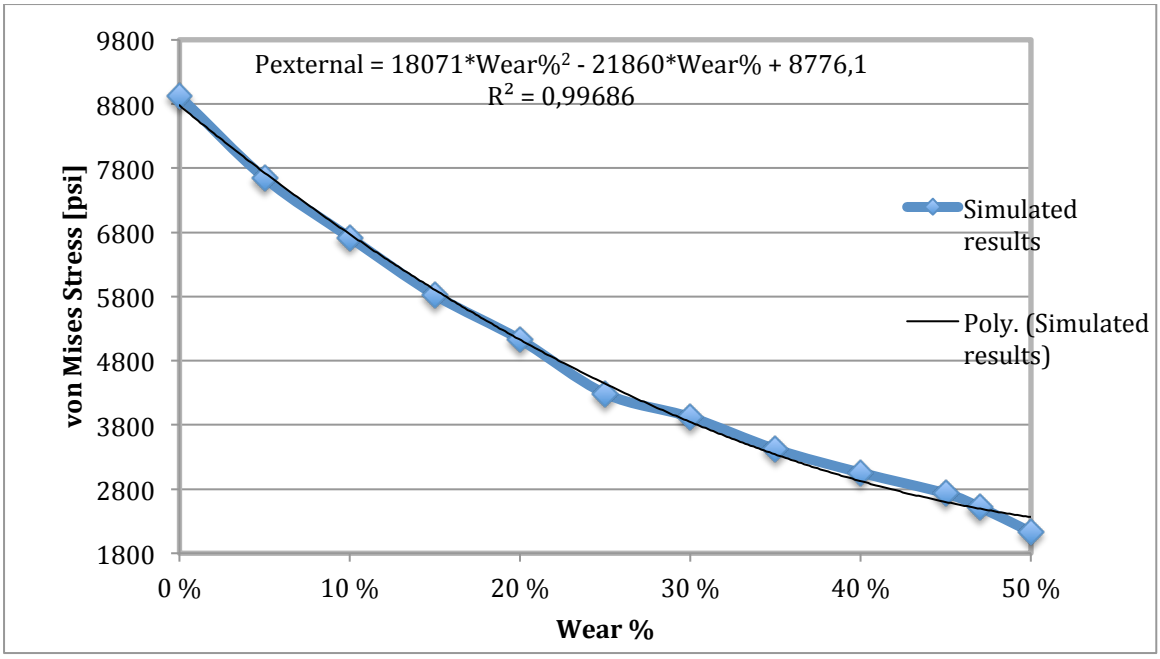

Figure 54: Safe/failure zone for operating external pressure for tubing with two wear scars.

Figure 55 shows a comparison of collapse pressure limit for tubing derived from one and two wear scars models. Similar to the burst, both cases overlaps almost entirely in the range of 0-30% wear depth. The curves start to diverge somewhat when the wear groove gets deeper than 30% of the wall thickness, as it did for burst as well.

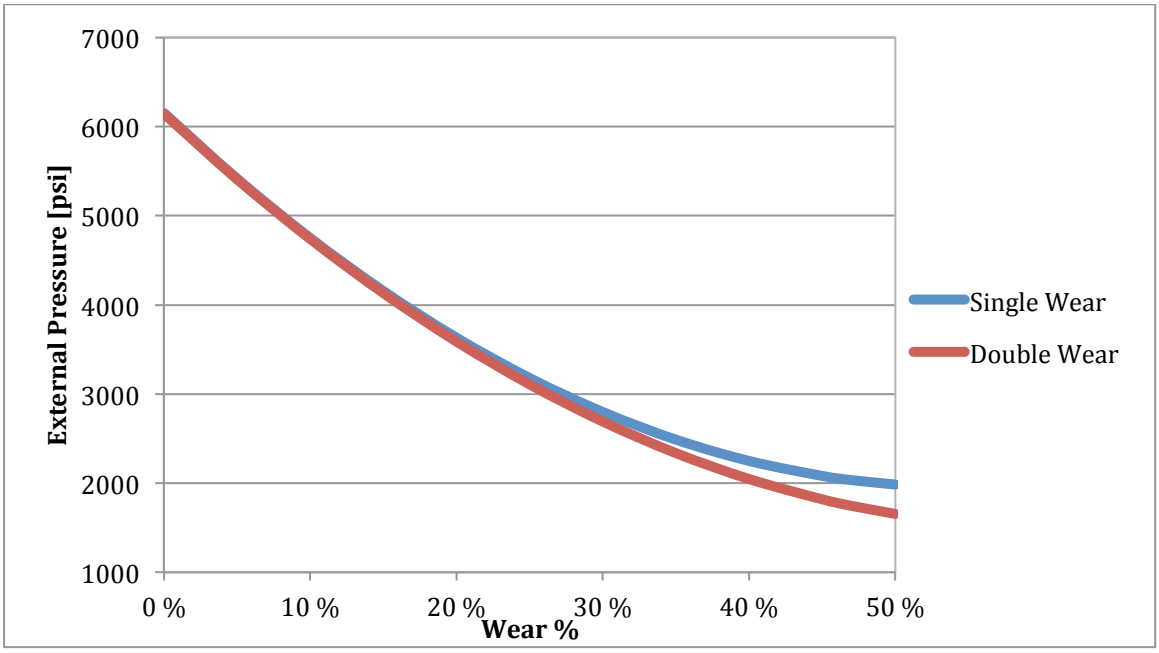

Figure 55: Comparison of collapse pressure limit for tubing with one and two wear scars.

7 Summary and Discussion

ConocoPhillips Norway (COPNO) detected local wear in the production tubing in some of their wells. The wear was of different severity and appeared in various sections of the tubing. In 2011, a brief study were conducted by ConocoPhillips on one of the wells, "Well Y", where the goal was to find the de-rated burst and collapse pressure due to worn tubing. The methods used in the study seemed to be based on Barlow's equation, thin-walled cylinder theory and uniform wear.

The most common tubing dimensions used by ConocoPhillips have a thickness-to-radius-ratio that determines them to be thick-walled cylinders. Considering the different failure mechanisms for the two cylinder types, a test simulation was done to check whether the approach by COPNO was correct or not. FEM analyses were performed to study the stress concentration and distribution in the tubing wall, and then compare the outputs for local and uniform wear. The main reason was that since the detected damage on the tubing was local and not uniform, the stress would probably be concentrated in the damaged area rather than uniformly distributed in the wall, like for uniform wear. The simulations were to verify this theory and to determine how elevated the stress is at the wear scar.

The test simulation showed that if in reality the detected wear is local and one uses uniform-wear theory to calculate the deterioration of the tubular, it could lead to an incorrect interpretation of both the distribution and magnitude of the stress in the tubing wall. By using Barlow's method and applying minimum wall thickness to the whole tubing, even though the wear was local, did not generate the same stress concentration in the tubing as for those models that had the geometry built with local wear. The local damage simulation showed a high stress concentration in the wear scar, for both burst and collapse scenarios. The magnitude of the accumulated stress in the wall was a great deal less for uniform damage, which can lead to estimating a considerably higher yield limit than the pipe actually can withstand. This can cause an over-estimation of the burst and collapse resistance, and can lead the pipe to yield before the estimated yield pressure has been reached.

The tubing models presented in this thesis were all built from scratch in the software Abaqus, which is a finite element analysis tool. The software both models and analyses mechanical components, and presents the results visually. This software is not a part of the curriculum for a petroleum student, something that is very unfortunate. Drilling softwares and simulation programs does not usually show how the stress is distributed in the tubulars when subjected to a variety of loads. Visualization of the stress in the models and how it deforms under different loads, gave a very good understanding of the mechanics and how it works.

Finite element method (FEM) modeling and analyses was done for three scenarios to assess the stress distribution during being subjected to different types of loading. The FEM modeling considers the axial-, radial- and hoop stresses to calculate the maximum and minimum Von Mises stress that arises in the pipe wall. The outputs from the simulations were without any safety design factor. This thesis was specifically based on the "Well Y", a real case from the Ekofisk field, where the maximum wear of 47% was detected at a depth of 1626 ft. in the production tubing. The tubing grade was L80 and had dimensions of 5,5 in. OD. and 4,892 in. ID. For the whole burst scenario, a constant external pressure of 727 psi was applied, which was supposed to represent the hydrostatic column of completion fluid in the A-annulus with density of 8,6 ppg. For the collapse scenario, a constant internal pressure of 488 psi was applied and was to represent the hydrostatic column of oil, with a gradient of 0,3 psi/ft., in a non-flowing well. The simulations do not take into account the effects of temperature and bending.

It is important to understand that the simulations and models generated in this thesis only apply for this particular case with these material properties and well parameters. In order to implement these models to a case under other circumstances, one would have to change the parameters and loading during modeling.

The purpose of the simulations were to determine at which pressure, either internal or external depending on the scenario, the pipe starts to yield and deform as it deteriorates for a given wear depth. By the use of linear interpolation, the intersection between the Von Mises equivalent stress (σ_{VME}) and material yield stress (σ_y) was

calculated. The values from the interpolation were then used to create a plot that indicates the safe operational window for the various scenarios. The area below the curve indicates a safe operational pressure zone. Exceeding this pressure for the given wear depth will lead the pipe to yield. The objective is to generate a model that predicts the deterioration of the tubing with increasing wear-depth.

In this thesis, three scenarios were simulated for the damaged tubing in "Well Y". Based on the specific input for material properties, well parameters and loads, the following scenarios were simulated for this case:

Burst – One wear scar

- High internal pressure can occur during for example a kick, production, well shut-in, acid stimulation and bull-heading.
- Constant external pressure of 727 psi exerted from completion fluid.
- Significant decrease in burst resistance with increasing wear-depth.
- Deformed into an oval shape when yield limit was exceeded.
- A model, with good approximation to the simulated data, was generated to create a safe operational window for burst pressure.
- A safety design factor was added and the model was compared to Barlow's model for uniform wear. There was a remarkable difference in the safe-operational window between the models. The model for local wear had significantly narrower window than uniform wear.

Collapse – One wear scar

- Inspired by a real-life case from a North Sea well.
- High external pressure can occur during for example a gaslift operation, leak in the tubing or arise due to temperature effects.
- Constant internal pressure of 488 psi exerted from the oil column at 1626 ft.
- Significant decrease in collapse resistance with increasing wear-depth.
- Deformed into an asymmetric, drop-like shape when yield limit was exceeded.
- A model, with good approximation to the simulated data, was generated to create a safe operational window for collapse pressure.

- A safety design factor of 0,7 was added to the model and compared to the collapse modes for uniform wear based on the slenderness ratio. Surprisingly, the models for local wear and uniform wear corresponded very well.

Burst and collapse – Two wear scars

- Based on different contact points between the tools and tubing during tripping in and out of the well (compression and tension).
- One additional wear scar was added to the models, and they were re-simulated in order to study if the distribution and magnitude of stress in the tubing wall changes from having only one wear scar, to having two. The wear depth of the scars was identical at all times.
- The stress appeared to be equally distributed between the two scars with the same magnitude, during both collapse and burst.
- Comparing the scenarios of one and two wear scars gave almost two indistinguishable curves. There seem to be a slight deviation between the curves when the wear depth increases to above 30% of wall thickness. One could not tell a big difference between the safe operational windows for neither the burst or collapse scenarios, with one and two wear scars.

8 Conclusion

Predicting the deterioration of production tubings after discovery of wear is very essential in order to maintain the integrity of the well. If the predictive models can be implemented, one can prevent downtime of the well by doing measures a step ahead, before the tubing yields or ruptures.

Abaqus is a very good tool for showing how the tri-axial stresses are distributed in the tubing wall and the mechanics of deformation. The fact that it visualizes where the stress is concentrated is very helpful for understanding. The results from FEM simulation in Abaqus can be compared against well-established theories and methods, and see how the models fit each other.

Based on the commonly used approaches and FEM simulation, the conclusions for this thesis are:

- The application of Barlow's equation, which is based on thin-walled cylinder model with uniform wall-loss, predicts a solution that yields a considerably higher pressure-limit than the FEM simulations for wear on production tubing. The safe operational window for Barlow's equation was significantly larger than the window for simulation of local wear. Barlow's equation is therefore not reliable to use for local damage on a thick/thin-walled tubing.
- Based on the burst scenarios, for both single and double wear scars, the simulated pressure limits were significantly less than the limits calculated with Barlow's equation. The safe operational pressure window generated from simulating local wear was shown to be much narrower than for Barlow's window for uniform wear. This can lead to an over estimation of the burst strength of the worn tubing.
- The collapse modes for uniform wear seem to coincide with the FEM simulations for local wear. The curves for the safe operational pressure window for the two methods were almost identical in the range of 0-35% wear depth. For wear depths of less than 35% of wall thickness, the observations obtained by comparing the simulated- and theoretical results, show that in this specific case the collapse mode for uniform wear can be applied for predicting the de-rated collapse pressure for local wear.

References

1. Aasen, J. A. and Aadnoy, B., 2006. *Three-dimensional well tubular design improves margins in critical wells.* Elsevier B. V. Journal of Petroleum Science and Engineering 56 (2007) 232-240.
2. Adams, P. M. and Payne, M., 2001. *On the calibration of design collapse strengths for quenched and tempered pipe.* Paper presented at Offshore Technology Conference, Texas, USA. doi:10.4043/13048-MS.
3. API Bulletin 5C3, 1994, with supplement 1999. *Bulletin on Formulas and Calculations for Casing, Tubing, Drill Pipe, and Line Pipe Properties.* 6th edition American Petroleum Instistute, Washington, USA.
4. API RP-7G, 1998. *Recommended Practice for Drill Stem Design and Operation Limits.*
5. Bellarby, J., 2009. *Well Completion Design.* Elsevier B.V., Amsterdam, The Netherlands.
6. Boresi, A. P. and Schmidt, R. J., 2003. *Advanced Mechancics of Materials.* 6th ed. ISBN 0-471-43811-2.
7. Bradley, W. B. and Fontenot, J.E., 1975. *The prediction and control of casing wear*. Journal of Petroleum Technology, SPE-5122-PA , 27:233–245.
8. Byrom, T., 2007. *Casing and Liners for Drilling and Completion.* Gulf Publishing Company, Houston, Texas, USA.
9. Craft, B. C., Holden, W. R., Graves Jr., E. D., 1962. *Well Design: Drilling and Production.* Prentice-Hall, Englewood Cliffs, New Jersey.
10. ConocoPhillips A. *Pressefoto.* Available from: http://www.conocophillips.no/NO/newsroom/Sider/press-photos.aspx, 20.04.2015.
11. ConocoPhillips B. *Ekofisk-området.* Available from: http://www.conocophillips.no/NO/our-norway-operations/greater-ekofisk-area/Sider/default.aspx, 20.04.2015.
12. ConocoPhillips C. *Ekofisk Senteret.* Available from: http://www.conocophillips.no/NO/our-norway-operations/greater-ekofisk-area/ekofisk/Sider/default.aspx, 20.04.2015.
13. ConocoPhillips Business Unit (COPNO), 2010. *Seawell: Memory Multi-Finger Caliper Log Results Summary,* by Oijord, M. and Sundvor, S.

14. ConocoPhillips Business Unit (COPNO), 2011. *Effect of Tubing Wear on "Well Y"*, by Dan Sturdee.
15. ConocoPhillips Business Unit (COPNO), 2012. *Data and Consulting Services: Final Report, Ekofisk field,* by McIntyre, W., Stavanger, Norway.
16. Oljefakta. *Ekofisk feltet.* Available from: http://oljefakta.petro.no/felt/ekofisk, 09.06.2015.
17. Dowling, N.E., 2012. *Mechanical Behaviour of Materials: Engineering Methods for Deformation, Fracture, and Fatigue.* Fourth Edition, Pearson Education Limited, Essex, England.
18. Felippa, C. A., 2014 A. *Chapter 6 - Finite Element Modelding: Introduction.* Available from: http://www.colorado.edu/engineering/CAS/courses.d/IFEM.d/IFEM.Ch06.d/IFEM.Ch06.pdf, 13.04.15.
19. Felippa, C. A., 2014 B. *Chapter 7 – Finite Element Modeling: Mesh, Loads, BCs.* Available from: http://www.colorado.edu/engineering/CAS/courses.d/IFEM.d/IFEM.Ch07.d/IFEM.Ch07.pdf, 13.04.15.
20. Fontenot, J. E. and McEver, J. W., 1974. *The Experimental Measurement of Casing Wear Due to Reciprocating Drillpipe and Wireline.* Paper presented at the Petroleum Mechanical Engineering Conference, Dallas, Texas, USA.
21. Holmquist, J. L., Nadai, A., 1939. *A theoretical approach to the problem of collapse of deep-well casing.* Drilling and Production Practice. American Petroleum Institute, pp.392-420.
22. Hibbeler, R.C., 2011. *Mechanics of Materials.* Eighth Edition in SI Units, Pearson Education South Asia PTE LTD, Singapore.
23. Holm, R., 1946. *Electric contacts*. Almqvist och Wiksell Forlag, Stockholm Sec. 40
24. Liu, G.R. and Quek, S.S, 2003. *The Finitie Element Method: A Practical Course.* Elsevier Science Ltd, Pxford, England.
25. NORSOK D-010. *Well Integrity in Drilling and Well Operations.* Rev 4, 2013.
26. Payne, M. L., 2001. *Modernization of OCTG Performance and Design Standards.* OTC 13053. Offshore Technology Conference, Houston, Texas.

27. Peloton. Available from: http://www.peloton.com/default.asp?id=13, 13.02.2015.
28. PetroWiki. *Gas lift.* Available from: http://petrowiki.org/Gas_lift, 07.04.15.
29. Song, J.S., Bowen, J. and Klementich, F., 1992. *The Internal Pressure Capacity of Crescent-Shaped Wear Casing*. Oil Technology Services Inc. IADC/SPE 23902, presented at the IADC/SPE Drilling Conference in New Orleans, Louisiana, February 1992.
30. Torbergsen, H. B., Haga, H. B., Sangesland, S., Aadnoy, B., Sæby, J., Johnsen, S., Rauland, M., Lundeteigen, M. A., 2012. *An Introduction to Well Integrity.* Rev 0. Well Integrity Forum.
31. Vignes, B., Andreassen, J. and Tonning, S. A., 2006. *PSA Well Integrity Survey, Phase 1 Summary report.*
32. Vignes, B. and Aadnoy, B., 2010. *Well-Integrity Issues Offshore Norway.* SPE-112535-PA, SPE Production & Operations, 25:02, p. 145-150.
33. White, J. P. and Dawson, R., 1987. *Casing Wear: Laboratory Measurements and Field Predictions.* SPE-14325-PA, Society of Petroleum Engineers.
34. Wikipedia A. *Well Intervention.* Available from: http://en.wikipedia.org/wiki/Well_intervention, 01.06.2015.
35. Wikipedia B. *Corrosion.* Available from: http://en.wikipedia.org/wiki/Corrosion, 08.06.2015.
36. Wikipedia C. *Well Integrity.* Available from: http://en.wikipedia.org/wiki/Well_integrity, 08.06.2015.
37. Wikipedia D. *Linear Interpolation.* Available from: http://en.wikipedia.org/wiki/Linear_interpolation, 15.05.2015
38. Wu, J., 2005. *Casing Burst Strength After Casing Wear*. SPE 94304. Presented at the SPE Production and Operations Symposium in Oklahoma City, Oklahoma, USA, April 2005.

Private communications

1. Belayneh, M., 2015. Personal communication.
2. Chow, H., 2015. Personal communication.
3. Rohde, J., 2015. Personal communication.
4. Toftkaer, J., 2015. Personal communication.

Appendix A

Derivation of burst models based on Thick-Walled cylinder

When assuming inside pressure only, the principal stresses for a thick-walled cylinder are [Boresi and Schmidt, 2003]:

$$\sigma_r = \frac{p_a a^2 - p_b b^2}{b^2 - a^2} - \frac{a^2 b^2}{(b^2 - a^2) r^2}(p_a - p_b) \quad \text{(A.1)}$$

$$\sigma_\theta = \frac{p_a a^2 - p_b b^2}{b^2 - a^2} + \frac{a^2 b^2}{(b^2 - a^2) r^2}(p_a - p_b) \quad \text{(A.2)}$$

$$\sigma_a = \frac{p_a a^2 - p_b b^2}{b^2 - a^2} \quad \text{(A.3)}$$

When setting $P_b = 0$ and $\sigma_z = 0$ these equations for the principal stresses are reduced to:

$$\sigma_r = \frac{p_a a^2}{b^2 - a^2} - \frac{a^2 b^2}{(b^2 - a^2) r^2}(p_a) \quad \text{(A.4)}$$

$$\sigma_\theta = \frac{p_a a^2}{b^2 - a^2} + \frac{a^2 b^2}{(b^2 - a^2) r^2}(p_a) \quad \text{(A.5)}$$

$$\sigma_z = \frac{p_a a^2}{b^2 - a^2} = 0 \quad \text{(A.6)}$$

Tresca Failure Criterion

For the Tresca failure criterion, insert the principal stress equations (A.4), (A.5) and (A.6) into the Tresca equation ($\sigma_y = \sigma_{max} - \sigma_{min}$) and solve for the inside yield pressure P_y. The Tresca failure criteria states that $\sigma_3 > \sigma_2 > \sigma_1$

Where

$\sigma_h = \sigma_3$

$\sigma_z = \sigma_2$

$\sigma_r = \sigma_1$

$\sigma_\gamma = \sigma_{max} - \sigma_{min}$

$\sigma_\gamma = \sigma_3 - \sigma_1 = \sigma_h - \sigma_r$

$$\sigma_\gamma = \left[\frac{p_a a^2}{b^2-a^2} + \frac{a^2 b^2}{(b^2-a^2)r^2}(p_a)\right] - \left[\frac{p_a a^2}{b^2-a^2} - \frac{a^2 b^2}{(b^2-a^2)r^2}(p_a)\right]$$

$$\sigma_\gamma = \frac{a^2 b^2}{(b^2-a^2)r^2}(p_a) + \frac{a^2 b^2}{(b^2-a^2)r^2}(p_a) = 2\frac{a^2 b^2}{(b^2-a^2)r^2}(p_a)$$

Solving for $P = P_\gamma$, and $r = a$

$$P_\gamma = \frac{\sigma_\gamma}{2}\left(1 - \frac{a^2}{b^2}\right) \qquad \text{(A.7)}$$

This is the Tresca failure criterion for thick-walled cylinders.

Von Mises Failure Criterion

Similarly, inserting the principal stress equations (A.4), (A.5) and (A.6) for thick-walled cylinder into the Von Mises equation:

$$\sigma_{VME} = \sqrt{{}^{1}/_{2}\{(\sigma_h - \sigma_r)^2 + (\sigma_r - \sigma_z)^2 + (\sigma_z - \sigma_h)^2\}}$$

Remember that $P_b = 0$ and $\sigma_z = 0$

$$\sigma_{VME} = \sqrt{{}^{1}/_{2}\left[({\sigma_h}^2 - 2\sigma_h\sigma_r + {\sigma_r}^2) + {\sigma_r}^2 + {\sigma_h}^2\right]}$$

$$\sigma_{VME} = \sqrt{{}^{1}/_{2}\left[2{\sigma_h}^2 + 2{\sigma_r}^2 - 2\sigma_h\sigma_r\right]}$$

$$\sigma_{VME} = \sqrt{{\sigma_h}^2 + {\sigma_r}^2 - \sigma_h\sigma_r} \qquad \text{(A. 8)}$$

When $r = a$, the equations for the principal stresses are again reduced to:

$$\sigma_h = \frac{p_a a^2}{b^2 - a^2} + \frac{a^2 b^2}{(b^2 - a^2) r^2}(p_a) = \frac{p_a \boldsymbol{a^2}}{b^2 - a^2} + \frac{b^2}{(b^2 - a^2)}(p_a) = \frac{p_a(a^2 + b^2)}{b^2 - a^2} \qquad \text{(A.9)}$$

$$\sigma_r = \frac{p_a a^2}{b^2 - a^2} - \frac{a^2 b^2}{(b^2 - a^2) r^2}(p_a) = \frac{p_a a^2}{b^2 - a^2} - \frac{b^2}{(b^2 - a^2)}(p_a) = \frac{p_a(a^2 - b^2)}{b^2 - a^2} \qquad \text{(A.10)}$$

$$\sigma_z = 0 \qquad \text{(A.11)}$$

Inserting the principal stresses into equation (A.8) yields:

$$\sigma_{VME} = \sqrt{{\sigma_h}^2 + {\sigma_r}^2 - \sigma_h \sigma_r}$$

$$\sigma_{VME} = \sqrt{\left(\frac{p_a(a^2+b^2)}{b^2-a^2}\right)^2 + \left(\frac{p_a(a^2-b^2)}{b^2-a^2}\right)^2 - \left(\frac{p_a(a^2+b^2)}{b^2-a^2}\right)\left(\frac{p_a(a^2-b^2)}{b^2-a^2}\right)}$$

$$\sigma_{VME} = \sqrt{\frac{{p_a}^2(a^2+b^2)^2}{(b^2-a^2)^2} + \frac{{p_a}^2(a^2-b^2)^2}{(b^2-a^2)^2} - \frac{{p_a}^2(a^2+b^2)(a^2-b^2)}{(b^2-a^2)^2}}$$

$$\sigma_{VME} = \sqrt{\frac{{p_a}^2}{(b^2-a^2)^2}\left[(a^2+b^2)^2 + (a^2-b^2)^2 - (a^2+b^2)(a^2-b^2)\right]}$$

$$\sigma_{VME} = \sqrt{\frac{{p_a}^2}{(b^2-a^2)^2}\left[a^4 + 3b^4\right]} = \frac{p_a}{\left(1-\frac{a^2}{b^2}\right)}\sqrt{\frac{a^4}{b^4}+3}$$

Solving for $P = P_Y$

$$P_Y = \frac{\sigma_{VME}\left(1-\frac{a^2}{b^2}\right)}{\sqrt{\frac{a^4}{b^4}+3}} \qquad \text{(A.12)}$$

This equation is the Von Mises failure criteria for a thick-walled cylinder.

Derivation of burst models based on Thin-Walled cylinder

Given for thin-walled cylinders, the principal stresses are [Boresi and Schmidt, 2003]:

$$\sigma_\theta = \frac{Pr}{t} \tag{A.13}$$

$$\sigma_z = \frac{Pr}{2t} \tag{A.14}$$

$$\sigma_r = 0 \tag{A.15}$$

Tresca Failure Criterion

Insert the principal stresses in equation (A.13), (A.14) and (A.15) into Tresca equation ($\sigma_\gamma = \sigma_{max} - \sigma_{min}$) and solve for the inside yield pressure P_y. The Tresca failure criteria states that $\sigma_3 > \sigma_2 > \sigma_1$

$$\sigma_\gamma = \sigma_{max} - \sigma_{min}$$
$$\sigma_\gamma = \sigma_\theta - \sigma_r$$
$$\sigma_\gamma = \frac{Pr}{t} - 0 = \frac{Pr}{t} \tag{A.16}$$

Solving for $P = P_y$ gives:

$$P_y = \frac{\sigma_\gamma t}{r} \tag{A.17}$$

This equation is the Tresca failure criterion for a thin-walled cylinder. Multiplying by 2 in the numerator and denominator gives the Barlow equation [Bellarby, 2009]:

$$P_y = \frac{\sigma_\gamma t}{r} * \frac{2}{2} = \frac{2\sigma_\gamma t}{D} \tag{A.18}$$

$\sigma_\gamma = Minimum\ yield\ strength$

$t = Nominal\ wall\ thickness$

$D = Tubing\ outside\ diameter$

Von Mises Failure Criterion

Similarly for Von Mises failure criteria, insert the principal stresses $(\sigma_h, \sigma_z, \sigma_r)$ into Von Mises equation:

$$\sigma_{VME} = \sqrt{{}^{1}/_{2}\{(\sigma_h - \sigma_r)^2 + (\sigma_r - \sigma_z)^2 + (\sigma_z - \sigma_h)^2\}}$$

$$\sigma_{VME}\sqrt{2} = \sqrt{(\sigma_h - \sigma_r)^2 + (\sigma_r - \sigma_z)^2 + (\sigma_z - \sigma_h)^2}$$

$$\sigma_{VME}\sqrt{2} = \sqrt{\frac{P^2r^2}{t^2} + \frac{P^2r^2}{4t^2} + \frac{P^2r^2}{4t^2}}$$

$$\sigma_{VME}\sqrt{2} = \sqrt{\frac{3}{2}\frac{P^2r^2}{t^2}}$$

Solving for $P = P_\gamma$:

$$P_\gamma = \frac{2}{\sqrt{3}}\frac{\sigma_\gamma t}{r} \qquad \text{(A.19)}$$

This equation is the Von Mises failure criteria for thin-walled cylinders.

Appendix B

Example: Calculation of indentation depth

Find the indentation depth of 45% wear

In order to build the geometry of the wear scar in Abaqus, one need the X and Y coordinates for the eccentricity and indentation depth. These coordinate positions can be calculated as follows:

$r_{i,tubing} = 2{,}446\ in.$

$r_{CT} = 1{,}4347\ in.$

$Eccentricity_{0\%wear} = r_{i,tubing} - r_{CT} = 2{,}446\ in. - 1{,}4347\ in. = 1{,}0085$ in.

$Wear\ Depth_{45\%\ wear} = 0{,}304 * 0{,}45 = 0{,}1368\ in.$

$$Eccentricity_{45\%wear} = Eccentricity_{0\%wear} + Wear\ Depth_{45\%\ wear}$$
$$= 1{,}0085 \text{ in.} + 0{,}1368\ in. = 1{,}1453\ in.$$

$$Indentation\ Depth_{45\%\ Wear} = r_{i,tubing} + Wear\ Depth_{45\%\ wear}$$
$$= 2{,}446\ in. + 0{,}1368\ in. = 2{,}5828\ in.$$

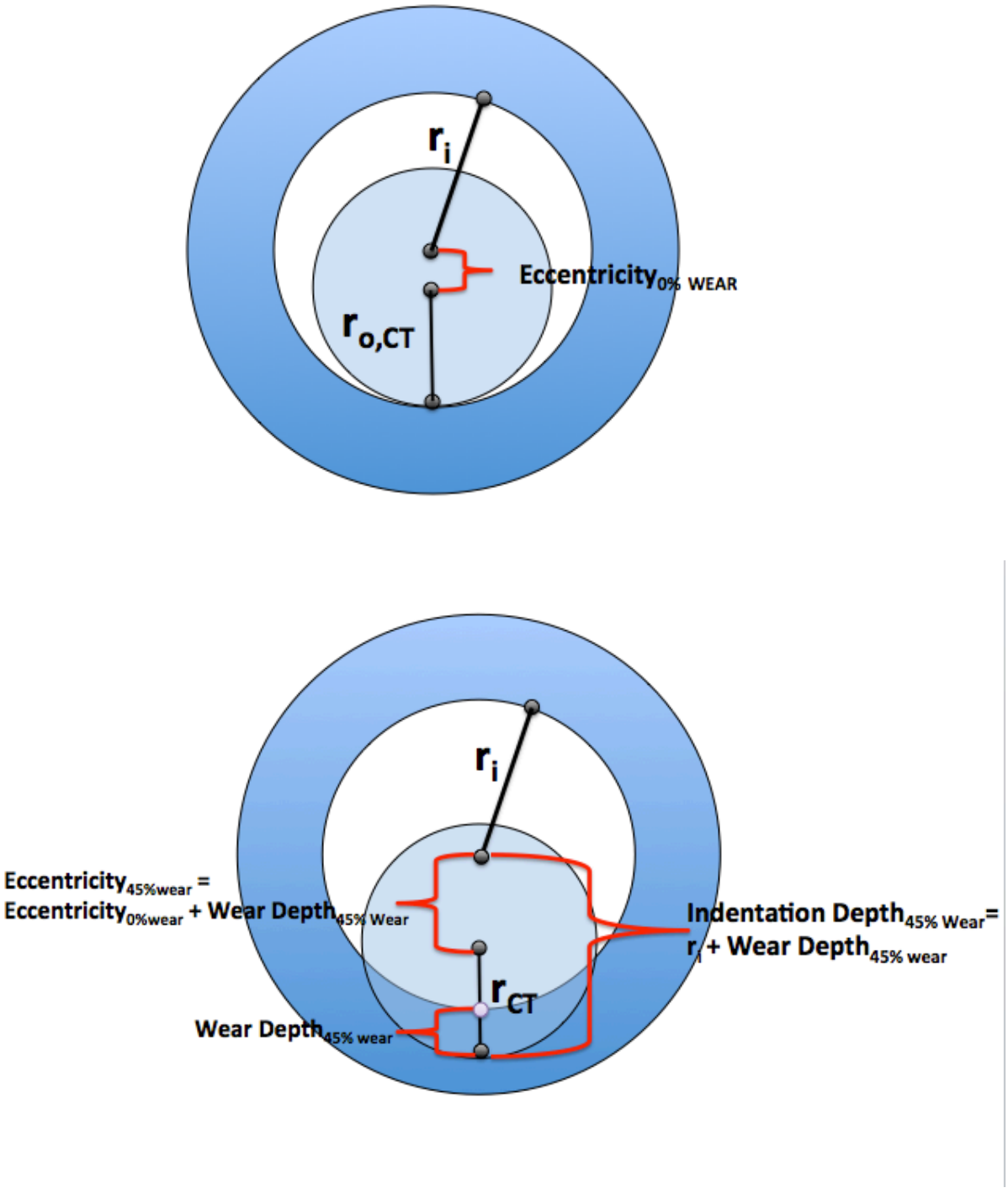

Figure B1: An illustration of how the eccentricity and indentation depth was calculated

Appendix C: Mesh dependent simulation results

Burst

At first, all the models were simulated using the same seed size equal to 0.2 for meshing. The models for 15% and 30% wear appears to be anomalies compared to the others. During meshing these two models, one could notice the meshing looked different from the others in the radial direction. These models only had one grid/mesh in the radial direction, while the others had two, like illustrated in the example below:

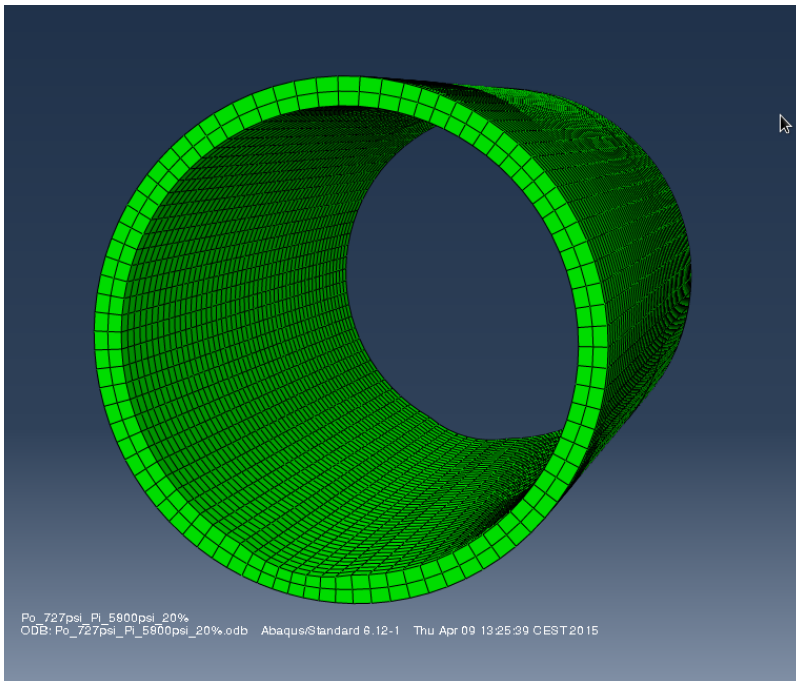

Figure C1: 20% wear model with two grids in the radial direction

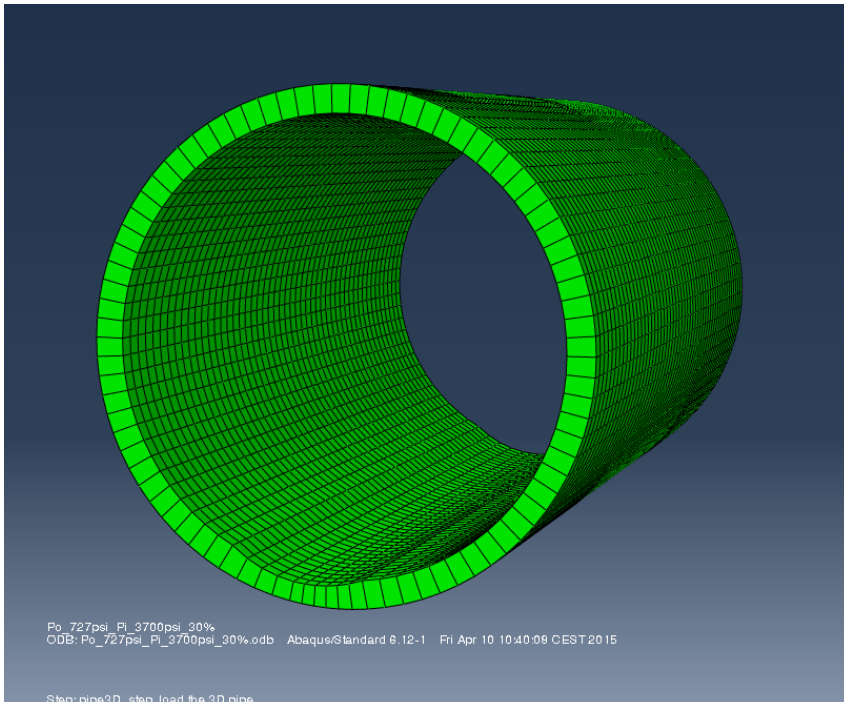

Figure C2: 30% wear model with only one grid in the radial direction

The results from the first simulation where all the models were built with the same seed size are shown in Table C1. The results from interpolation represent the intersection between the σ_{VME} and σ_y.

Table C1: Linear interpolation results

Linear interpolation	
Wear %	**Pressure [psi]**
0,00 %	9677,53
5,00 %	8162,04
10,00 %	7 546,61
15,00 %	5 693,83
20,00 %	5 557,23
25,00 %	4 926,56
30,00 %	3 871,37
35,00 %	3 993,50
40,00 %	3 638,04
45,00 %	3 287,58
47,00 %	3 159,09
50,00 %	3 002,27

Figure C3 shows the plotted results from the interpolation. A model was generated from the plot

$$y = 25683x^2 - 25544x + 9531{,}1 \qquad \text{(C.1)}$$

As seen in Figure C3, the anomalies are at the points of 15% and 30% wear depth. At these points the simulation-based model does not seem to fit the simulated data, where one can notice that the slope of the curve varies a lot. The steepest slope seems to be between 10% and 15% wear positions. The pressure where the material starts yielding at 10 % wear depth is 7546.61 psi, and drops drastically down to 5693.83 psi at 15% wear. Another odd phenomenon is that the 30% wear model has a lower pressure limit than the 35%, while logically 30% wear should have a higher limit.

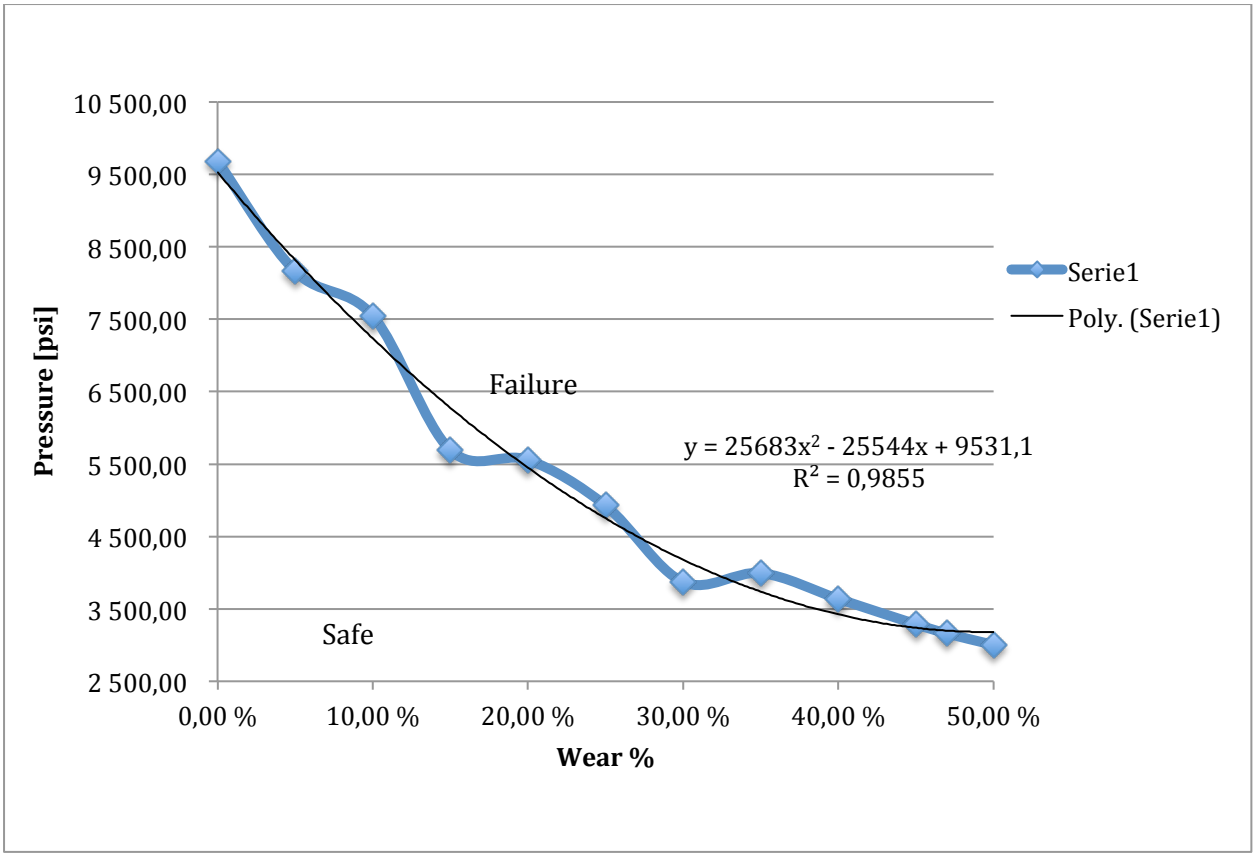

Figure C3: Safe/Failure Zone for Operating Internal Pressure, “True Burst”

Re-building and re-simulating 15% and 30% wear models for Burst

The two models were re-built with another seed size for meshing to see if it would make a difference for the result. Instead of the seeding with 0.2, the size was reduced to 0.15 to achieve same number of grids in the radial direction. Simulating these models with reduced seed size gave a higher tolerance for the internal pressure than the first time. The results from the linear interpolation for the re-simulated models for 15% and 30% are given in Table C2:

Table C2: Linear interpolation of re-simulated models

Linear interpolation	
Wear %	**Pressure [psi]**
0,00 %	9677,53
5,00 %	8162,04
10,00 %	7546,61
15,00 %	6141,89
20,00 %	5557,23
25,00 %	4926,56
30,00 %	4288,00
35,00 %	3993,50
40,00 %	3638,04
45,00 %	3287,58
47,00 %	3159,09
50,00 %	3002,27

From interpolation one can see that the point of intersection between σ_{VME} and σ_Y is at a higher internal yield pressure. For the 15% wear model, decreasing from seed size 0.2 to 0.15 lead to an increase in internal pressure limit from 5693.83 psi to 6141.89 psi. Similarly for the 30% wear model, the pressure increased from 3871.37 psi to 4288.00 psi.

By keeping the seed size constant, the meshing turned out differently for some of the models. It may seem that by adjusting the seed size, the final results became more adequate. When modifying the seed size, the models became more similar grid-wise. The re-simulated models had all the same number of grids in the radial direction, and the curve produced from these results was more logically satisfying. With this in mind, it appears that it is more essential to keep the grid number of the models similar, rather than keeping the seed size constant when modeling.

Figure C4 and Figure C5 plots and compares the results from the simulations with different seed sizes. Both plots show a clear difference for the safe operational pressure limit within the same wear percent model.

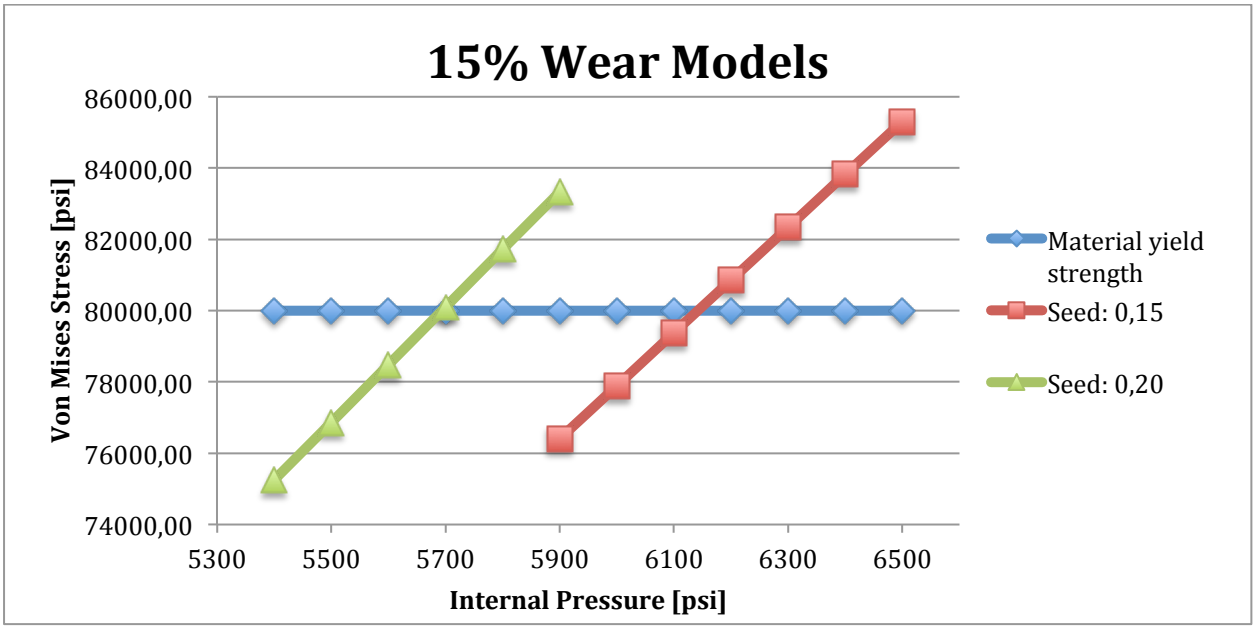

Figure C4: Comparison of 15% wear models with different seed sizes.

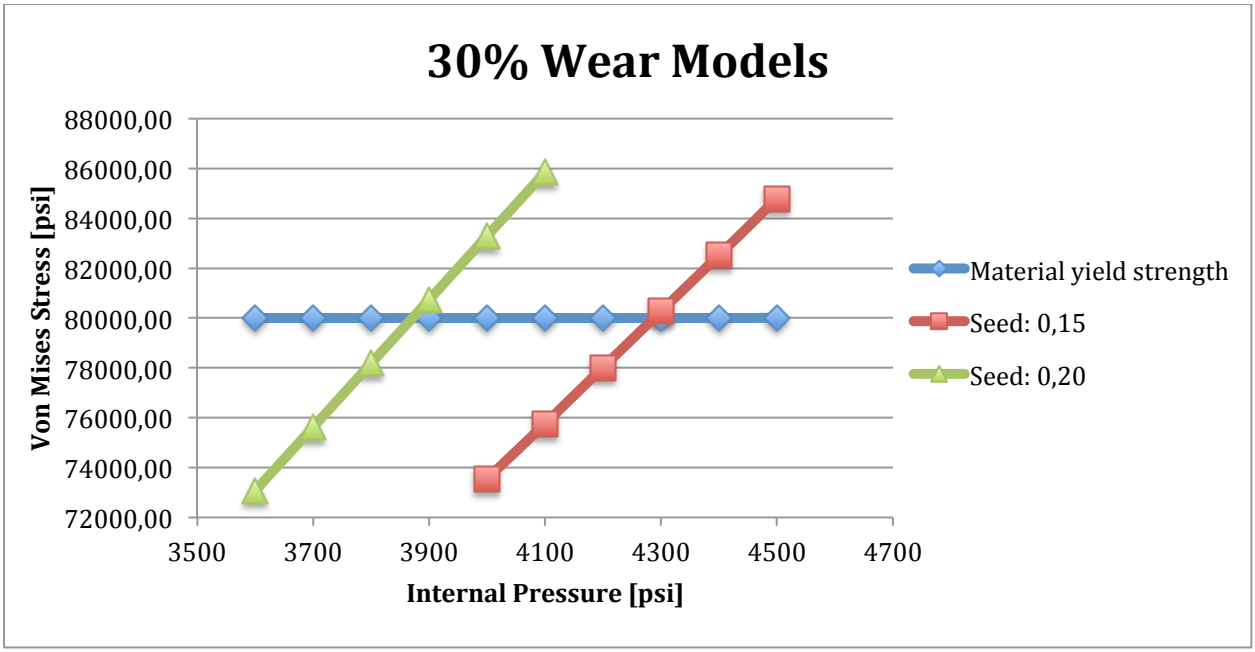

Figure C5: Comparison of 30% wear models with different seed sizes.

Plotting these re-simulated results in the "true-burst for operational internal pressure" provides a much more smooth curve, and the simulated data fits the models better:

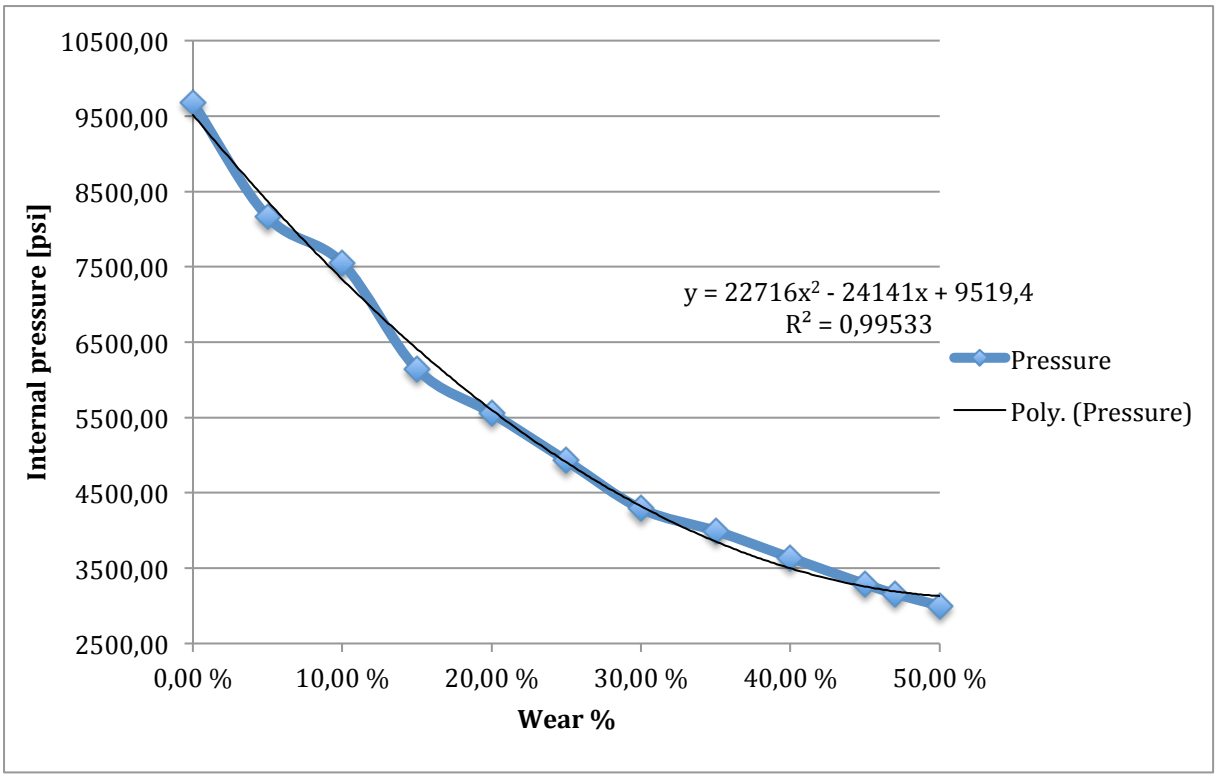

Figure C6: Results of data after re-simulating the models for 15% and 30% with adjusted mesh size.

Collapse

The same problem occurred for the 15% and 30% wear depth during modeling for collapse. Similar as for burst, the two models show anomalies during meshing, leading to an unsatisfying result. The data do not match very well with the generated model at certain points of the curve:

$$y = 23173Wear\%^2 - 23420Wear\% + 8802 \qquad \text{(C.2)}$$

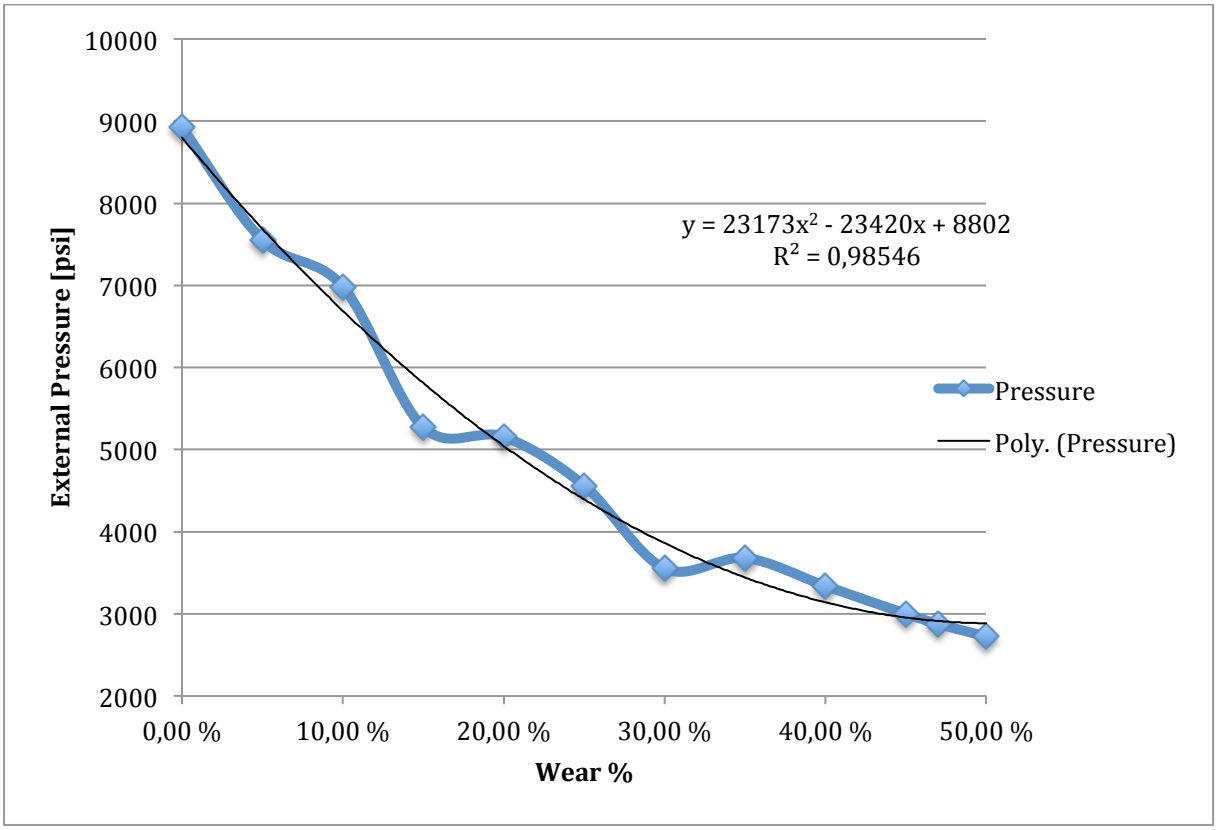

Figure C7: Safe/failure zone for operational external pressure, "True Collapse"

Re-building and re-simulating 15% and 30% wear models for Collapse

The same procedure was carried out for re-simulating the 15 and 30% wear models for collapse, as it did for burst. The ending result showed a much better match with the generated model and looks as follows:

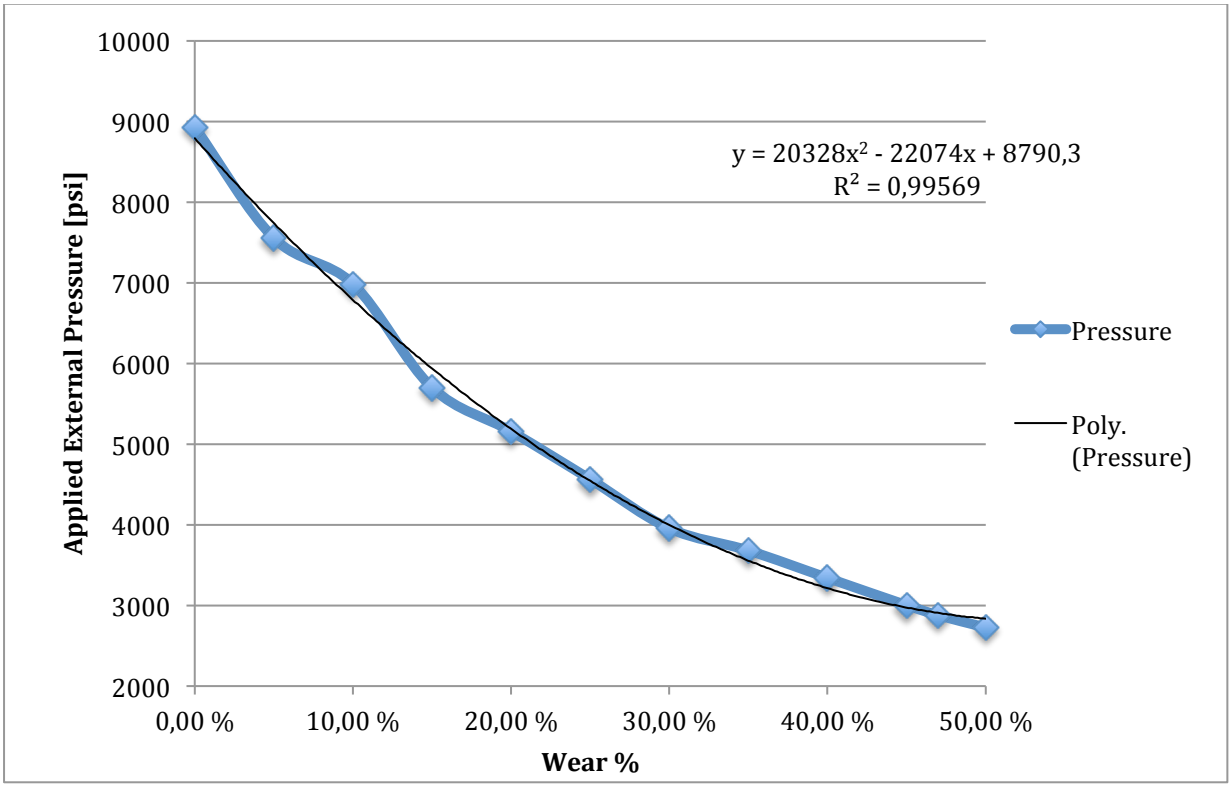

Figure 56: Safe/failure zone for operational external pressure, “True Collapse” for the re-simulated data.